Structural Performance of Steel Buildings under Travelling Fires and Blast

A thesis submitted for the degree of Doctor of Philosophy and the Diploma of Imperial College London

By

Adeyanju Ashabi Teslim-Balogun

Department of Civil and Environmental Engineering

Imperial College London

February 2020

Declaration of originality

I hereby confirm that the research work undertaken in this thesis is my own work and all other materials from published and unpublished work have been appropriately referenced.

Copyright declaration

Abstract

Previous records of fire and blast incidents have shown the extensive damage that these actions can cause in building structures in general and steel buildings in particular. Therefore, it is crucial that strategic facilities are designed to withstand these extreme loads with as little damage as possible. However, the design of structures to resist blast and fire actions has typically been carried out prescriptively and without consideration for the uneven distribution of temperatures in large building compartments typical of today's architectural practice. Blast pressures due to explosions are also likely to be followed by travelling fires in these compartments. Moreover, due to the significant level of uncertainty involved, a performance-based framework is likely to be more suited for the design and assessment of structures subjected to these loads. This thesis aims to investigate the structural performance of steel structures under travelling fires as well as multi-hazard conditions involving blast and travelling fires from a performance-based perspective.

Non-linear finite element analyses are carried out on steel frames considering various travelling fires and post-blast travelling fire scenarios. The PEER performance-based framework, originally developed for seismic actions, is tailored and used to assess the building performance under these actions. The results show that the structural response could be underestimated or overestimated by up to 30 % when there is significant correlation between the maximum compartment temperature and the length of travelling fire for very low probabilities of exceedance. Under post-blast travelling fires, the first storey is likely to be the most critical storey, and blast and fire parameters can significantly affect the structural response. Moreover, correlation effects between maximum compartment temperature and blast overpressure are found to be more significant when low exceedance rates are considered.

The results of this research demonstrate that a performance-based assessment can be used to examine the response of steel structures under these extreme loads and to assess the efficiency of different structural systems. It can also potentially lead to great savings in the cost of blast and fire protection required.

Acknowledgements

I wish to express profound gratitude to my supervisors, Dr Christian Málaga-Chuquitaype and Dr Peter J Stafford for their support and expert supervision during the course of my research. I am also grateful for the constructive feedback they have given me on my thesis as well as all other publications and reports I have submitted during the PhD.

The financial support of the Petroleum Technology Development Fund (PTDF) and the National Universities Commission (NUC) in Nigeria is duly acknowledged. I also wish to thank all the staff of PTDF and NUC for their support and guidance.

I am very grateful for the administrative support provided by the staff of the Civil and Environmental Engineering Department of Imperial College London, especially Ms Fionnuala Donovan and Ms Sarah Willis who supported me especially during my pregnancy and after the birth of my daughter. I am indeed thankful for my friends from the Emerging Structural Technologies Group with whom I have shared good memories with during the course of my research.

The PhD process is a very tough and challenging one and I do not think I would have made it this far without the support of my friends and family. I want to thank my parents for believing in me all these years and making my education a priority and last but not the least, I wish to appreciate my husband, Dolapo Oluwa for being a pillar of support over the years and I am eternally grateful for your love and care.

Table of Contents

Abstract 2

Acknowledgements 3

Table of Contents 4

List of Figures 8

List of Tables 13

Notations 14

Chapter 1 Introduction 16

1.1 Research background 16

1.2 Objectives of the research 18

1.3 Organization of the thesis 19

Chapter 2 Literature Review 20

2.1 Introduction 20

2.2 Fire 20

2.2.1 Fire dynamics 20

2.2.2 Properties of steel and concrete under elevated temperatures 22

2.2.3 Experimental and numerical studies on fire 23

2.2.4 Structural fire design methods and their limitations 26

2.2.5 Fire tests and accidental fires in large compartments 28

2.2.6 Travelling fires 29

2.3 Blast 34

2.4 Blast and fire 37

2.5 Performance-based design 39

2.6 Research gaps 42

Chapter 3 Finite Element Modelling 43

3.1 Introduction 43

3.2 Modelling in OpenSees 43
3.2.1 Structural element modelling 43
3.2.2 Composite beam modelling 44
3.2.3 Material models 45
3.3 Numerical analyses 45
3.3.1 Static analysis 45
3.3.2 Blast analysis 45
3.3.3 Heat transfer analysis 47
3.3.4 Fire analysis 47
3.4 Model validation 48
3.4.1 Structures subjected to fire 48
3.4.2 Structures subjected to blast 53
3.4.3 Structures subjected to blast and fire 55
3.5 Prototypical building model 57
3.5.1 Sensitivity analyses 59
3.6 Conclusions 61
Chapter 4 Assessment of Efficiency of Travelling Fire Intensity Measures for Performance-based Assessment 62
4.1 Introduction 62
4.2 Structural and fire parameters 63
4.3 Regression analyses 65
4.3.1 Intensity measures and Engineering demand parameters 65
4.3.2 Univariate regression 66
4.3.3 Efficiency of intensity measures 71
4.3.4 Multivariate regression 73
4.4 Performance-based travelling fire assessment 76
4.4.1 Hazard analysis 76

4.4.2 Structural analysis 80
4.4.3 Discussion 82
4.5 Conclusions 84
Chapter 5 Effects of Blast and Travelling Fires on Steel Frames 85
5.1 Introduction 85
5.2 Blast and fire parameters 85
5.3 Preliminary studies 88
5.3.1 Blast and horizontally travelling fire 89
5.3.2 Blast and multi-floor horizontally travelling fire 91
5.3.3 Blast and vertically travelling fire 95
5.3.4 Discussion 99
5.4 Effects of blast pressures 100
5.4.1 North-south travel direction 100
5.4.2 East-west travel direction 103
5.5 Effects of maximum compartment temperature 106
5.5.1 North-south travel direction 106
5.5.2 East-west travel direction 108
5.6 Effects of fire size 111
5.6.1 North-south travel direction 111
5.6.2 East-west travel direction 113
5.7 Conclusions 115
Chapter 6 Performance-based Post-blast Travelling Fire Assessment of Steel Frames 116
6.1 Introduction 116
6.2 Effects of steel beam-to-column stiffness ratio 116
6.2.1 North-south travel direction 118
6.2.2 East-west travel direction 122
6.2.3 Fire protection 126

6.2.4 Discussion 128
6.3 Performance-based post-blast travelling fire assessment 129
6.3.1 Regression analyses 129
6.3.2 Hazard analysis 132
6.3.3 Structural analysis 134
6.3.4 Discussion 140
6.4 Conclusions 141
Chapter 7 Conclusions and Future Work 142
7.1 Conclusions and Recommendations 143
7.2 Limitations of research 146
7.3 Future work 147
References 148

List of Figures

Figure 2.1. Course of a fire in a building compartment (from Drysdale, 2011). 21
Figure 2.2. Stress-strain relationship of steel at different temperatures (from BSI, 2005). 22
Figure 2.3. Stress-strain relationship of concrete at different temperatures (from BSI, 2005). 23
Figure 2.4. The standard temperature-time curve. 27
Figure 2.5. The parametric temperature-time curve. 27
Figure 2.6. Temperature–time history of a compartment using the Fire Cell Method (adapted from Clifton, 1996). 29
Figure 2.7. Movement of fire across a compartment floor for (a) 5 % fire size and (b) 25 % fire size (from Law et al., 2011). 30
Figure 2.8. Temperature-time history of a travelling fire (from Stern-Gottfried & Rein, 2012b). 31
Figure 2.9. Reflection of blast pressures on a building from Ngo et al. (2007)..... 34
Figure 2.10. Positive blast wave parameters (from UFC, 2008)..... 35
Figure 2.11. Pressure-time history of a typical blast wave (from Ngo et al., 2007). 36
Figure 2.12. Probability plots for (a) IM hazard curve (b) EDP hazard curve (c) DM fragility curve and (d) Downtime consequence curve (from Lange et al., 2014)..... 41
Figure 3.1. Fibre section beam element modelling in OpenSees. 44
Figure 3.2. Composite beam modelling alternatives..... 45
Figure 3.3. Temperature distribution in a steel column and composite beam section. 47
Figure 3.4. Temperature-time history of the beam. 48
Figure 3.5. The pin-ended beam in the study. 49
Figure 3.6. Vertical displacement response of the pin-ended beam. 49
Figure 3.7. Longitudinal section and cross-section of the beam from Jiang et al. (2015). 50
Figure 3.8. Mean temperatures at different locations in the beam (Wainman & Kirby, 1988). 50
Figure 3.9. Vertical displacement response of the composite beam at mid span. 51
Figure 3.10. The steel frame in the study with F1 = 74 kN, F2 = 2.5 kN, L = 1.2 m and h = 1.18 m (from Izzuddin et al., 2000). 52
Figure 3.11. Horizontal displacement response of the frame. 52
Figure 3.12. Column geometric configuration and blast history from Chen & Liew (2005). 54

Figure 3.13. Vertical displacement at top of column adapted from Chen & Liew (2005). 54
Figure 3.14. The 3-storey frame in the study from Izzuddin et al. (2000). 55
Figure 3.15. Horizontal displacement response of the side column from Izzuddin et al. (2000). 56
Figure 3.16. Plan of the prototypical office building. 58
Figure 3.17. Numerical model for the 9 m composite beam. 58
Figure 3.18. Movement of fire along the compartment for a fire size of 10 % of the floor area. 60
Figure 3.19. Temperature time history of the travelling fire and composite beam at 2 m and 8 m from the left edge of the compartment. 60
Figure 3.20. Vertical displacement at mid span of the 9 m composite beam for increasing number of elements. 61
Figure 4.1. Temperature-time curves at different locations in a 9 m beam. 64
Figure 4.2. Scatter plot matrix showing the regression models of the natural logarithm of the EDPs against the natural logarithm of T_{max}, L_f, S and T_{tot}. 68
Figure 4.3. Scatter plot matrix showing the regression models of the natural logarithm of the EDPs against the natural logarithm of t_b, FS, FLD and HRR. 69
Figure 4.4. Plot of natural log of maximum relative beam displacement against natural log of length of fire showing the regression line with and without the lower lnMBD data values. 71
Figure 4.5. Scatter plot matrix for residuals of natural log of MBD, MBC and MBT for T_{max} against natural log of T_{max}, L_f and S. 75
Figure 4.6. PDF and POE curves of maximum compartment temperature and length of fire. 78
Figure 4.7. Joint POE of maximum compartment temperature and length of fire. 79
Figure 4.8. Joint PDF of maximum compartment temperature and length of fire (surface and contour plots). 79
Figure 4.9. PDF of maximum relative beam displacement given the IMs. 80
Figure 4.10. PDF of maximum relative beam compressive force given the IMs. 81
Figure 4.11. Probability of exceedance of maximum relative beam displacement. 81
Figure 4.12. Probability of exceedance of maximum relative beam compressive force. 82
Figure 4.13. Ratio of maximum relative beam displacement for the high positive and negative correlation to the zero correlation case for different probabilities of exceedance. ... 83

Figure 4.14. Ratio of maximum relative beam compressive force for the high positive and negative correlation to the zero correlation case for different probabilities of exceedance. 83
Figure 5.1. Position of a blast source from the centre of the beam (in dotted lines) and directions of travel for a travelling fire of 10 % of the floor area. 86
Figure 5.2. Typical pressure-time histories of the blast loads. 87
Figure 5.3. Typical temperature-time curves of the travelling fire scenarios. 88
Figure 5.4. Deformation of the frame when the 1st, 3rd and 5th storeys are subjected to the blast load (5x magnification of displacements). 90
Figure 5.5. Deformation of the frame when the 1st, 3rd and 5th storeys are subjected to the subsequent travelling fire (5x magnification of displacements). 91
Figure 5.6. Structural response at different storey levels as number of floors under fire increases for blast at the 1st storey (dotted lines represent tension and pink rectangles indicate storeys under fire)..... 93
Figure 5.7. Structural response at different storey levels as number of floors under fire increases for blast at the 4th storey (dotted lines represent tension and pink rectangles indicate storeys under fire)..... 94
Figure 5.8. Deformation of the frame during multiple floor fires for an initial blast at the 1st storey (5x magnification of displacements). 95
Figure 5.9. Deformation of the frame during multiple floor fires for an initial blast at the 4th storey (5x magnification of displacements). 95
Figure 5.10. Envelope of structural response showing the maximum values at different storey levels for a 30 kg blast at the 1st storey and a vertically travelling fire (dotted lines represent tension and ignition time of each storey is indicated). 97
Figure 5.11. Deformation of the frame during the vertically travelling fire for an initial blast at the 1st storey (5x magnification). 97
Figure 5.12. Envelope of structural response showing the maximum values at different storey levels for a 30 kg blast at the 4th storey followed by a vertically travelling fire (dotted lines represent tension and ignition time of each storey is indicated). 98
Figure 5.13. Deformation of the frame during the vertically travelling fire for an initial blast at the 4th storey (5x magnification of displacements). 99
Figure 5.14. Structural response for increasing blast pressures and fire travelling in the north-south direction. 102

Figure 5.15. Structural response for increasing blast pressures and fire travelling in the east-west direction. 105
Figure 5.16. Deformation of the frame during the blast and during the fire. 106
Figure 5.17. Structural response showing the effect of increasing maximum temperatures for fire travelling in the north-south direction. 107
Figure 5.18. Structural response showing the effect of increasing maximum temperatures for fire travelling in the east-west direction. 109
Figure 5.19. Deformation of the frame under the 133 kPa blast and travelling fire for different maximum temperatures 110
Figure 5.20. Structural response of the frame for fire travelling in the north-south direction showing the effect of increasing fire sizes. 112
Figure 5.21. Structural response of the frame for fire travelling in the east-west direction showing the effect of increasing fire sizes. 114
Figure 6.1. Structural response under the 133 kPa blast and fire travelling in the north-south direction for different beam-to-column stiffness ratios. 119
Figure 6.2. Structural response under the 183 kPa blast and fire travelling in the north-south direction showing the effect of different beam-to-column stiffness ratios. 121
Figure 6.3. Structural response under the 133 kPa blast and fire travelling in the east-west direction showing the effect of different beam-to-column stiffness ratios. 123
Figure 6.4. Structural response under the 183 kPa blast and fire travelling in the east-west direction showing the effect of different beam-to-column stiffness ratios. 125
Figure 6.5. Temperature-time history in the beam section for the protected and unprotected beams. 127
Figure 6.6. Beam displacement response for the protected and unprotected beams. 127
Figure 6.7. Scatter plot matrix of the natural logarithm of maximum beam displacement, maximum column displacement and maximum beam compressive force against the natural logarithm of the maximum compartment temperature, blast overpressure and length of fire. 130
Figure 6.8. Probability distribution and Probability of exceedance curves for the maximum compartment temperature and blast overpressure. 133
Figure 6.9. Joint probability of exceedance of maximum compartment temperature and blast overpressure. 133
Figure 6.10. Joint probability distribution of maximum compartment temperature and blast overpressure (surface and contour plots). 134

Figure 6.11. Probability distribution of the EDPs considering a Vector IM of T_{max} and B_p. 135
Figure 6.12. Probability of exceedance curves of the EDPs for the three values of correlation when $\alpha = 0.18$. 136
Figure 6.13. Probability of exceedance curves of the EDPs for the three values of correlation when $\alpha = 0.31$. 137
Figure 6.14. Probability of exceedance curves of the EDPs for the three values of correlation when $\alpha = 0.49$. 138
Figure 6.15. Probability of exceedance curves of the EDPs for the three values of correlation when $\alpha = 0.67$. 139

List of Tables

Table 3.1. Temperature distribution in the structural elements from Izzuddin et al. (2000) .. 56
Table 3.2. Beam lengths and section sizes for the columns and beams. 57
Table 4.1. Range of values of structural and fire parameters considered in this study. 64
Table 4.2. Intensity measures considered in this study. 66
Table 4.3. The engineering demand parameters adopted in this study. 66
Table 4.4. Standard deviation of the IMs based on the selected EDPs. 70
Table 4.5. Ranking of IMs based on the mean standard deviation. 73
Table 4.6. Standard deviation of the Vector IMs. 74
Table 4.7. Ranking of Vector IMs..... 76
Table 5.1. Blast parameters. 87
Table 5.2. Travelling fire parameters. 87
Table 5.3. Structural response when individual storeys are subjected to blast and travelling fire. 90
Table 5.4. Ignition pattern of the vertically travelling fire for blast load at the 4^{th} storey. 96
Table 6.1. Element sizes for different steel beam-to-column stiffness ratios. 117
Table 6.2. Intensity measures and engineering demand parameters used in this study. 130
Table 6.3. Standard deviation values of EDP|IM. 132
Table 6.4. EDP values at a probability of exceedance of 0.001. 140
Table 6.5. Probability of exceedance of MBD at a failure criterion of L/20 (for λE = 1.0). 141

Notations

Alphabetic symbols

a	Coefficient of thermal expansion
B_p	Blast overpressure
E	Elastic modulus of steel
e	Standard error of regression
H	Distance between ceiling and the floor, height of compartment
I_b	Second moment of area of steel beam
I_c	Second moment of area of steel column
L^*	Dimensionless parameter which represents fire size
L	Length of the compartment
l_b	Span of steel beam
l_c	Height of steel column
L_f	Length of fire
n	Number of records
$P(DM\|EDP)$	Conditional probability of exceeding DM for a given value of EDP
$P(DV\|DM)$	Conditional probability of exceeding DV for a given value of DM
$P(EDP\|IM)$	Conditional probability of exceeding EDP for a given value of IM
$P(IM)$	Probability of exceeding IM
p_o	Peak uniformly distributed blast load
P_o	Pressure in ambient conditions
P_{so}^-	Blast underpressure
P_{so}	Peak pressure of the blast
$\bar{p}(t)$	Normalised blast overpressure
$p(t)$	Uniformly distributed blast load with respect to time
$\dot{Q}$	Heat release rate
$\dot{Q}''$	Heat release rate per unit area
q_f	Fuel load density
r	Distance to centre of fire
R	Standoff distance
s	Fire spread rate
t_b	Burning duration
T_∞	Ambient temperature in the compartment
t_A	Blast arrival time
t_d	Blast duration
T_{ff}	Far field temperature
T_{max}, T_{nf}	Maximum compartment temperature, near field temperature
T_{nf}	Near field temperature
T_{tot}	Total fire duration
W	Charge weight
w	Compartment width
x^*	Distance between point of interest and edge of compartment
X	Variable
Z	Scaled distance

Abbreviations

CDF	Cumulative distribution function
DM	Damage measure
DV	Decision variable
EDP	Engineering demand parameter
FLD	Fuel load density
FS	Fire size
HRR	Heat release rate
IAC	Increase in base column axial force due to fire
IM	Intensity measure
MBC	Maximum relative beam compressive force
MBD	Maximum relative beam displacement
MBT	Maximum relative beam tensile force
MCD	Maximum relative column lateral displacement
MJD	Maximum relative joint horizontal displacement
MJR	Maximum relative joint rotation
PDF	Probability distribution function
POE	Probability of exceedance
S	Fire spread rate

Greek letters

α	Beam to column stiffness ratio
α_0, α_1	Regression coefficients
$\beta_0, \beta_1, \beta_2$	Regression coefficients
ΔT	Change in temperature
$\varepsilon_{mechanical}$	Mechanical strain
$\varepsilon_T, \varepsilon_{thermal}$	Thermal strain
ε_{total}	Total strain
$\lambda(DV)$	Annual rate of exceeding DV
λ_E	Annual rate of occurrence of an event
$\lambda(EDP)$	Annual rate of exceeding the EDP
$\lambda(IM)$	Annual rate of exceeding the intensity measure
μ	Mean
ρ	Correlation between variables
$\sigma_{EDP\|IM}$	Standard deviation of an EDP given a particular IM
$\sigma_{EDP\|IM_1,IM_2}$	Standard deviation of an EDP given IM_1 and IM_2
Σ	Covariance matrix

Chapter 1
Introduction

1.1 Research background

The world has seen a dramatic change in the field of structural engineering especially with the demand for more aesthetically pleasing tall buildings. This has had a major effect on structural design as it has birthed novel design methods to ensure the stability of structures and safety of occupants. These structures also have to be designed to withstand extreme loading conditions which might occur during their design life. Fire is one of such loads that can cause serious structural damage putting the stability of the building and the safety of its occupants at risk. The impact of an inadequate fire safety design in buildings can be catastrophic as observed in the World Trade Centre and, more recently, the Grenfell Tower fire.

The World Trade centre fire has revolutionised structural fire design as it has made structural engineers understand the need for alternative load paths as well as the importance of designing structures to resist multiple extreme loading conditions. The towers were actually designed to resist impact loading because of their height. However, subsequent fire loads which impacted the integrity of the connections were not considered. This was obvious during the disaster as the towers were still standing after the impact but collapsed during the fire. The Grenfell Tower fire has also enlightened building regulators and the world at large on the need to ensure that proper fire resistant materials are used for cladding systems. This is because once the cladding was burning on a particular floor in the building, the fire travelled vertically, igniting other floors. Although the Grenfell Tower fire did not result in structural collapse, numerous lives were lost.

These and many more fire accidents have shown the significance of an adequate fire safety design in building structures. Besides, an understanding of the behaviour of structural materials in fire especially steel, which is widely used in building construction, is essential for the provision of an adequate level of safety against this extreme loading condition. This is because steel loses its strength at elevated temperatures. As a result, steel members are usually coated or covered with fire protection materials to reduce the penetration of heat.

Structural fire design is an important fire safety strategy that will ensure that structural elements can withstand elevated temperatures when active protection systems become inadequate. Usually the design is performed considering uniform temperature distributions in the compartment. This has been found to be unrealistic in larger compartments based on records of previous fire accidents as fire was observed to travel. This can result in an uneven spatial distribution of fire temperatures across the compartment (Stern-Gottfried & Rein, 2012a). Also, there are limitations in current methods of structural fire design that make them unsuitable for larger compartments, which are typical of modern day structures (Law et al., 2011). It is therefore important that travelling fires are considered in structural fire design within a full performance-based framework.

Blast loads can also cause serious damage to structures. This is due to the large amount of energy that is released in a short period of time during the action of a blast. Structures not designed for blast loads and exposed to it can collapse depending on the amount of blast pressure and the proximity to the structural elements. The progressive collapse of the Ronan point building in London and the Alfred P. Murrah Federal building in Oklahoma have shown the need for structures to adequately resist blast pressures. In the event of a blast followed by a fire, the damage can be disastrous due to the instability of the frame from the initial blast loads which can decrease the fire resistance of the structure. Moreover, several explosion incidents have resulted in very large fires. It is therefore imperative that for large building compartments, multiple hazard scenarios consisting of blast and travelling fires are adequately taken into consideration.

Prescriptive design codes have been found to be impractical and sometimes over conservative for the design of structures to resist extreme loading conditions (Lange et. al., 2014). As a result, performance-based approaches have been adopted in these cases so that the structure can be designed for a specific level of performance. Performance levels are usually characterised based on immediate occupancy, life safety and collapse prevention as recommended by FEMA (1997). A premier example of a performance-based design and assessment framework is the Pacific Earthquake Engineering Research (PEER) framework which was formulated to design structures subjected to earthquake action based on specified performance objectives and to provide relevant information on acceptable levels of associated risk. The application of the PEER framework has not been extended to travelling fires. Also, the framework has not been

used for the design and assessment of structures to resist multi-hazard scenarios involving blast and travelling fires.

Therefore, this thesis aims to study the structural performance of steel structures under blast pressures and travelling fires from a performance-based perspective. In particular, the PEER framework is adapted and employed to assess steel structures under both actions. It is expected that the outcome of this research will provide valuable information and design recommendations that will be useful when designing for such loading scenarios.

1.2 Objectives of the research

The structural performance of selected steel frames to travelling fires as well as blast and travelling fires will be examined in this thesis. The PEER performance-based framework will also be adapted for both actions in order to access the performance of selected steel frames under both loading scenarios. Therefore, the objectives of this thesis are to:

1. Assess the suitability of several intensity measures related to travelling fire events that have significant influence on the structural response of steel buildings and evaluate the most efficient intensity measures to be used within a performance-based context.
2. Adapt the PEER framework for travelling fires in order to assess the probability of exceedance of selected engineering demand parameters.
3. Determine the effects of blast pressure, maximum compartment temperature, fire size and different travel directions on the structural performance of steel frames under blast and horizontally travelling fires. Preliminary studies will be carried out to determine the most critical floor for a single floor horizontally travelling fire as well as multi-floor simultaneous and vertically travelling fire scenarios.
4. Assess the performance of steel frames under blast and travelling fires. The effects of steel beam-to-column stiffness ratio will be investigated and the probability of exceedance of structural systems with different beam-to-column stiffness ratios will be determined.

1.3 Organization of the thesis

The thesis is organised into seven chapters:

Chapter 1 offers an introduction to the research themes and sets out the objectives of the research. The organization of the thesis is also outlined in this chapter.

Chapter 2 is a review of past studies on fires, blast and performance-based design. It also discusses the research gaps that will be addressed by this thesis.

Chapter 3 discusses the finite element modelling approach employed throughout the research. It also describes the numerical analyses that will be carried out in this thesis. The validation of building models constructed in OpenSees is also presented.

Chapter 4 presents an assessment of the efficiency of several intensity measures for performance-based travelling fire assessment. It also reformulates relevant parts of the PEER performance-based framework for the assessment of steel structures under travelling fires.

Chapter 5 investigates the effects of different parameters on the performance of steel buildings subjected to blast and travelling fires. It also presents initial studies to determine the most critical floor for different travelling fire scenarios.

Chapter 6 presents an adaptation of the PEER performance-based framework to blast and travelling fires and investigates the effects of steel beam-to-column stiffness ratio on the response of steel frames under blast and travelling fires.

Chapter 7 presents the summary of the research as well conclusions and recommendations for future work.

Chapter 2
Literature Review

2.1 Introduction

Structural fire engineering is very important in building design since the damaging effects of fires in buildings can be catastrophic. Several studies have been carried out to determine the effect of fires on building structures. Besides, multi-hazard scenarios in particular explosions and fire have also been studied to understand their effect on structures. Moreover, probabilistic methods such as performance-based design frameworks have also been developed to provide more robust hazard design and assessment. This chapter will review previous research in these areas. Also, the research gaps that will be addressed by this research will be identified.

2.2 Fire

2.2.1 Fire dynamics

The design of structures to resist fire is determined by the behaviour of its structural members and their end restraints under increasing thermal loads. The thermal behaviour of a structural member is described by Equation 2.1.

$$\varepsilon_{total} = \varepsilon_{thermal} + \varepsilon_{mechanical} \tag{2.1}$$

where $\varepsilon_{thermal}$ is the thermal strain, $\varepsilon_{mechanical}$ is the mechanical strain and ε_{total} is the total strain in the member (Usmani et al., 2001). The stresses in the member are governed by the mechanical strains while its deformed shape is based on the total strains in the structural member. The strains in the structural member due to thermal expansion are characterized by an increase in length or curvature depending on whether a uniform temperature or thermal gradient is applied to the section. Thermal bowing can occur as a consequence of the curvature from thermal gradients, which can result in deflections. Moreover, translational restraints at the ends of a structural element can induce large displacements due to thermal expansion and large compressive stresses can be generated in the element. Tension can occur in structural members with translational restraints but no rotational restraint, especially when thermal bowing is dominant (Usmani et al., 2001). Thermal strains can be calculated using Equation 2.2.

$$\varepsilon_T = a\Delta T \tag{2.2}$$

Where ε_T is the thermal strain, a is the coefficient of thermal expansion and ΔT is the change in temperature. It follows from the previous discussion that the type of thermal load applied and the end restraint will determine how a structural member will behave under an increase in temperature and that this can result in different stress states in the member. This information is necessary for understanding how buildings will respond when subjected to fires with a view to implement appropriate measures to avoid excessive displacements of structural members.

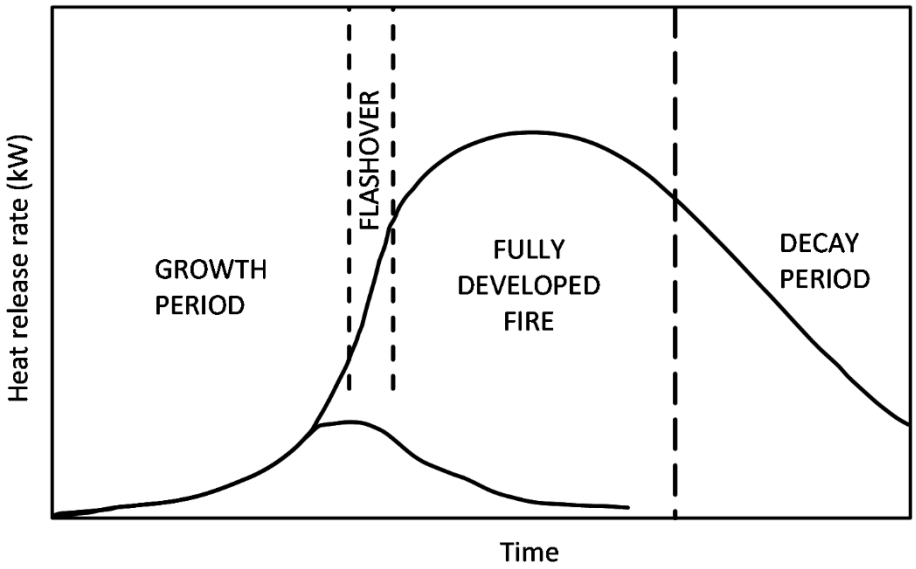

Figure 2.1. Course of a fire in a building compartment (from Drysdale, 2011).

Three main stages can be identified in a building compartment during a fire attack. The first stage is the growth period in which the temperature of the compartment rises from the ambient temperature and grows into the fully developed stage. The transition from the growth stage to the fully developed stage is referred to as 'flashover' and during this period all combustible objects in the compartment are burning. Structural damage is expected to occur during the fully developed stage which can eventually lead to collapse. The final stage of a fire is the decay period in which there is a decrease in temperature and the heat release rate of the fire. The evolution of a compartment fire is illustrated in Figure 2.1 (Drysdale, 2011) which depicts how the heat release rate of a fire grows and decays over time in a compartment. The flashover point is also highlighted in the figure.

Some fires might not reach flashover or the fully developed stage because they are put out quickly following a notification from fire detection systems or suppressed through active fire protection systems like sprinklers. In all cases, structural fire design is very important to ensure that structural members do not deflect excessively during a fire so that collapse can be avoided. This design is usually carried out by using the passive resistance of the structural members and by adding fire protection where necessary. This will require an understanding of the properties of structural materials when subjected to high temperatures as in the case of a fire.

2.2.2 Properties of steel and concrete under elevated temperatures

Experiments on structural materials such as steel and concrete have shown that their material properties degrade under high temperatures. The Eurocodes (BS1, 2005) provide guidance on how the mechanical and thermal properties of different structural materials degrade with increasing temperatures and reduction factors are proposed for their strength at elevated temperatures. Also, equations are provided for the specific heat and the thermal conductivity for different temperature ranges. The stress-strain relationships for steel and concrete up to the ultimate strain are also provided.

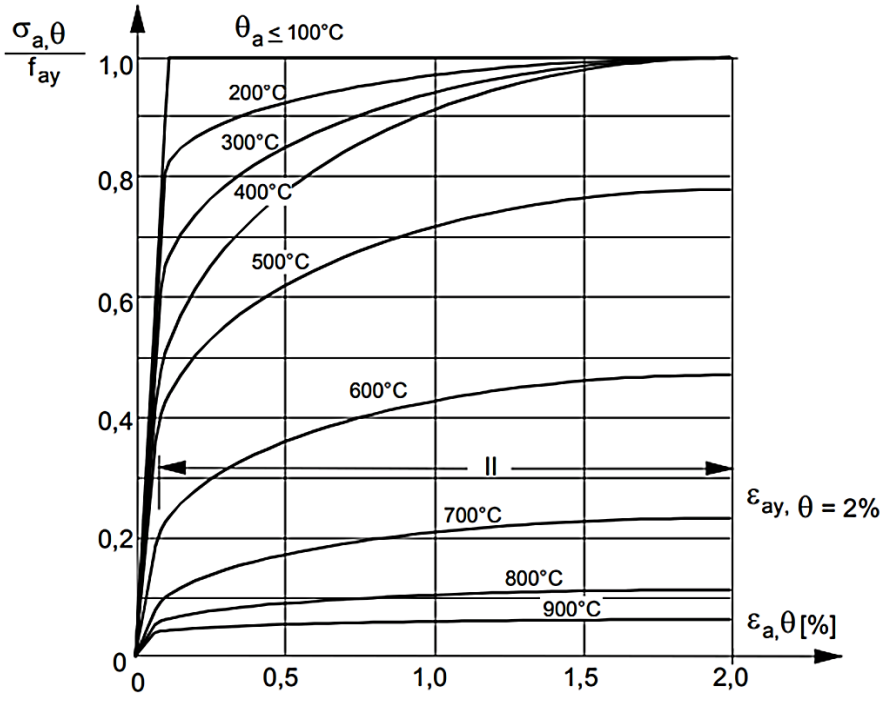

Figure 2.2. Stress-strain relationship of steel at different temperatures (from BSI, 2005).

The stress-strain curves of steel for increasing temperatures are shown in Figure 2.2. In the figure, θ_a is the steel temperature, σ_a,θ is the stress of steel at temperature θ_a, ε_a,θ is the strain

of steel at temperature θ_a, f_{ay} is the yield strength of the steel (at ambient temperature) and $\varepsilon_{ay,\theta}$ is the yield strain of steel which is equal to 2 %. Also, Figure 2.3 illustrates the stress-strain curve of concrete at different temperatures. In the figure, $\sigma_{c,\theta}$ is the stress of concrete at a particular temperature, f_c is the compressive strength of concrete, $\varepsilon_{c,\theta}$ is the strain at temperature θ and $E_{co,\theta}$ is the young modulus of concrete at temperature θ. Figure 2.2 and Figure 2.3 show that the yield strength of steel and the compressive strength of concrete decreases as temperature increases. Therefore, when these structural materials are exposed to excessive temperatures, they might lose their load bearing capacity which can lead to failure.

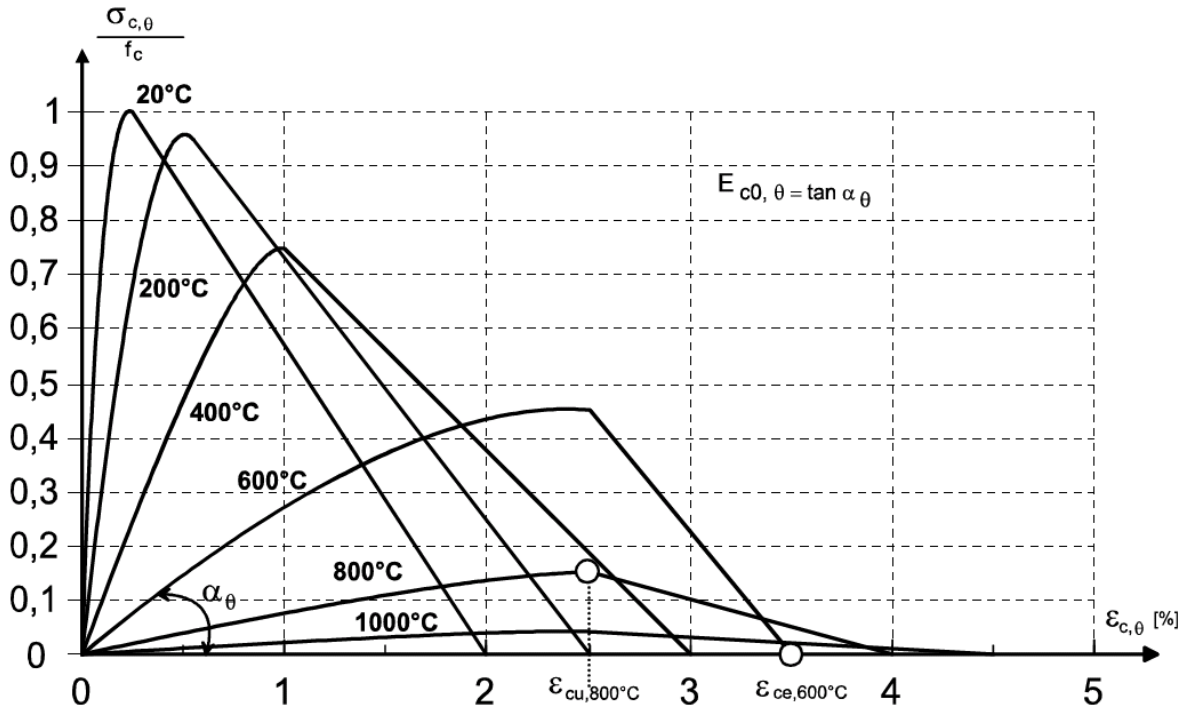

Figure 2.3. Stress-strain relationship of concrete at different temperatures (from BSI, 2005).

2.2.3 Experimental and numerical studies on fire

Numerous experiments have been carried out on structural elements to understand their structural and thermal response when subjected to fire. The most widely known experiments on fire were the series of tests carried out on an 8-storey composite steel building at Cardington in the United Kingdom and temperatures between 800 °C and 1100 °C were recorded during the fire as described by Martin et al. (1999). The results of the experiments revealed the effect of the surrounding structural elements in increasing the resistance of framed structures under high temperatures. As a result, members in a structural frame will have a higher structural fire resistance due to redistribution of floor loads from the affected element to surrounding

elements. This resistance is higher than the calculated structural fire resistance of individual structural elements.

Numerical studies have also been performed using various finite element analysis programs such as ABAQUS (Dassault Systèmes, 2008), VULCAN (Huang et al., 2003), SAFIR (Franssen, 2005), OpenSees (McKenna, 1997) etc. to simulate the response of structures under the effects of fire. Wang (2000) carried out numerical analyses to simulate the response of the frame for two of the tests carried out at the Cardington facility. The results of the study indicated the need for more advanced numerical models to predict the tensile membrane action of the concrete slab and also the possibility of large sagging moments occurring during the cooling phase of the fire.

The performance of a three dimensional frame subjected to a natural compartment fire was accessed by Liew & Ma (2004). It was concluded that it was unnecessary to provide fire protection on some structural members based on the results of the analyses which can lead to savings in the overall cost of the building project. Full scale fire tests and numerical simulations were performed by Mesquita et al. (2005). It was established that the critical temperature of the beams from the studies was higher compared to that of the simplified design method in Eurocode. Foster et al. (2007) used numerical simulations to study the effects of vertical support conditions and fire protection on the 8-storey structure tested at Cardington. The results of the study were very similar to the results of the experiment and it was deduced that a better representation of the support conditions was needed in order to obtain a higher level of accuracy in the structural response. The nonlinear behaviour of steel elements subjected to fire was studied by Lien et al. (2009) using the Vector Form Intrinsic Finite Element (VFIFE) method. The study was carried out considering both the heating and cooling phase of the fire, and it was concluded that temperature distributions, boundary conditions and properties of the steel at high temperatures will have a significant effect on the fire response.

Torero (2011) discussed the process leading to failure of structures under fire using the World Trade Centre fire as illustration. Structural performance, fire growth, egress analysis and performance of protection systems were highlighted as important features that can be used to understand the failure of a structure under fire. The author explained the importance of reducing the uncertainty associated with the modelling of fire with a parametric analysis of the structure considering several representative fire scenarios.

The robustness of a steel-composite car park subjected to a localised fire was assessed by Fang et al. (2011) using numerical models. The study concluded that the floors above the fire-affected floors can provide an alternative load path if the vertical loads can be resisted by the upper floors under a double span configuration. The collapse mechanisms for tall buildings subjected to fires was assessed by Lange et al. (2012). It was concluded that a weak floor mechanism can occur when failure occurs in the floor closest to the floor subjected to fire and then propagates to other floors due to large moments in the fire-affected floor, while a strong floor mechanism is induced by large moments in the column around the affected area. The response of steel beams subjected to localized fires was investigated by Zhang et al. (2013). They concluded that the standard fire cannot be used to predict the response accurately when the beam is subjected to localized fires because temperature distributions may vary along the length of the beam and also in the beam section due to thermal gradients induced by the localized fire. Rackauskaite & El-Rimawi (2014) studied the behaviour of multi-storey steel framed structures subjected to compartment fires and concluded that the redistribution of loads to surrounding members improves the performance of steel frames in fires. Also, fire compartmentation is necessary in unprotected steel structures and fire spread should be limited across bottom floors and between storeys for improved performance.

Gernay & Franssen (2015) proposed the duration of heating phase and fire resistance time as performance indicators for structural members subjected to fire. The performance indicators proposed can provide significant information on post-flashover fires in relation to the extent of a standard fire. From the study, the authors deduced that the structure has theoretically collapsed if fire resistance time is shorter than post-flashover time of heating and the structure is theoretically safe if duration of heating phase is longer than heating time after flashover. This information can be useful during fire-fighting operations. It was also concluded that there is a possibility of failure occurring during the cooling phase of a fire.

Fischer & Varma (2017) studied the fire response of composite beams with simple connections subjected to fire. The effect of different design fire scenarios, fire resistance rating, continuity of composite slab across bays, composite deck type, connections and slab reinforcement type was investigated. No premature failure of the connections was observed for the 2 hour fire rating and it was also deduced that the continuity of the steel reinforcement and composite slabs across bays greatly influence the performance of the connections. Torero et al. (2017) examined the role of thermal performance and the thermal boundary conditions of structures, and

highlighted their importance in the design process when designing protective structures to withstand high temperatures from fires. It was concluded that the thermal performance of a structure can only be predicted adequately when the correct thermal boundary conditions are established. The authors also discussed the influence of the 'biot number' and deduced that as the biot number increases, the effect of the fire on the deformation of the structure decreases. Biot number is a dimensionless parameter determined by the product of the convective heat transfer coefficient and the thermal conductivity of the solid divided by the characteristic length.

Xu et al. (2018) presented a global optimization approach which can be used to determine the critical fire scenarios that can result in the instability of an unbraced steel frame. Analyses were carried out on single-storey unbraced steel frames and it was observed that instability of the frame caused by the highest temperature scenarios were as a result of fire starting in non-critical compartments with 'weak' columns, while the lowest temperature scenarios that caused instability were due to localized fires starting in critical compartments with 'strong' columns. Qin & Mahmoud (2019) studied the collapse performance of composite steel beams subjected to the standard fire and parametric temperature-time curves, and it was concluded that failure of the shear connections can occur when confined compartment fires result in large lateral deformations in the composite slab and beam. It was also suggested that a performance-based approach should be adopted to ensure that fire protection is used where appropriate to avoid material waste while ensuring structural fire safety.

2.2.4 Structural fire design methods and their limitations

Structural fire design is usually carried out by determining the fire resistance of a member based on the time to failure, temperature to cause failure or load capacity at elevated temperatures. These checks are performed using temperature-time curves that may represent the fire temperatures in a building compartment. The most widely used temperature-time curve for structural fire design is the standard fire. The standard temperature time curve is provided in BSI (2002) and it only specifies the fire temperature at a particular time in the heating phase and has no provisions for temperatures during the cooling phase. Also, it does not fully represent the realistic nature of fires in building compartments as it was determined based on experiments carried out in a furnace. Figure 2.4 illustrates the standard temperature-time curve and it shows the rise in temperature for a given fire duration.

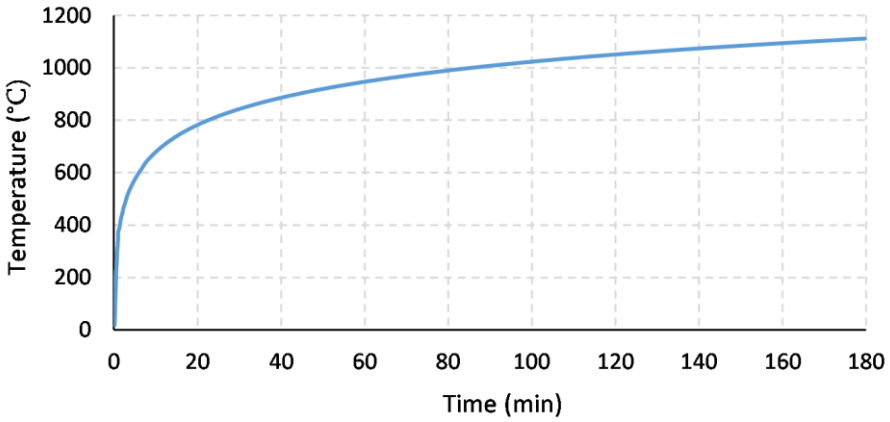

Figure 2.4. The standard temperature-time curve.

A more realistic representation of compartment fires is the parametric temperature-time curve which considers both heating and cooling of the compartment. Also, parameters such as openings in the walls and thermal properties of different layers of structural materials in the compartment are considered. This information is used as input into the parametric fire equations in Eurocode 1 which is then used to develop a more realistic temperature-time history of the fire in a building compartment. Maximum temperature in the compartment is determined based on whether the fire is fuel controlled (i.e. is based on the composition of the fuel in combustible materials in the compartment) or ventilation controlled (i.e. is based on the amount of ventilation in the compartment from the wall openings). The parametric temperature time curve for a given compartment is illustrated in Figure 2.5 and it depicts the temperature regime in a compartment as it rises to maximum temperature and decays back to ambient temperature.

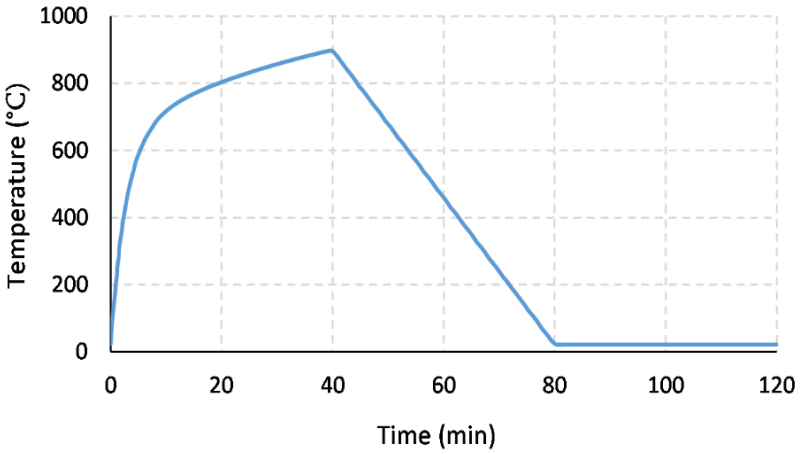

Figure 2.5. The parametric temperature-time curve.

Although the parametric temperature time curve seems to be a more practical representation of compartment fires, there are some limitations that hinder its use in design. From BSI (2002), the parametric temperature time curve is only suitable for compartments with storey heights up to 4 m, compartments without ceiling openings, thermal inertia (i.e. rate at which thermal energy is absorbed or released into the compartment) of linings of compartments between 1000 and 2200 $Jm^{-2}s^{-½}K^{-1}$ and floor areas up to 500 m^2. Modern building structures with large compartments do not fall within this range, which means that the parametric temperature time curve is only suitable for small compartments and cannot be used to represent fire scenarios in larger compartments (Law et al., 2011; Stern-Gottfried & Rein, 2012a).

Another important aspect to note is that in design, a uniform distribution of fire temperatures is usually assumed in the building compartment so that the fire is burning at the same time throughout the compartment, which is unrealistic for open plan offices with larger compartments subjected to post-flashover fires (Buchanan, 2002). Moreover, Majdalani & Torero (2011) stated that fuel controlled fires are expected in large compartments and might be more severe in comparison with ventilation controlled fires which are assumed as worst case in design. The next section also explains why current design methods might be impractical based on previous fire accidents.

2.2.5 Fire tests and accidental fires in large compartments

The results of the experiments carried out by Kirby et al. (1994) indicate that fire moved rapidly from the fire source to other parts of the compartment. Also, fire tests carried out by Lennon & Moore (2003) and Rein et al. (2007) revealed a temperature variation in the compartment with maximum temperatures ranging from 23 % to 75 % above the average temperature and minimum temperatures between 29 % and 88 % below the average compartment temperatures.

A review of the collapse of the World Trade Centre Towers due to the impact and subsequent fire by Pitts et al. (2005) revealed that fire can travel across large floor compartments and also between floors (Law et al., 2011). Pitts et al. (2005) also stated that a shift in the burning areas of the fire affected floors was noticed horizontally across the compartment floors and vertically between the floors, based on observations of the fire of World Trade Centre Towers 1 and 2. All the above explanations point to the fact that current methods of design cannot be relied upon to adequately replicate the fire scenarios in large building compartments and therefore, an improved design method that considers the travelling nature of fires needs to be considered.

2.2.6 Travelling fires

The importance of considering travelling fires in buildings, especially those with large compartments, has been discussed in previous sections based on experimental studies, reviews of accidental fires and the limitations of current design methods have been highlighted. This realization has spurred research in order to understand how structures behave under the effect of travelling fires. Clifton (1996) was the first to study the travelling nature of fires and proposed fire models that represent the temperature-time history of a fire travelling through a compartment of a building which was referred to as a fire cell. Different stages in the temperature history were defined. The first was the fire stage followed by the pre-heat, smoke-logged and burnout out stages. Clifton (1996) specified a range of temperatures between 400 °C and 800 °C for the pre-heat and delayed cooling period. Nevertheless, Clifton (1996) explained that there was inadequate data to verify the fire cell method and it might only be useful for research purposes or to determine the fire resistance of structural members. The temperature time history for the fire cell method is illustrated in Figure 2.6 and it describes how the temperature in the compartment increases from the pre-heat period to a maximum temperature and decreases to a constant temperature during the delayed cooling period before decreasing back to ambient temperature.

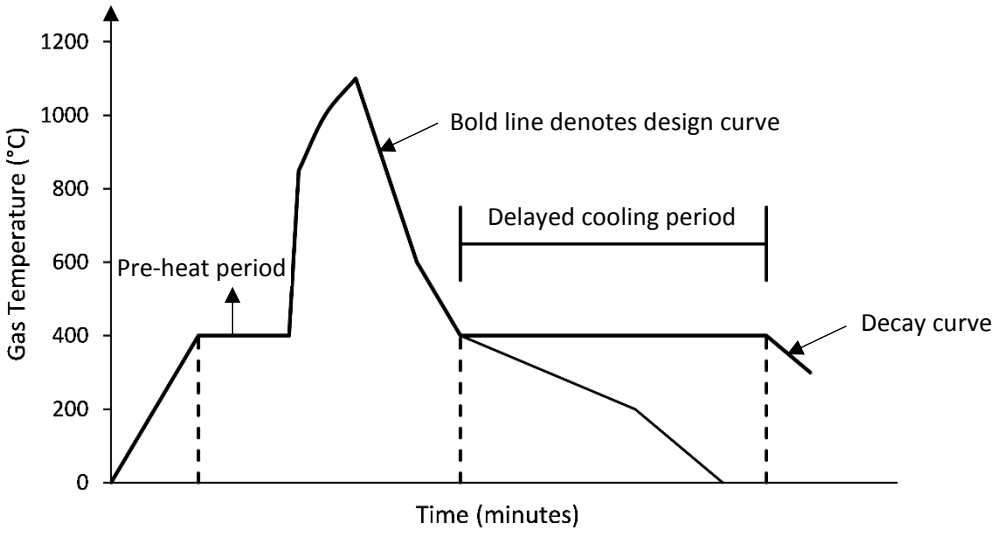

Figure 2.6. Temperature–time history of a compartment using the Fire Cell Method (adapted from Clifton, 1996).

The Travelling Fire Methodology (TFM) which is a more recent approach to the travelling nature of fires was developed by Law et al. (2011) and Stern-Gottfried & Rein (2012a). The TFM considers a range of fire sizes travelling across a floor compartment and it divides the

compartment into two temperature regions which are the near field and far field regions (Law et al., 2011). The near field region is the part of the compartment which is burning at a particular time while the far field region is the part of the compartment that is exposed to smoke from hot combustion gases (Stern-Gottfried & Rein, 2012a). The design is carried out considering large fire sizes which burn for a shorter duration and smaller fire sizes with longer fire durations (Law et al., 2011). Figure 2.7 illustrates the concept of travelling fires as it shows how the compartment is divided into different temperature regions for different fire sizes travelling across the compartment. Computational Fluid Dynamics (CFD) was used in the initial TFM studies to determine the temperature distribution of travelling fires in different parts of a building compartment. However, a simplified method using the Alpert jet correlation method (see Equation 2.3), which considers the heat release rate, distance to source of fire and floor to ceiling height, was later adopted to determine the temperature distribution in the compartment. The temperature distribution using the simplified method was found to yield similar results to that of the CFD tests (Stern-Gottfried & Rein, 2012a; 2012b).

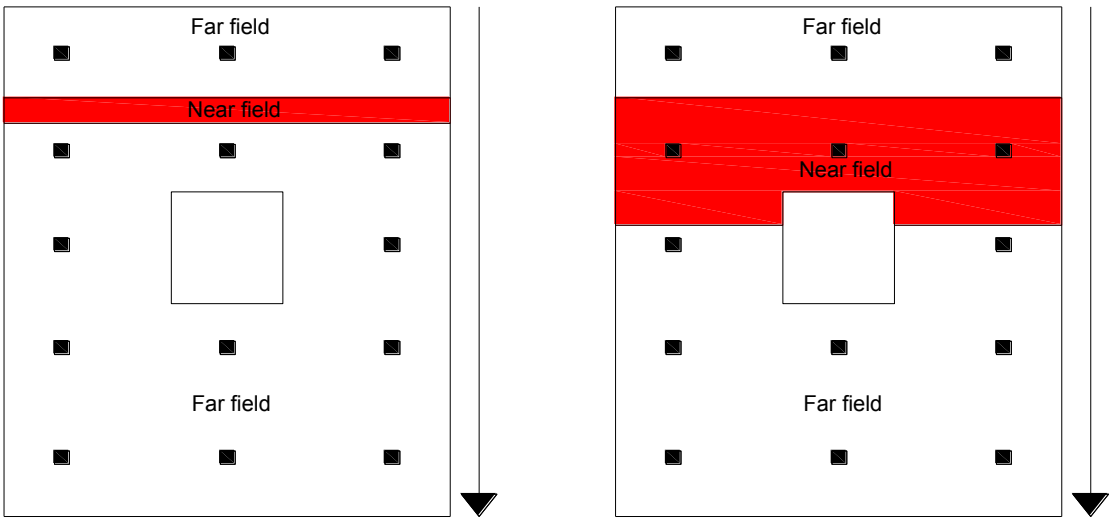

(a) (b)

Figure 2.7. Movement of fire across a compartment floor for (a) 5 % fire size and (b) 25 % fire size (from Law et al., 2011).

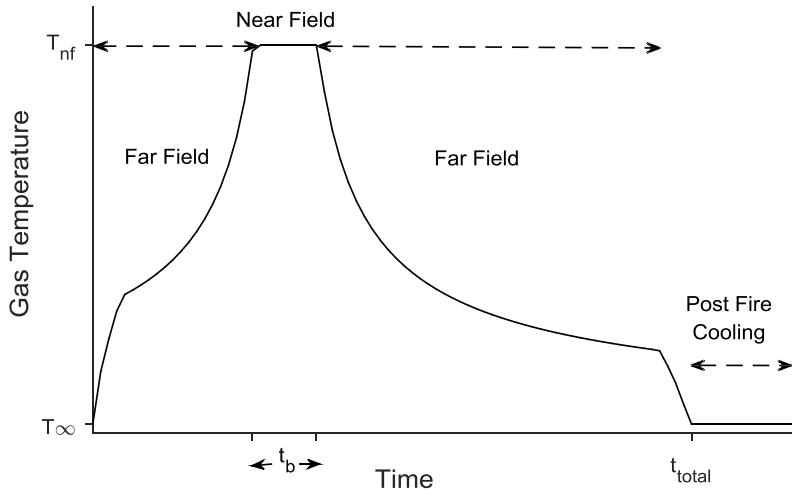

Figure 2.8. Temperature-time history of a travelling fire (from Stern-Gottfried & Rein, 2012b).

The TFM is implemented by specifying the heat release rate per unit area $\dot{Q}''$ (MW/m^2), fuel load density q_f (MJ/m^2) and the near field temperature T_{nf} (°C). The burning duration t_b is calculated as fuel load density divided by heat release rate per unit area. The TFM assumes a uniform value of q_f and $\dot{Q}''$ (Stern-Gottfried & Rein, 2012a). Maximum compartment fire temperatures are typically between 800 °C and 1200 °C. However, the TFM assumes a near field temperature of 1200 °C (Law et al., 2011) as the worst case although other temperature values can be used. The temperature-time history at a random location in the compartment using the TFM is illustrated in Figure 2.8 which shows an increase from ambient temperature T_∞ in the far field region to the maximum temperature T_{nf} in the near field region of the fire (with a constant burning duration of t_b) and then a decay back to ambient temperature. The TFM initially considered a constant far field temperature distribution and the far field temperatures were calculated using the ceiling jet correlation formula in Alpert (1972) which is presented in Equation 2.3.

$$T_{max} - T_\infty = \frac{5.38\left(\frac{\dot{Q}}{r}\right)^{2/3}}{H} \tag{2.3}$$

where $\dot{Q}$ is the heat release rate (kW), which is calculated as the area of floor compartment multiplied by the heat release rate per unit area, r is the distance between the location considered and the centre of fire (m), H is the distance between the ceiling and the floor in metres, T_∞ is the ambient temperature in the compartment (°C) and T_{max} is the near field temperature (°C), which is the maximum temperature in the compartment (Stern-Gottfried & Rein, 2012a). The TFM temperature distribution was modified by Rackauskaite et al. (2015)

such that temperature values can be evaluated at different locations in the compartment without dividing the compartment into discrete nodes as specified in Stern-Gottfried & Rein (2012b). Equations 2.4 to 2.7 were proposed by Rackauskaite et al. (2015) to determine the temperature-time histories at different locations in the compartment:

$$s = L_f \,/t_b \tag{2.4}$$

$$x^* = s\,.t \tag{2.5}$$

$$L^* = L_f/L \tag{2.6}$$

$$T_{max}(x,t) \; - \; T_\infty = \frac{5.38}{H}\left(\frac{LL^*{}_t w\dot{Q}''}{x + 0.5LL^*{}_t - x^*{}_t}\right)^{\frac{2}{3}} \tag{2.7}$$

$$T_{max}(x,t) = T_{nf} \; if \;\; \begin{cases} T_{ff} > T_{nf} \\ x + 0.5LL^*{}_t - x^*{}_t \leq 0.5L_f \end{cases} \tag{2.8}$$

where T_{nf} is the near field temperature, T_{ff} is the far field temperature, $\dot{Q}''$ is the heat release rate per unit area, s is the fire spread rate, H is the height of compartment, w is the compartment width, L is the length of the compartment, L^* is a dimensionless parameter which represents the fire size, x^* is the distance between the point of interest and the edge of the compartment and L_f is the length of fire (Rackauskaite et al., 2015). When considering a performance-based design, stochastic components in the equations above will include the maximum compartment temperature or near field temperature, heat release rate per unit area, fire spread rate, fire size and length of fire. This can then be used to produce the likely temperature-time histories in the compartment.

Numerical studies on travelling fires

Several numerical studies have been carried out to determine the effect of horizontally and vertically travelling fires in building structures. The effect of a vertically travelling fire on a multi-storey steel building was investigated by Röben et al. (2010) and it was observed that thermal expansion can induce cyclic loading in the columns when fire travels vertically between floors. Law et al. (2011) carried out parametric analyses on a concrete frame subjected to a horizontally travelling fire to determine the effects of fire path and shape as well as varying far field temperatures. The study highlighted the impact of horizontally travelling fires with medium fire sizes over parametric fires in concrete frames. Stern-Gottfried & Rein (2012b) investigated the influence of structural and fire parameters on the bay temperatures in a concrete frame subjected to a horizontally travelling fire. The results of the study showed that the fuel

load density, fire size, near field temperature and rebar depth had a significant influence on the bay temperatures in the frame.

The effects of multi-floor, vertically and horizontally travelling fires in tall steel-composite buildings were studied by Kotsovinos (2013) and it was concluded that horizontally travelling fires can result in higher deformations. Also, multi-floor fires burning simultaneously and rapid vertically travelling fires were observed to have a very similar response while slow vertically travelling fires resulted in large cyclic deformations. Kotsovinos et al. (2013) also studied the effect of vertically travelling fires on the collapse of tall buildings considering both the weak floor and strong floor systems, and highlighted that multiple floor fires burning simultaneously can be more conservative for the global structural behaviour compared to vertically travelling fires. The study also showed that strong floor collapse is unlikely for slow vertically travelling fires. The thermal response of a steel building with composite beams under horizontally travelling fires was investigated by Jiang et al. (2013). The study showed that higher peak temperatures can occur in the concrete slab under the effect of travelling fires with smaller fire sizes while large fire sizes might significantly affect the failure time of steel beams.

The TFM was modified by Rackauskaite et al. (2015) to consider the effect of the flapping angle of the flame which can essentially reduce the near field temperature. Also, a method to determine the realistic range of fire sizes was proposed based on fire spread rates from experiments and accidental fires. Parametric analyses were carried out in their study and they demonstrated the influence of the fire spread rate and fire size on the location of the maximum temperature in the compartment. Nevertheless, Rackauskaite et al. (2015) explained the need for more experimental studies to verify their results. Numerical analyses were carried out by Rezvani & Ronagh (2015) on a steel moment resisting frame designed to resist seismic loads in order to determine its response under the effect of traveling fires considering a maximum temperature of 1000 °C. The study showed the significant influence the fire size has on the failure time of the steel frame. Rackauskaite et al. (2017) also studied the response of a steel frame under horizontally and vertically travelling fires and concluded that the type of fire and the number of floors subjected to fire can influence the collapse mechanism of steel frames.

In offshore structures, Thyer et al. (2008) conducted experiments in the Health and Safety Laboratory in Buxton to study the effects of an unrestrained hydrocarbon pool fire in a simulated offshore deck. It was observed that the deck deformed such that the seams and welds failed and there was a split in the deck through which burning fuel was able to flow through.

The Health and Safety Executive in HSE (2008) explained that the implications of the splitting of the deck can be severe as it could cause a vertical fire spread. Also, buckling of the deck can cause continuous movement of the pool fire across the deck plate as the deck buckles. Ufuah (2012) stated that the results of the experiments conducted at the HSL showed that the structural integrity of steel-plated decks may not achieve the required fire resistance period. The author then investigated the effect of travelling pool fires on a steel-plated deck using ABAQUS and deduced that the alternating tension and compression in the steel deck due to the travelling fires can significantly affect the failure mode of the deck and the integrity of the welded connections.

It can be appreciated from the above discussion that a number of studies have compared the response of building structures under the effect of standard fires and parametric fires with that of travelling fires. These studies have shown the impact of travelling fires on structures and have stressed the need to consider them in structural fire design. Another extreme loading scenario which can cause significant damage in multi-storey structures is blast and this will be discussed in the next section.

2.3 Blast

Blast pressures can cause significant damage to building structures. They are applied on structures due to explosions from bombs, chemicals or gas. Explosions result in a rapid release of energy and can be very destructive to anything near them (Ngo et al., 2007). The reflection of a blast wave on a surface based on the stand-off distance is illustrated in Figure 2.9.

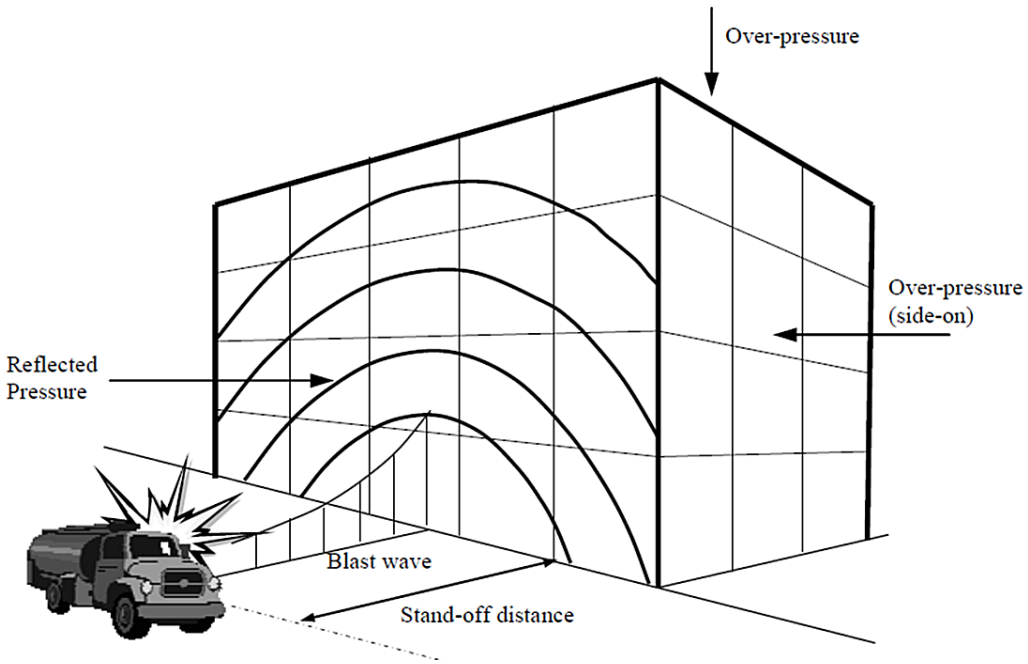

Figure 2.9. Reflection of blast pressures on a building from Ngo et al. (2007).

The ability of the structure to absorb the energy from the blast and the dynamics characteristics will govern the response of the structure when it is subjected to blast pressures (Elliot, 2009). Usually, blast resistant design is carried out based on the standoff distance R and the charge weight W. The standoff distance refers to the distance between the source of the blast and the target structure while the charge weight is the mass of the explosive designed for, which is usually expressed in terms of TNT (Trinitrotoluene) (Ngo et al., 2007). The reflected pressure, blast duration and impulse from the blast can be determined from charts or equations considering a scaled distance $Z = R/W^{1/3}$ where R is the distance to source of blast and W is the weight of the explosive in kg (Smith & Cormie, 2009). The scaled distance is based on the Hopkinson-Cranz law.

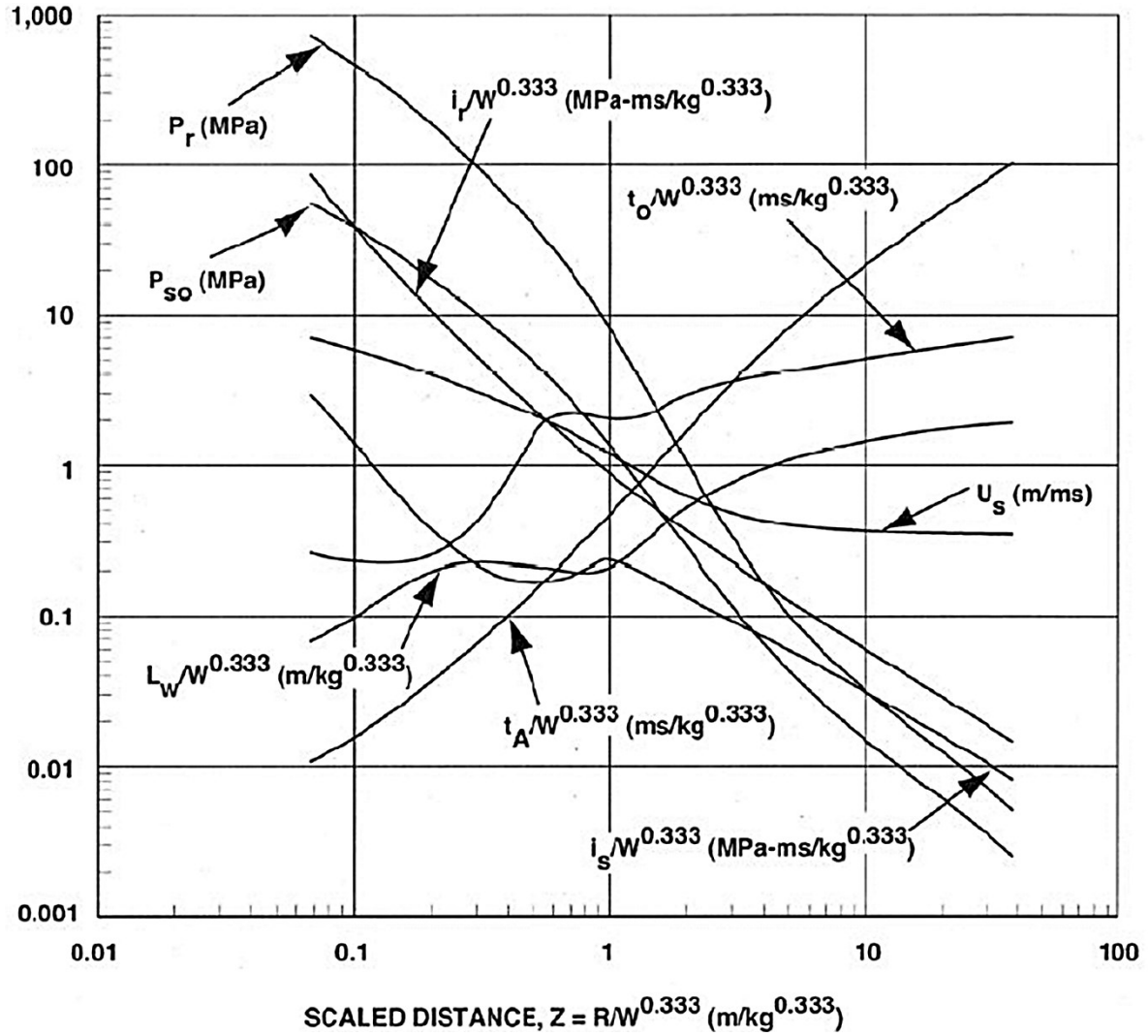

Figure 2.10. Positive blast wave parameters (from UFC, 2008).

The chart in Figure 2.10 from UFC (2008) is usually used to determine the blast wave parameters. A typical pressure-time history of a blast wave is shown in Figure 2.11 where P_o is the pressure in ambient conditions, P_{so} is the peak pressure of the blast, P_{so}^- is the underpressure after the decay of the blast pressure below ambient conditions, t_d is the blast duration and t_A is the blast arrival time.

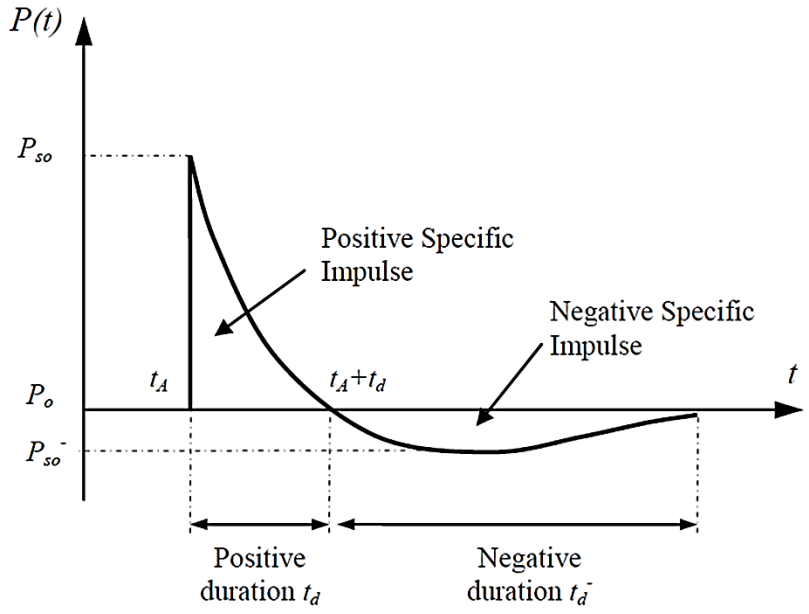

Figure 2.11. Pressure-time history of a typical blast wave (from Ngo et al., 2007).

Several experimental and numerical studies have been carried out on structures subjected to blast. Schleyer & Hsu (2000) presented a simplified method for determining structural deformations under pulse pressure loading from explosions, which was found to show good agreement with finite element methods. It was however stated that the method was limited to structures where elastic deformations are significant and loading is in quasi-static to dynamic regime. Louca & Boh (2004) analysed stainless steel profiled blast walls subjected to blast loading from hydrocarbon explosions and deduced that the use of an elastic-perfectly plastic material for the steel can give unconservative deflection predictions after yielding has occurred. Also, the correct modelling of boundary restraint conditions and connections should be adopted for a more accurate response.

Liew (2008) studied different modelling approaches for steel columns with different end supports subjected to a blast pressure. This study explained that the difference between the natural period of the structure and the duration of the blast was an important factor in the blast response of the structure. Nassr et al. (2012) investigated the experimental performance of steel

buildings to blast considering different charge weights and standoff distances. Their study compared the blast pressures from the experiments with that of UFC (2008) and numerical simulations of the experiments were performed considering single degree of freedom analysis and different dynamic increase factors. The importance of properly accounting for strain rate effect in order to achieve a higher accuracy of structural response was highlighted. Fallah et al. (2013) studied the shape effects of pulse loading on the dynamic response of continuous beams. The study also presented a method of determining the maximum displacement of elastic-plastic and elastic continuous beams, based on the study carried out on the Pressure-Impulse diagrams for continuous systems. The results showed three distinct P-I regimes and provides an improved solution which reduces continuous systems to single degree of freedom systems.

Elsanadedy et al. (2014) studied the response of a steel building subjected to a blast attack and the results of the study showed that progressive collapse might occur when an explosive with a high charge weight is detonated close to exterior columns. The importance of having an appropriate standoff distance to restrict vehicle access to buildings was highlighted. Khan et al. (2017) developed fragility curves to investigate the effects of standoff distance, structural configurations and member orientations on steel frames subjected to blast pressures. It was concluded that the orientation of the columns is important for effective blast mitigation. Also, the ability of the structural configuration to dissipate blast pressures increases as standoff distance increases. Thil et al. (2019) presented a theoretical model to determine the dynamic plastic response of beams under localized blast pulse loads. A strain rate sensitivity study was also conducted. The study showed the presence of travelling plastic hinges as a result of the critical pressure. Nevertheless, the results of the study showed good correlations with numerical results.

These studies explain the damage that can be caused by blast loads on structures and the different ways of designing structures to resist them effectively. There are instances where multi-hazard scenarios such as blast followed by a fire can occur and this should be accounted for in design. The next section discusses several numerical studies on blast and fire.

2.4 Blast and fire

There is a high likelihood of a fire occurring after a blast has occurred and this needs to be considered in the design of strategic facilities and important buildings that can be subjected to

this multi-hazard scenario during their design life. Some numerical studies have been carried out to understand how structural members behave under these loading conditions. The first numerical attempt at structures subjected to blast and fire was carried out by Izzuddin et al. (2000) in which an explicit dynamic method was adopted for the blast analysis and an implicit method was used for the fire analysis. A mixed-element method was proposed by Chen & Liew (2005) for structures subjected to blast and fire. In their study, beam elements were adopted for structural members unaffected by the actions while shell elements were employed for the structural members exposed to the blast and fire.

Liew (2008) studied the response of a steel frame subjected to blast and fire, and deduced that the fire resistance of a steel structure can be reduced if there is an initial exposure to blast actions. It was stated that local buckling and initial deformation of the structural members under blast loads was responsible for the decreased fire resistance and this can cause instability of the frame under subsequent fire action. The effect of mechanical and geometrical damage of steel tubular columns under blast and fire was investigated by Ding et al. (2013) and a method to predict the level of damage was proposed. The study showed that peak pressure, fire exposure time and impulse had a significant effect on the level of damage of the columns when they were subjected to blast and fire actions.

Málaga-Chuquitaype et al. (2014) studied the influence of secondary frames on the collapse response of steel frames under the effect of earthquake, blast and fire actions. The study showed that the secondary connection strength has a significant effect on the progressive collapse capacity of the steel frames. Also, the secondary frame can increase the sidesway collapse resistance of the frames under these actions. However, the study did not consider the response under subsequent fire loads for an initial blast event. Tan et al. (2017) examined the effect of the shape of the blast load (pulse load) on the blast and fire resistance of a steel beam. The study showed that the effect of the pulse shape on the performance of the beam in fire decreases as dynamic load ratio increases.

All these studies show that under multiple hazard scenarios especially in building structures, blast and fire can cause immense damage to the structure and possibly collapse. These studies however did not consider the travelling nature of fires in large compartments. The uncertainty associated with these loading scenarios makes it necessary to consider a performance-based approach for design and assessment of structures that might be subjected to these type of

actions. The next section discusses the performance-based design process and its importance in design.

2.5 Performance-based design

The use of prescriptive design codes might be limited in the design or assessment of structures subjected to extreme loads such as blast and fire due to the uncertainty associated with these actions. The performance-based design framework allows for more flexibility in design as it enables different performance objectives to be defined and facilitates the comparison of alternative design solutions for meeting the desired objectives. It can also provide a risk based assessment to determine the most effective design solution based on acceptable risks.

The PEER performance-based design framework originally proposed by Cornell & Krawinkler (2000) was developed for the design of structures to resist seismic actions. However, it has been adapted to consider other extreme loading conditions such as hurricane (Barbato et al., 2013), fire (Lange et al., 2014) and blast (Whittaker et al., 2003). Equation 2.9 illustrates this framework in probabilistic form.

$$\lambda(DV) = \iiint P(DV|DM)\, dP(DM|EDP)\, dP(EDP|IM)\, |d\lambda(IM)| \tag{2.9}$$

where EDP is the engineering demand parameter, IM is the intensity measure, DV is the decision variable, DM is the damage measure, $\lambda(DV)$ is the annual rate of exceeding DV and $P(DV|DM)$ is the conditional probability of exceeding DV for a given value of DM (Cornell & Krawinkler, 2000). Equation 2.9 is a triple integral based on the Total Probability Theorem, which can be evaluated numerically in four stages. The first part of the equation is the hazard analysis which is initiated by choosing an appropriate intensity measure that describes the severity of the action. Examples of intensity measures include spectral acceleration, maximum compartment temperature, etc. The hazard analysis produces the mean annual rate of exceeding the intensity measure $\lambda(IM)$.

The second stage of the PEER performance-based framework is the structural analysis in which non-linear analysis is carried out on a numerical model and the response of the structure to the action is computed. The structural response is recorded with reference to specified engineering demand parameters such as inter-storey drifts, deflections, axial forces etc. In the structural

analysis stage, the annual rate of exceeding the EDP, $\lambda(EDP)$ is determined which is the integral of $P(EDP|IM)$ with respect to $\lambda(IM)$.

The third stage is the damage analysis where fragility functions of $P(DM|EDP)$ are produced. Different levels of damage expressed as damage measures (DM) are considered based on a range of values of the EDP as a means of quantifying the extent of damage to structural members, finishes etc. (Hamilton, 2011).

The final stage is the loss analysis where decisions are taken based on mean annual losses that will be incurred for different damage levels. Consequence curves which are plots of $P(DV|DM)$ against selected decision variables (DV) are usually produced for the different damage measures in this stage. Examples of decision variables include dollar loss, repair costs, downtime etc.

Some studies have considered extending the performance-based approach to the extreme loads considered in this thesis i.e. fire and blast. Whittaker et al. (2003) proposed performance levels, engineering demand parameters and intensity measures for blast resistant design based on the PEER performance-based framework and stated that an understanding of the risk of loss was necessary in performance-based engineering to improve structural design and construction practices. The significance of a performance-based structural fire design was demonstrated in Rini & Lamont (2008) as it was found to produce a fire safe solution as well as an optimised structural fire design for the steel structure studied. Asprone et al. (2010) proposed a probabilistic model which can be used to determine the annual risk of collapse of a structure subjected to multi-hazard conditions involving blast and seismic loads. The blast fragility was determined based on the probability of progressive collapse occurring using Monte Carlo simulation technique. A reinforced concrete framed structure was used as the case study and the results of the analyses showed that given a blast event occurs, the probability of progressive collapse is about 18% and it was stated that the blast fragility can be multiplied by the annual rate of blast to determine the annual risk of collapse.

Hamilton (2011) used the PEER framework to illustrate the variability in post-flashover fires. The study demonstrated the ability of performance-based design to consider a wide range of loading scenarios for structural fire design. Lange et al. (2014) used the PEER framework to design a steel frame to resist fires modelled with the parametric temperature-time curve. Significant information relating to annual costs, downtime and repair costs were determined from the study which can help designers to make informed decisions on the appropriate fire

protection strategy for the structure. Figure 2.12 shows examples of probability plots for the PEER performance-based structural fire design.

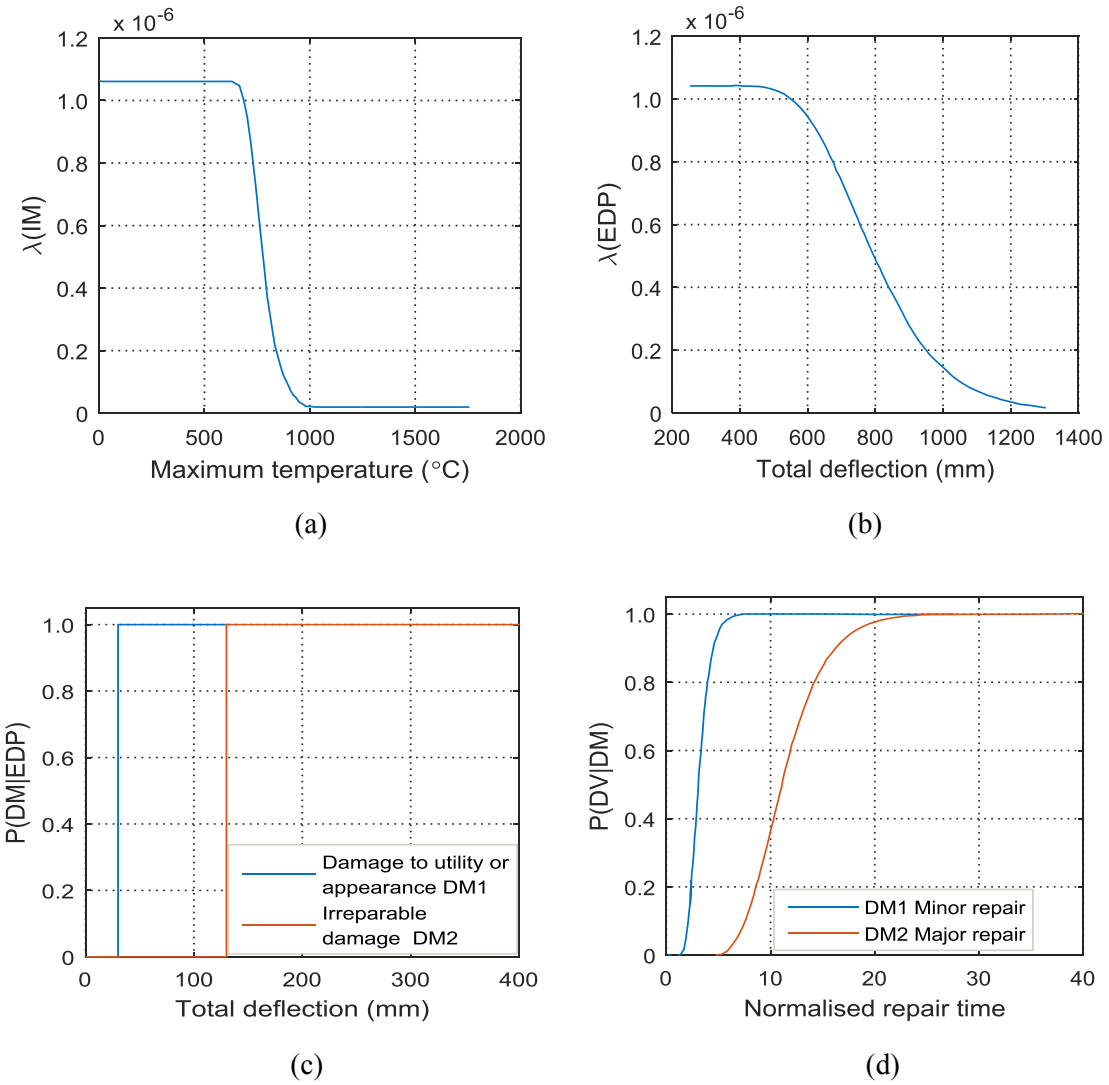

Figure 2.12. Probability plots for (a) IM hazard curve (b) EDP hazard curve (c) DM fragility curve and (d) Downtime consequence curve (from Lange et al., 2014)

Nigro et al. (2014) proposed a probabilistic method for assessing the probability of failure of a structure under fire using Monte Carlo simulation techniques and plastic limit state analysis. A steel framed structure used for car parking was employed as the case study and the results of the analyses showed that for a full parking lot, a probability of failure of about 90% is expected for a fire burning for about 3 hours. When different occupancy rates are considered, the probability of failure is about 35% after 3 hours of fire. The authors however stated that the effect of active fire protection systems was not considered. Rush et al. (2014) assessed the residual strength capacity of a reinforced concrete column by performing fragility analyses based on the PEER performance-based probabilistic framework. The results of the analyses

showed that there were other fire intensity measures besides the peak fire temperature that influenced the residual strength capacity of the column such as the ventilation opening factor (a parameter related to the amount of openings in the walls) and the fire duration. Coile & Bisby (2017) investigated the adequacy of the deflection-based criterion for structural performance of concrete floors subjected to fire using probabilistic methods and suggested an approach which efficiently approximates the strength-limit state in which the slab load is increased in a stepwise manner to the value that corresponds to the deflection limit. The authors explained that this allows the use of commonly used distribution types to appropriately represent the maximum distributed load for performance-based fire assessment.

The above review demonstrates the importance of the performance-based framework in the assessment of structures subjected to extreme loading conditions, in particular fire and blast. However, the studies neither provided a detailed assessment of fire intensity measures nor determined the most efficient intensity measure to be used with the framework. Also, the effect of blast and travelling fires has not been considered. The research gaps that were identified based on the extensive review carried out in this Chapter are discussed in the next section.

2.6 Research gaps

An extensive review has been carried out on structures subjected to fire, travelling fire, blast, as well as multi-hazard conditions involving blast and fire. The stages of the PEER performance-based framework have been explained and the findings of previous studies that adopted the framework have been discussed. The review reveals that although studies have been carried out on structures subjected to an initial blast load followed by fire, the travelling fire scenario has not been considered. Since records of accidental fires have shown that fires can travel in large compartments, which is typical of modern day structures, it is important to consider travelling fires when designing for multiple hazards in the structure. This thesis will study the performance of selected steel frames under different combinations of blast loads and travelling fires in order to address this research gap.

Furthermore, the review shows that the PEER performance-based design framework has been used to assess structures subjected to fires as well as blast loads. However, it has not been applied to travelling fires and the efficiency of the intensity measure adopted has not been established. Moreover, the framework has not been applied to multi-hazard conditions involving blast and travelling fires. This research will also extend the PEER framework to assess structures under travelling fires as well as blast and travelling fires.

Chapter 3
Finite Element Modelling

3.1 Introduction

The estimations of structural and thermal response of steel structures in this thesis are based on the results of the open source finite element analysis program OpenSees (McKenna, 1997). This program is widely employed to analyse structures subjected to gravity loads, thermal loads and dynamic loads, which are the loading conditions studied in this research. This Chapter describes the steps taken to model structural elements in OpenSees as well as the numerical approaches followed for analysing structures under different loading conditions. The suitability of the modelling procedures adopted are verified by comparing their results against those of other numerical tools and experimental studies. Finally, the case study and corresponding numerical model employed in this research are presented in detail.

3.2 Modelling in OpenSees

OpenSees is a finite element analysis program developed by McKenna (1997). It boasts of a strong community of researchers who have the ability to improve the program by adding more classes and objects to the source codes in order to widen its applicability to solve engineering problems. The modelling approaches adopted for steel and concrete structural elements are presented in the following sections.

3.2.1 Structural element modelling

Several elements types are available in OpenSees but only those used in the present research are discussed in this section. Displacement-based beam-column elements are used throughout this thesis to model steel beams and columns as well as concrete slabs. This type of element considers the spread of plasticity along the element axis and section. It also considers the large deflection response of structural elements subjected to elevated temperatures by combining it with suitable geometric transformations. Five integration points per element and co-rotational transformation are adopted in this thesis. This is based on initial sensitivity studies and past studies as the number of integration point adopted takes into account the smooth distribution

of stresses and the co-rotational transformation considers geometric non-linearity of the elements.

Moreover, the structural elements are modelled with a minimum of 44 fibre sections to improve the prediction accuracy. The *patch* command in OpenSees is used to construct the different shapes that make up the structural section while the *layer* command is used to model a number of fibres along a line or an arc typically representing steel reinforcement. The steel sections in this thesis are discretized with 16 fibres in the flanges and 8 fibres in the web based on initial sensitivity analyses. Fibre section elements have been found to predict structural response more accurately and require a smaller number of elements when compared with beam elements (Spacone et al., 1996). Figure 3.1 illustrates fibre section modelling of an I-shaped beam element in OpenSees. The figure describes an I-beam section being discretised into smaller rectangular elements, which improves accuracy and allows a more accurate prediction of structural response in comparison with beam elements.

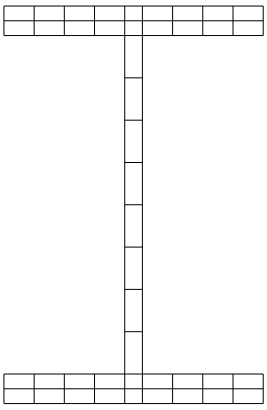

Figure 3.1. Fibre section beam element modelling in OpenSees.

3.2.2 Composite beam modelling

A composite beam consisting of a concrete slab and a steel beam can be modelled in OpenSees using two different methods (Jiang et al., 2015). Firstly, the composite beam can be modelled using a single composite section consisting of concrete and steel fibre sections based on their location in the beam. The second option is to model the steel beam and concrete slab separately and join them with rigid links that represent full composite action between the two members. Figure 3.2 shows the different modelling approaches for composite beam modelling in

OpenSees and it illustrates how the steel beam and concrete slab are connected to form a composite section using the single section and the two section approach.

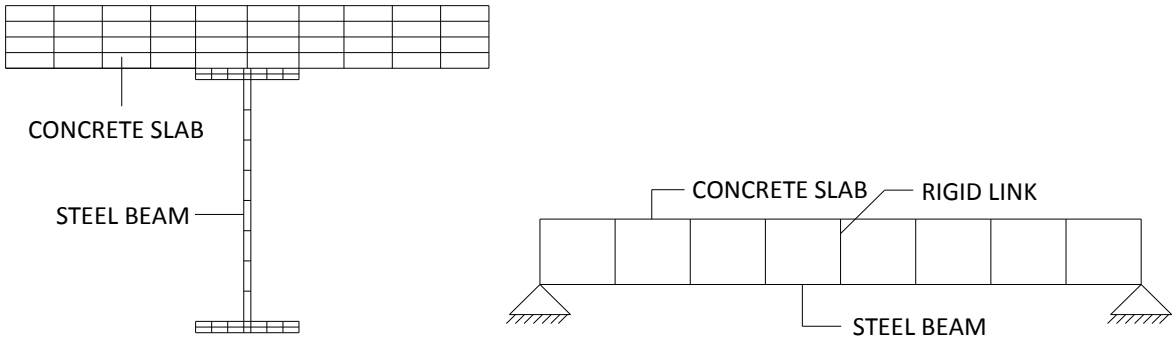

(a) Single section (b) Two sections joined via rigid links

Figure 3.2. Composite beam modelling alternatives.

3.2.3 Material models

The *Steel01Thermal* material model in OpenSees has been adopted for the steel members. This material model is able to simulate the Eurocode stress strain curve for steel which includes temperature dependent properties that consider material degradation under elevated temperatures. *Concrete02Thermal* is employed as the material model for the concrete slabs. This material model represents the stress strain behaviour of concrete in compression and tension. It also includes temperature dependent properties from Eurocode 1 to account for mechanical degradation under high temperatures.

3.3 Numerical analyses

3.3.1 Static analysis

To determine the structural response under the effect of dead and imposed floor loads, static analysis is carried out using the *Newton* algorithm and *Load Control* integrator in OpenSees. Loads are typically applied as either point loads or distributed loads on each element. The *Static* analysis type in OpenSees is used to perform the static analyses presented in this thesis.

3.3.2 Blast analysis

Blast analysis is carried out in OpenSees by applying equivalent dynamic loads unto the affected structural members in the numerical model. Strain rate effects due to blast loading are

not embedded in the definition of the constitutive materials in OpenSees, however, based on recommendations proposed by UFC (2008), the yield strength of the steel sections and the compressive strength of the concrete sections are amplified by 1.2 in order to account for the effects of high strain rates. This has been used in previous blast studies to estimate the response of structures under blast loading (Nassr et al., 2012). Amplifying the yield strength to account for strain rate effects is usually used in single degree of freedom (SDOF) analyses. It is expected that in a finite element model, a more realistic representation should be used. However, this is best achieved using programs that have constitutive models which consider the effects of strain rate. At a stress level close to the yield stress, the effects of strain rate will be more significant but a smaller increase in strain rate can be expected at higher strain values for mild steel. As a result, the amplification of the yield strength for strain rate effects was not considered at the ultimate or fracture strain in the steel model. Validation studies are carried out in this Chapter which showed that the OpenSees results compared well with previous blast studies.

As the thesis mainly focuses on previously damaged steel frames subjected to travelling fires, a simplistic approach has been adopted for the blast analyses such that strain rate effects have been considered by amplifying the yield strength of steel and compressive strength of concrete. The estimated blast pressure-time histories in OpenSees are applied using the *timeSeries* command. In this thesis, the blast analyses are carried out using the *Krylov-Newton* solution algorithm, *Newmark* integrator ($\gamma = 0.5$ and $\beta = 0.25$) and *Transient* analysis type in OpenSees.

In order to couple the blast and fire analyses in OpenSees, strain rate effects has to be suppressed for the subsequent fire analysis. This is because the effects of strain rate when structural elements are subjected to temperature loading are not as significant as when they are subjected to blast loading. In order to combine both analyses in OpenSees, the residual displacements of the structural members affected by the dynamic loading from the blast are recorded considering the increased yield and compressive strength due to strain rate effects. A separate static analysis is then performed (with the actual yield and compressive strength of the members) using a suitable dynamic increase factor for the blast loads which would result in the same displacements recorded during the dynamic analyses. This would imply that an equivalent static analyses is carried out for the blast analyses so that the actual yield and compressive strength can be used in the OpenSees script for both loading scenarios. It is expected that this would allow a closer simulation with more realistic reserves of strength for both the blast and fire analyses.

3.3.3 Heat transfer analysis

The thermal analysis program SAFIR (Franssen, 2005) is used to determine the histories of temperature in the structural members affected by fire. To this end, the temperature histories caused by the fires are applied on each individual structural section exposed to fire in SAFIR and then an analysis is carried out to determine the evolution of temperatures in the sections. A convective heat transfer coefficient of 4 W/m^{2}K is used for the sections not exposed to the fire while 25 W/m^{2}K is taken as the coefficient for members directly exposed to the fire. The ambient temperature is assumed to be 20 °C and the radiative emissivity is taken as 0.7 for all the analyses. Figure 3.3 illustrates the distribution of temperatures in a steel column and composite beam section obtained from heat transfer analyses in SAFIR. The composite beam figure shows that the heat transfer analysis results in higher temperatures in the steel section (red region in the figure) while the concrete slab experiences lower temperatures. In the steel column, the flange exposed to the fire will experience hotter temperatures compared to the other flange in the column section.

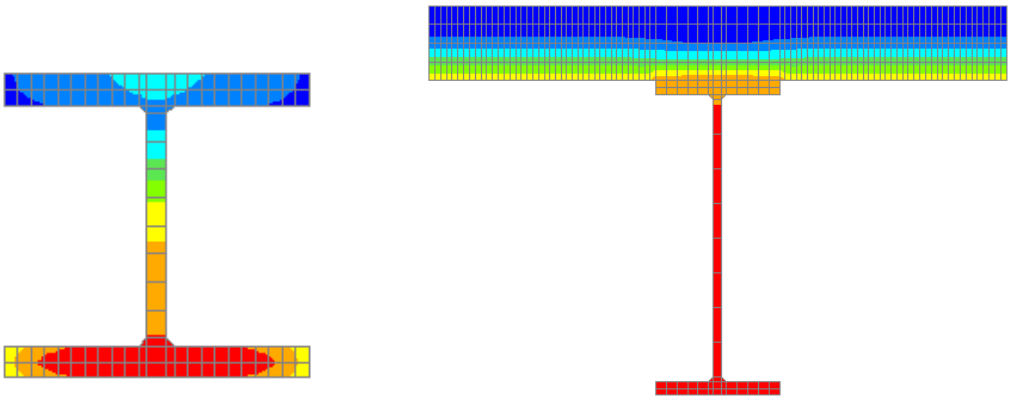

Figure 3.3. Temperature distribution in a steel column and composite beam section.

3.3.4 Fire analysis

The temperature history over the structural sections determined from the output file of the heat transfer analyses carried out in SAFIR as described above, is applied as an element load on the structural members subjected to fire using the *Fire pattern* and *timeSeries* command in OpenSees. These OpenSees models are then used to determine the thermal and structural responses under temperature loads. In this thesis, 5 temperature points are adopted in the beam and column sections. The fire analyses are carried out using the *Krylov-Newton* algorithm, the *Hilber-Hughes-Taylor* integrator with a numerical damping factor of 0.7 and the *Transient*

analysis type in OpenSees. The *Hilber-Hughes-Taylor* integrator has been found to be more numerically stable when dealing with extreme temperatures (Hilber et al., 1977).

3.4 Model validation

3.4.1 Structures subjected to fire

The thermal module in OpenSees was developed at the University of Edinburgh by Usmani et al. (2012) and it has been widely used to analyse structures under thermal loads (Kotsovinos, 2013; Rezvani & Ronagh, 2015; Jiang et al., 2015). In this section, OpenSees is used to reproduce the results of numerical and experimental studies on the effect of fire on steel beams, composite beams and steel frames in order to gain confidence on the adopted modelling strategies.

Steel beam subjected to fire

The pin-ended steel beam with a uniformly distributed load of 20 kN/m and a span of 8 m examined by Burgess & Alexandrou (2014) is studied first. In the original study, the beam was subjected to the standard fire for 90 mins. A UB 457x191x98 was employed for the steel beam. The yield strength of the steel is 355 MPa while its elastic modulus is 210 GPa. Moreover, the beam was assumed to have fire protection which is accounted for by subjecting the web and lower flanges to 70 % of the fire temperature and the upper flange to 60 % of the fire temperatures. The temperature-time curves of the standard fire at different locations in the beam section are shown in Figure 3.4. The beam is illustrated in Figure 3.5.

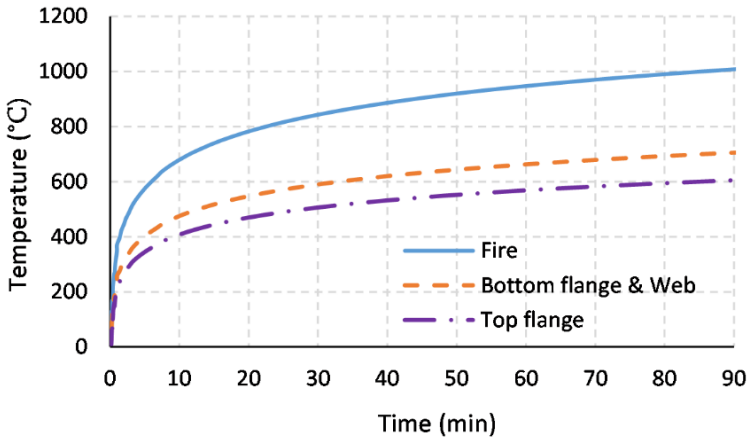

Figure 3.4. Temperature-time history of the beam.

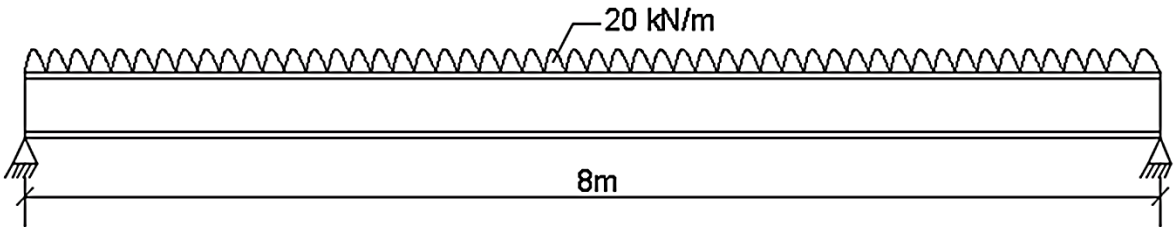

Figure 3.5. The pin-ended beam in the study.

The beam is modelled in OpenSees using 8 displacement-based beam-column elements with 5 integration points per element. *Steel01Thermal* material model is adopted for the beam. The maximum vertical beam displacement at mid-span is recorded and is compared with the results of the benchmark studies by Burgess & Alexandrou (2014) in Figure 3.6. The finite element analyses program VULCAN was used in the initial study. It can be observed from Figure 3.6 that the displacement response predicted by OpenSees is very similar to that of the original study. Although the displacements in OpenSees are slightly higher than the original estimations, this difference is more pronounced in the initial phase of the fire. Moreover, the difference between the displacement values in both studies decreases as the fire duration increases. Overall, Figure 3.6 shows that the modelling strategy adopted can be used to obtain consistent estimates of the response of steel members exposed to fire.

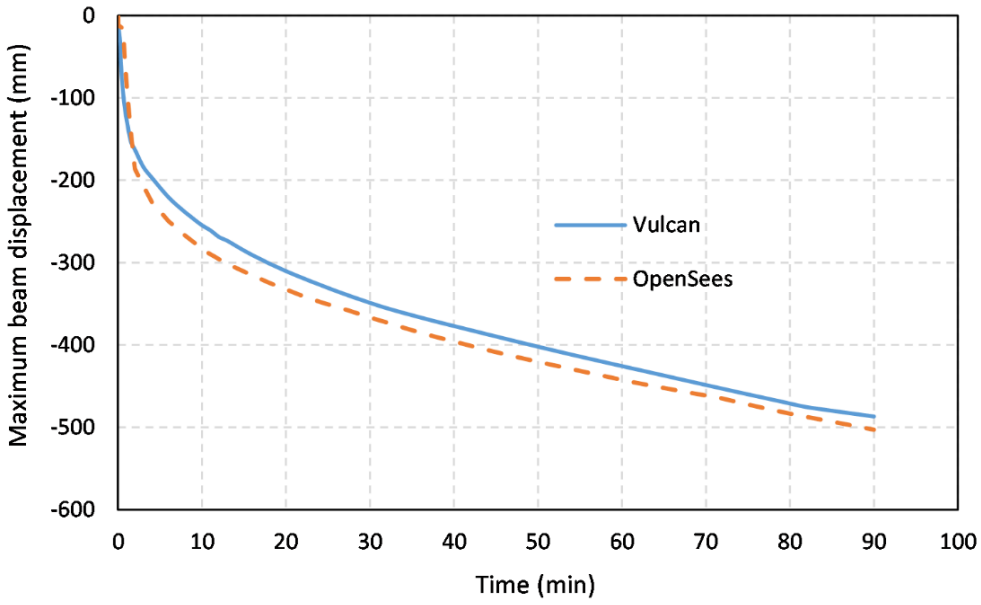

Figure 3.6. Vertical displacement response of the pin-ended beam.

Composite beam subjected to fire

The majority of the study in this thesis have numerical models with composite beams. Therefore, it is necessary to establish that OpenSees has the capacity to predict the response of composite beams reasonably well. Experiments have been carried out by Wainman & Kirby (1988) to determine the response of steel members under thermal loads. In particular, Test 15 from the study is examined herein. In the test, a simply supported composite beam was subjected to a standard fire for 40 mins. The span of the beam is 4.53 m. The concrete slab is 130 mm thick with a compressive strength of 30 MPa while the yield strength of the steel beam is 255 MPa with an elastic modulus of 210 GPa. Figure 3.7 shows the cross-section and longitudinal section of the beam which was obtained from Jiang et al. (2015). The letter 'P' in Figure 3.7 represents a point load of 32.47 kN. Figure 3.8 shows the average temperatures at different locations in the beam section.

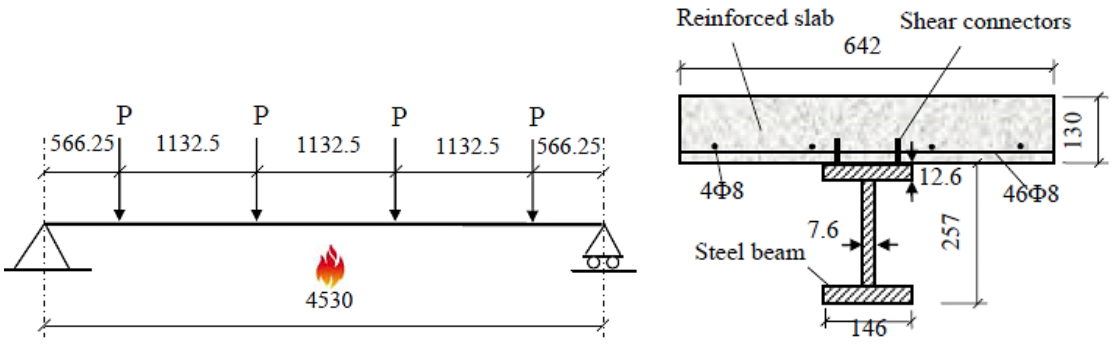

Figure 3.7. Longitudinal section and cross-section of the beam from Jiang et al. (2015).

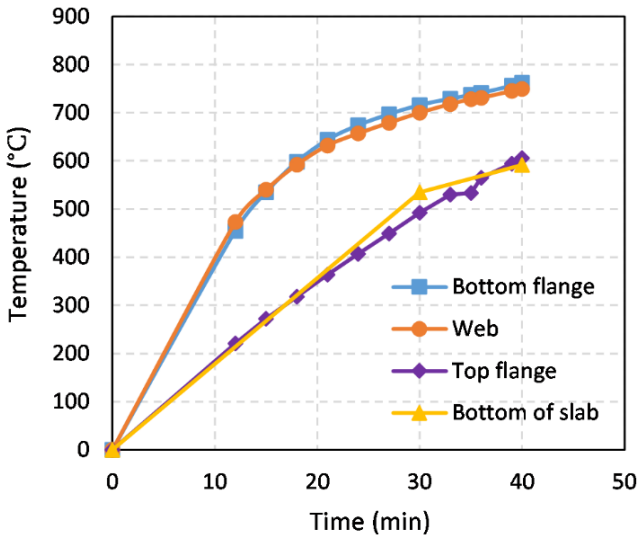

Figure 3.8. Mean temperatures at different locations in the beam (Wainman & Kirby, 1988).

The results from the two modelling techniques for composite beams discussed (see Section 3.2.2) are compared in Figure 3.9. For the single section method, the composite beam is modelled with 5 displacement-based beam-column elements and 5 integration points per element in OpenSees. For the two section alternative, 5 beam elements are adopted for both the concrete slab and the steel beam. The two members are then joined with 6 rigid links to represent full composite action. *Concrete02Thermal* material is adopted for the concrete slab while *Steel01Thermal* is employed for the steel beam in all cases.

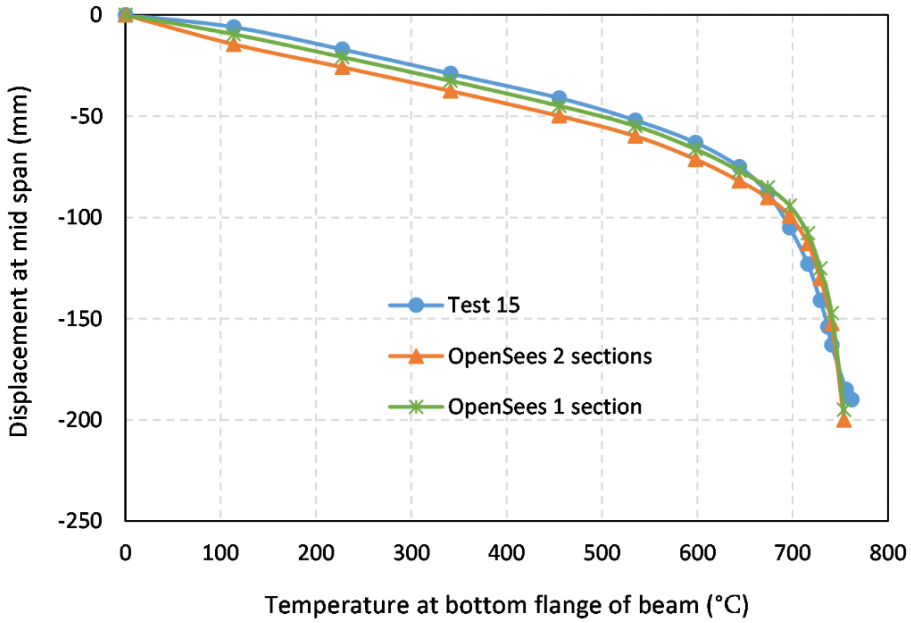

Figure 3.9. Vertical displacement response of the composite beam at mid span.

The vertical displacement of the composite beam experimentally observed at mid span is shown in Figure 3.9 together with the predictions from the two modelling approaches. These results show that both modelling approaches have a very similar response to that of the experiment. The displacement response from OpenSees is slightly higher in the beginning but from 680 °C, the numerical and experimental displacement values became very similar. This shows that the modelling strategy adopted leads to good estimations of the response of composite beams subjected to elevated temperatures.

Steel frame under fire

The single storey steel frame studied by Izzuddin et al. (2000) is examined herein to determine the structural response under fire. The steel frame is a two-bay frame and only the structural

members in the left bay are subjected to the fire. Izzuddin et al. (2000) employed the finite element analysis program ADAPTIC (Izzuddin, 1991) to analyse the structure. Besides, their numerical predictions were validated against experiments performed by Rubert & Schaumann (1986). In the original study, an IPE 80 section was employed for the column and beam sections. The yield strength of the steel is 355 MPa while its elastic modulus is 210 GPa. Figure 3.10 shows the frame under consideration.

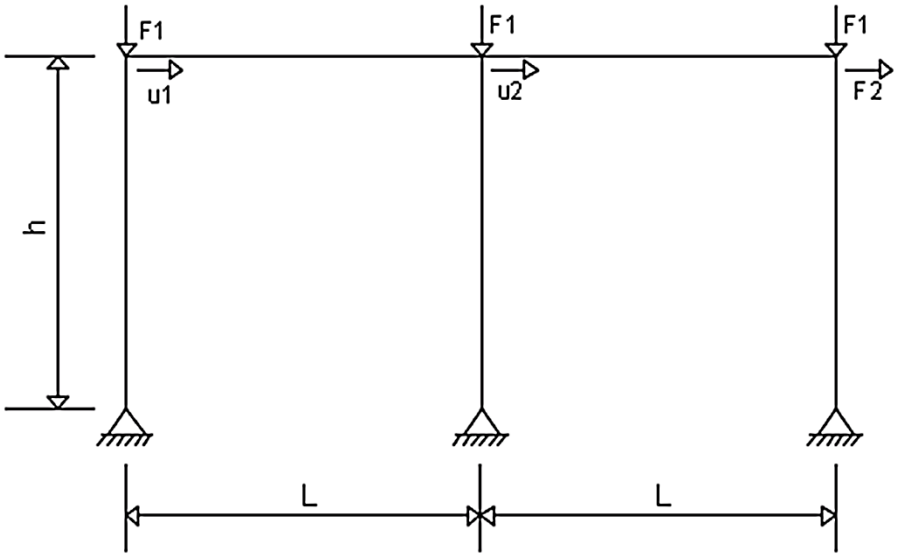

Figure 3.10. The steel frame in the study with F1 = 74 kN, F2 = 2.5 kN, L = 1.2 m and h = 1.18 m (from Izzuddin et al., 2000).

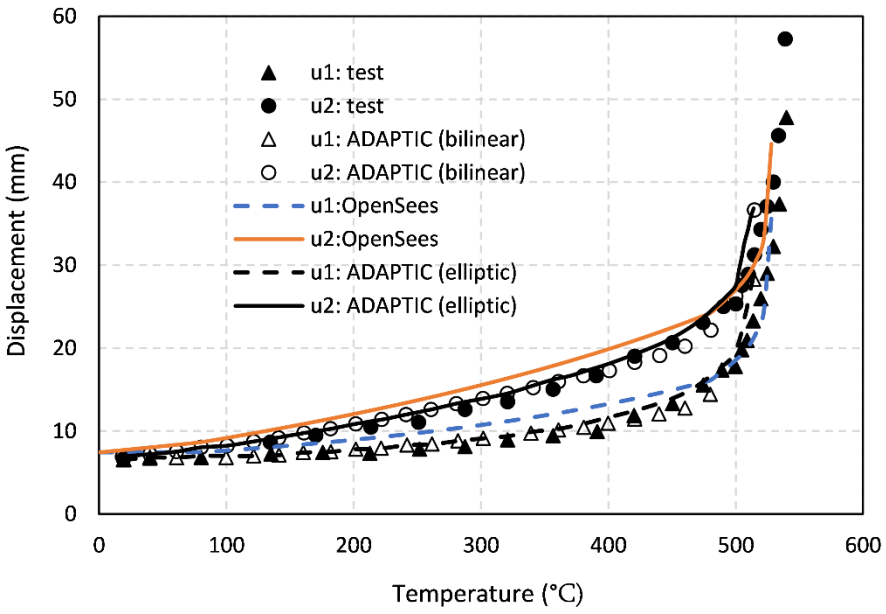

Figure 3.11. Horizontal displacement response of the frame using ADAPTIC (from Izzuddin et al., 2000) and OpenSees.

In this study, comparisons are established between the experimental response and numerical estimations obtained with OpenSees. To this end, the beams and columns of the frame under consideration are modelled with 4 displacement based beam-column elements and the *Steel01Thermal* material model is used for the steel sections. The horizontal displacement response of the frame is shown in Figure 3.11 for experimental results and finite element estimations made by Izzuddin et al. (2000) with ADAPTIC considering bilinear and elliptic stress-strain curves for the steel material as well as displacements from the OpenSees model. From the figure, it can be observed that there is a good prediction of the horizontal displacement when the response from OpenSees is compared with that of ADAPTIC and the experiments. Figure 3.11 shows that the horizontal displacement increases linearly as the temperature increases up to about 480 °C after which the response becomes non-linear up to 520 °C. After this temperature is exceeded, a large increase in displacement is observed which marked the beginning of failure of the frame. The results of the study demonstrate that the modelling approach adopted in OpenSees has the capacity to effectively analyse steel frames subjected to fire.

3.4.2 Structures subjected to blast

In this section, the prediction capability of the numerical models put forward in this thesis when subjected to blast loads is examined. The numerical study selected to establish the comparisons was carried out by Chen & Liew (2005) and it is used to determine the blast resistance of a steel column. In the original study, the finite element analysis software ABAQUS was employed. The column was subjected to the blast profile depicted in Figure 3.12. The longitudinal section of the column is also shown in Figure 3.12. The section size adopted was UC 254x254x89. The yield strength of the steel is 275 MPa while its elastic modulus is 205GPa. An imperfection of L/1000 is assumed for the column and it is linearly varying along its height reaching a maximum at mid-height. A compression load F equal to 30 % of the axial capacity is applied at the top of the column. Moreover, the axial capacity of the column was determined to be 3100 kN. The blast pressure is represented by a uniformly distributed load $p(t) = p_o\bar{p}(t)$ where $\bar{p}(t)$ is the normalised blast overpressure. In OpenSees, six displacement based beam-column elements are used to model the column with 5 integration points per element. *Steel01Thermal* is used as the material model for the column. The column is then analysed for different blast pressures so as to determine the blast resistance of the column.

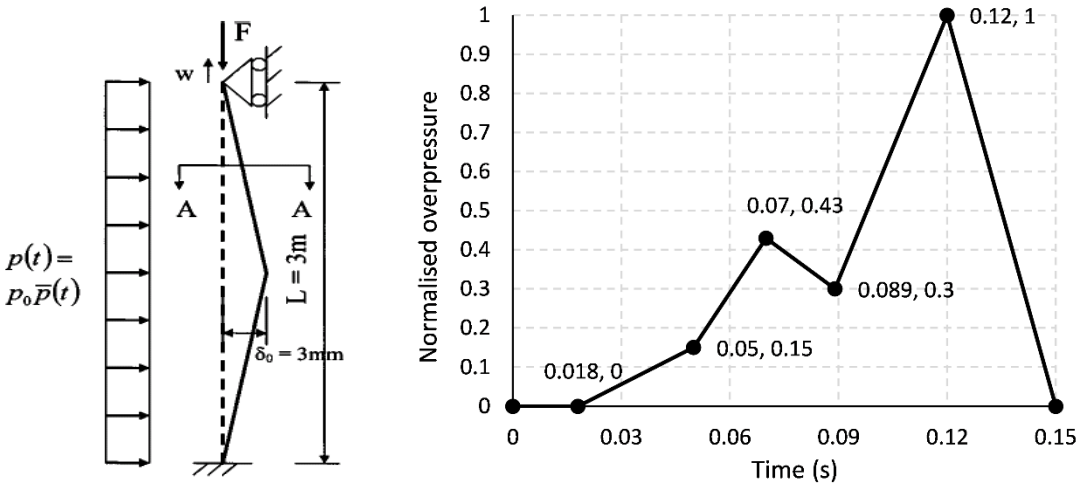

Figure 3.12. Column geometric configuration and blast history from Chen & Liew (2005).

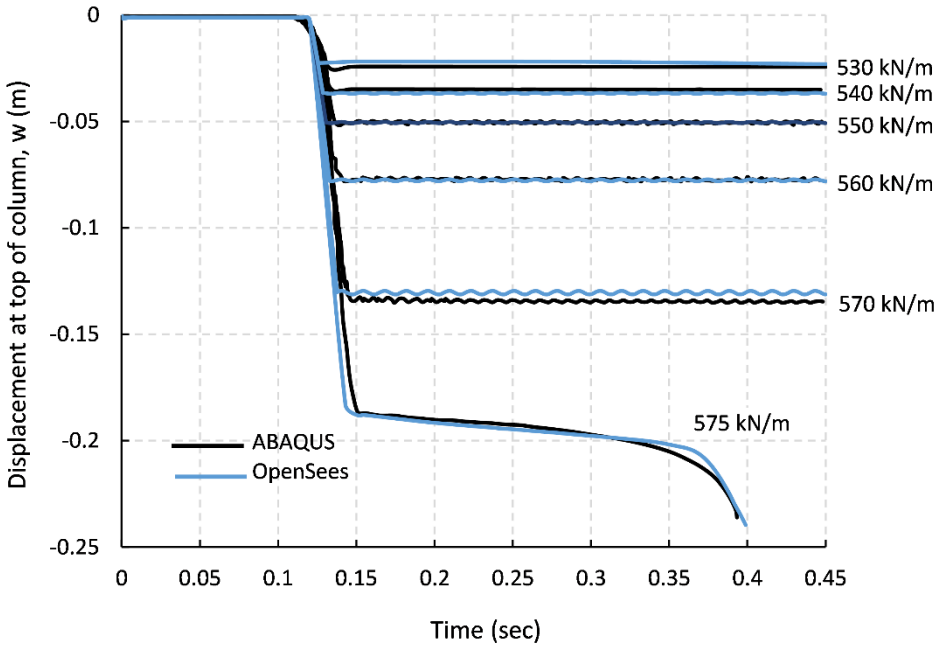

Figure 3.13. Vertical displacement at top of column adapted from Chen & Liew (2005).

The vertical displacement at the top of the column as estimated by Chen & Liew (2005) using ABAQUS and the numerical predictions of OpenSees are presented in Figure 3.13. A comparison between both results show that the displacement response from OpenSees is very similar to the response from the original study by Chen & Liew (2005). Figure 3.13 shows that the blast load is not large enough to cause significant change in the displacement until the maximum pressure was reached at 0.12 secs. A sudden increase in displacement is then noticed based on the magnitude of the blast pressure up to about 0.15 secs. The blast resistance of the

column is deduced to be 574 kN/m (Chen & Liew, 2005) since a blast pressure of 575 kN/m results in an excessive displacement of the column. The result of the study shows that the modelling strategy adopted can adequately predict the blast resistance of structural members.

3.4.3 Structures subjected to blast and fire

The ability of the finite element models proposed to predict the response of multi-hazard scenarios involving blast and fires is also studied. In this section, OpenSees is used to analyse a 3-storey steel frame subjected to blast and fire. The frame was taken from a numerical study by Izzuddin et al., (2000) and is shown in Figure 3.14. The finite element analysis program ADAPTIC was used in the original study. The section of the beams is UB 686x254x152 while the section of the internal columns is UC 203x203x46 and that of the side columns is UC 152x152x23. The yield strength of the steel used was assumed to be 399 MPa while its elastic modulus was 210 GPa. Six displacement based beam-column elements are used to model each beam in OpenSees while four elements with five integration points are adopted per column. *Steel01Thermal* material model is used in the study.

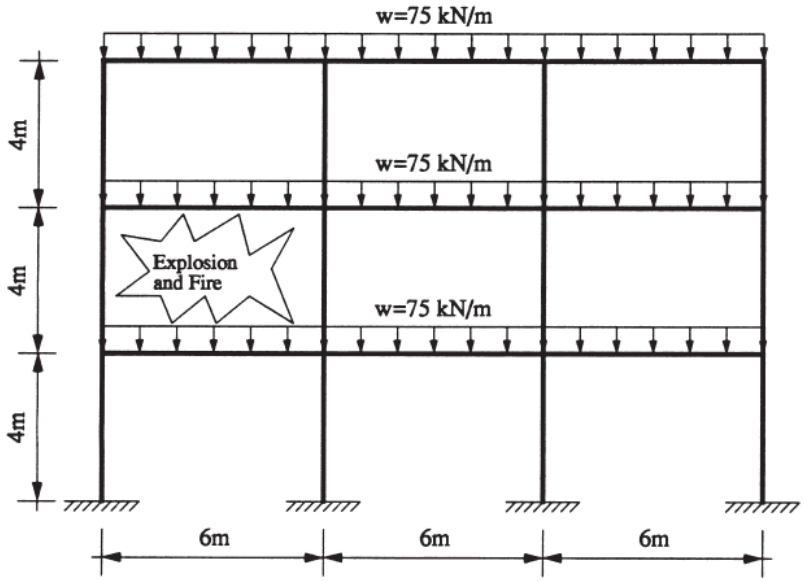

Figure 3.14. The 3-storey frame in the study from Izzuddin et al. (2000).

A static load of 75 kN/m is initially applied to the beams followed by a blast pressure of 125 kN/m acting in the left compartment of the middle storey. Fire temperatures which increased monotonically from 20 °C until failure are subsequently applied to the compartment affected by the blast. The temperature distribution in the structural members is shown in Table

3.1. The temperature parameter 'T' in Table 3.1 is used to represent the maximum temperature in the compartment. The analysis was carried out with the assumption that the lower beam in the blast affected compartment was unaffected by the fire and that the side columns had fire protection (Izzuddin et al., 2000). The frame is first analysed considering only the fire. It is then analysed for an initial blast load followed by fire.

Table 3.1. Temperature distribution in the structural elements from Izzuddin et al. (2000)

Top beam		**Lower beam**	**Internal column**	**Side column**	
Lower flange	Upper flange	Both flanges	Both flanges	Internal flange	External flange
T	0.75T + 5	20	T	0.5T+10	0.25T+15

The horizontal displacement response at mid-height for the column on the left-hand side is illustrated in Figure 3.15 for the original study and OpenSees. Considering only the fire, the side column is observed to buckle at about 500 °C. This is as a result of the reduced stiffness of the column which is quite low in comparison to the other structural members in the compartment. However, failure of the frame occurred at 900 °C when a displacement of about 500 mm was recorded.

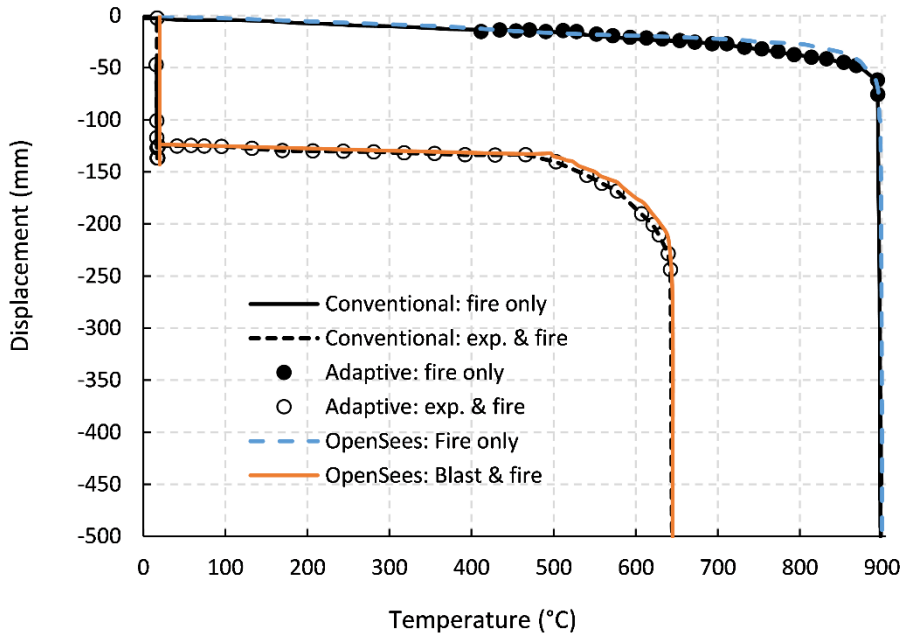

Figure 3.15. Horizontal displacement response of the side column from Izzuddin et al. (2000).

For the blast and fire analysis, an initial plastic deformation of the side column is observed due to the blast pressure which resulted in a residual lateral displacement of 125 mm. Buckling of the side column is observed during the subsequent fire analysis at about 500 °C. Moreover, buckling of the internal column occurred at about 650 °C which led to failure of the frame. The suitability of the modelling approach adopted in this thesis to predict blast and fire response is validated as seen in Figure 3.15 which shows that the response from the OpenSees model reproduces that of the original study. All the studies carried out so far have shown good agreement with previous studies which therefore makes OpenSees suitable for use in this research.

3.5 Prototypical building model

The prototypical building adopted throughout this research is a 7 storey steel office building with composite beams. In particular, the slice under consideration is supported on one end by a column and on the other end by a reinforced concrete core. The reinforced concrete core is represented in the model by a pinned support. The plan of the building is shown in Figure 3.16 which highlights the frame section selected for this research. Three beam lengths (9 m, 12 m and 15 m) are considered in the study denoted by 'L' in Figure 3.16 and the height of the column is assumed to be 4 m which is typical for office buildings. Different section sizes are adopted for the composite beams and they are summarized in Table 3.2. Figure 3.17 shows the elevation of a typical numerical model employed in this thesis as well as the cross-section of the composite beam as illustrated in Teslim-Balogun et al. (2017). An imperfection of 1/1000 at mid-height is assumed for the column. Three different axial loads are applied at the top of the column to represent the floor loads coming from upper floors of 10, 12 and 14 storey buildings. The imposed load and partitions are assumed to be 3.5 kN/m^2 and 1 kN/m^2, respectively. The dead load is assumed to consist of the self-weight of a 130 mm thick concrete slab and steel beam as well as finishes, which results in a total dead load of 5 kN/m^2. The 130 mm concrete slab was found to be adequate for the composite beam based on preliminary structural analyses.

Table 3.2. Beam lengths and section sizes for the columns and beams.

Beam length	Beam section	Column section
9 m	UB 533x210x138	UC 356x406x340
12 m	UB 533x312x182	UC 356x406x340
15 m	UB 533x312x272	UC 356x406x340

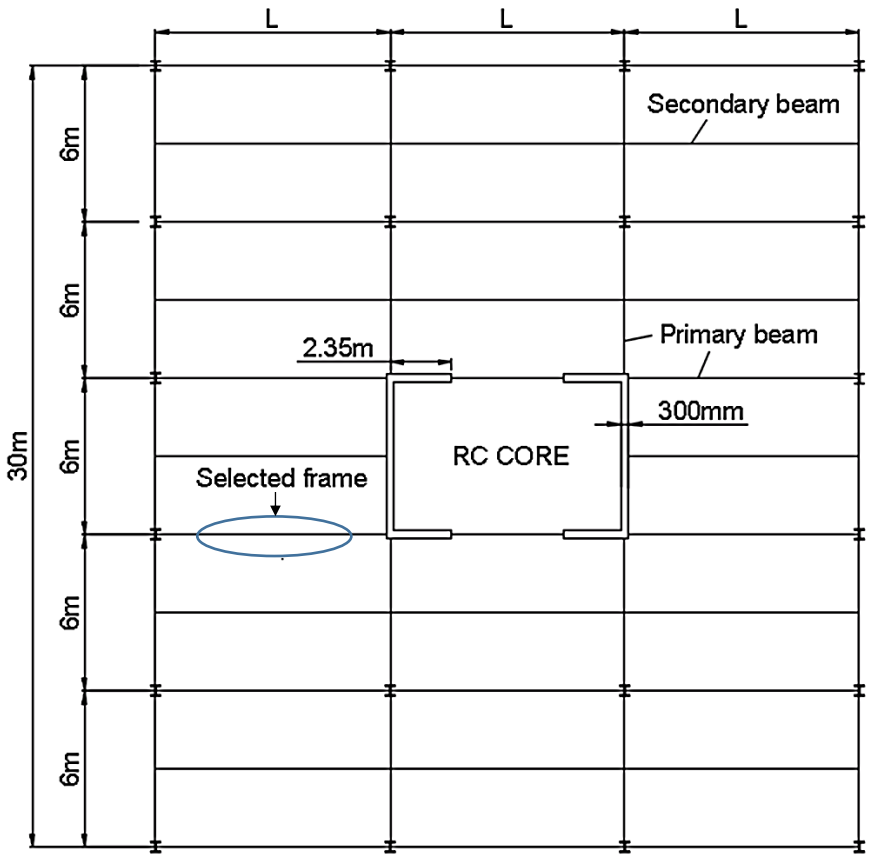

Figure 3.16. Plan of the prototypical office building.

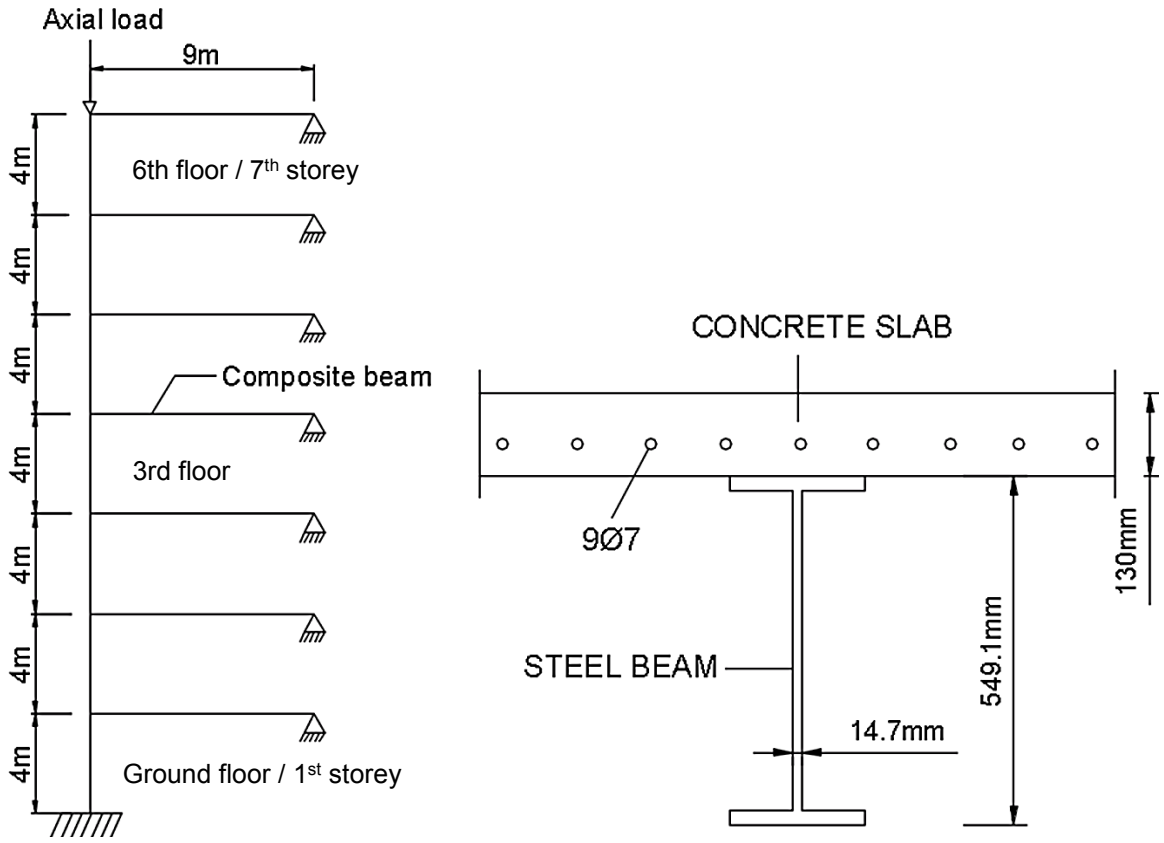

Figure 3.17. Numerical model for the 9 m composite beam.

The steel frame is modelled in OpenSees using displacement based beam-column elements with 5 integration points per element. Full composite action is assumed for the composite beam and the single section modelling method is used to represent the composite beam in OpenSees. The steel mesh in the concrete slab is modelled in OpenSees using 9 no 7 mm diameter reinforcement bars and the composite beams are assumed to be fully fixed to the columns. The yield strength of the steel is assumed to be 355 MPa while that of the reinforcement is taken as 460 MPa. An elastic modulus of 210 GPa is assumed for the steel. The compressive strength of the concrete is taken as 30 MPa. The steel material used for the study is *Steel01Thermal* while *Concrete02Thermal* is adopted for concrete. It is important to note that the structural members are assumed to be unprotected which represents a worst case condition of the structure. It is assumed that the beams and columns are connected by fully rigid connections and has been modelled as such. This may reduce the prediction of strength and estimates of failure. Other types of connections such as pin and semi-rigid connections may be more usual in the building considered. Although, this might affect the overall response, it is expected that the numerical configuration adopted is adequate for this study and further studies in this area can consider the influence of other type of connections.

3.5.1 Sensitivity analyses

Sensitivity analyses are carried out to determine the suitable number of beam elements that will be required for an accurate prediction of the thermal and structural response of the composite beam under the travelling fire scenarios. A near field temperature of 1000 °C is assumed for this purpose. Also, a fuel load density of 570 MJ/m^2 is adopted and a heat release rate per unit area of 500 kW/m^2 is assumed for the study which results in a burning time of 19 mins. The numerical model presented in Figure 3.17 is used for the study with a column axial load of 690 kN corresponding to floor loads from 5 extra storeys.

The travelling fire is assumed to occur at the fourth storey while the third floor beam is assumed to remain at ambient temperature. Six, eight, twelve and twenty beam elements are considered for the composite beam while the column is modelled using 8 beam elements. The steel frame is initially analysed for static loads from dead and imposed floor actions. Subsequently, the model is subjected to a travelling fire of 10 % of the floor area travelling from the left edge of the compartment as illustrated in Figure 3.18. This fire size was chosen because, Law et al. (2011) and Stern-Gottfried & Rein (2012b) concluded that low and medium fire sizes can have a higher impact on the structural response. Figure 3.19 shows the temperature time curves of

the travelling fire and at different points in the beam section at 2 m and 8 m from the left edge of the compartment.

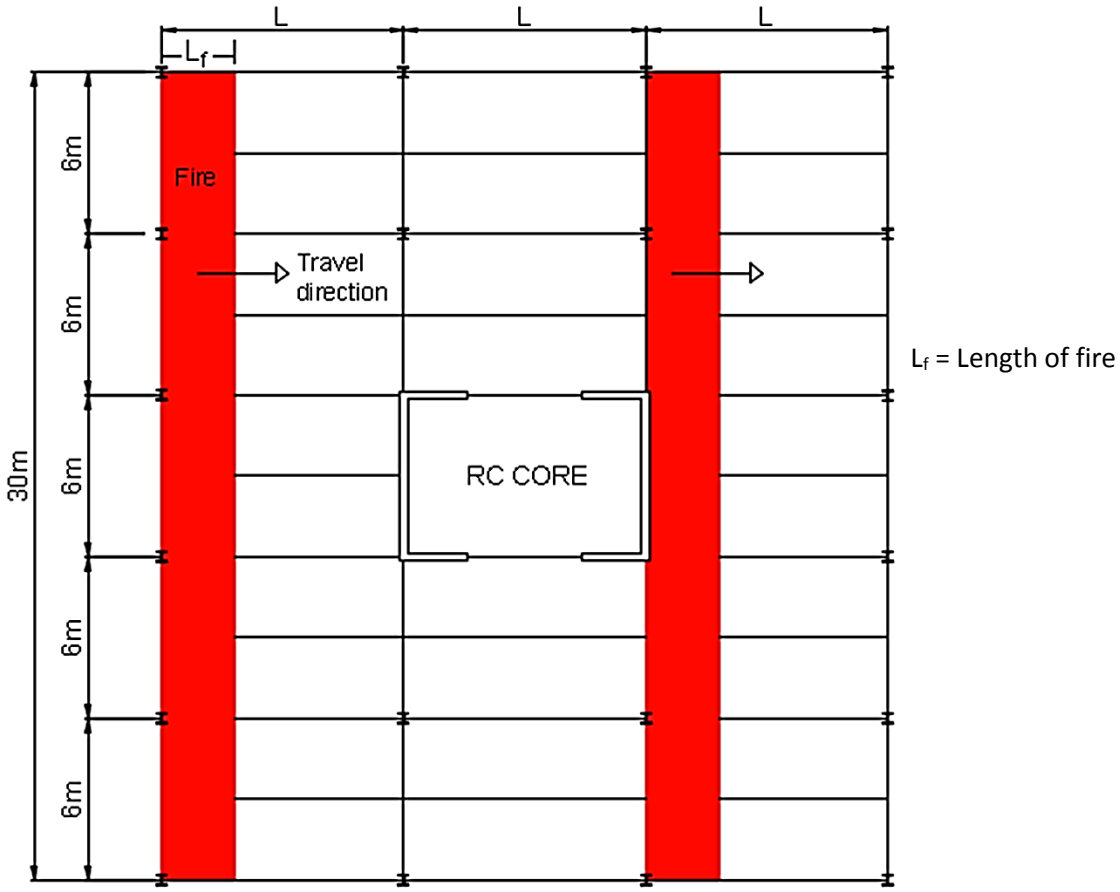

Figure 3.18. Movement of fire along the compartment for a fire size of 10 % of the floor area.

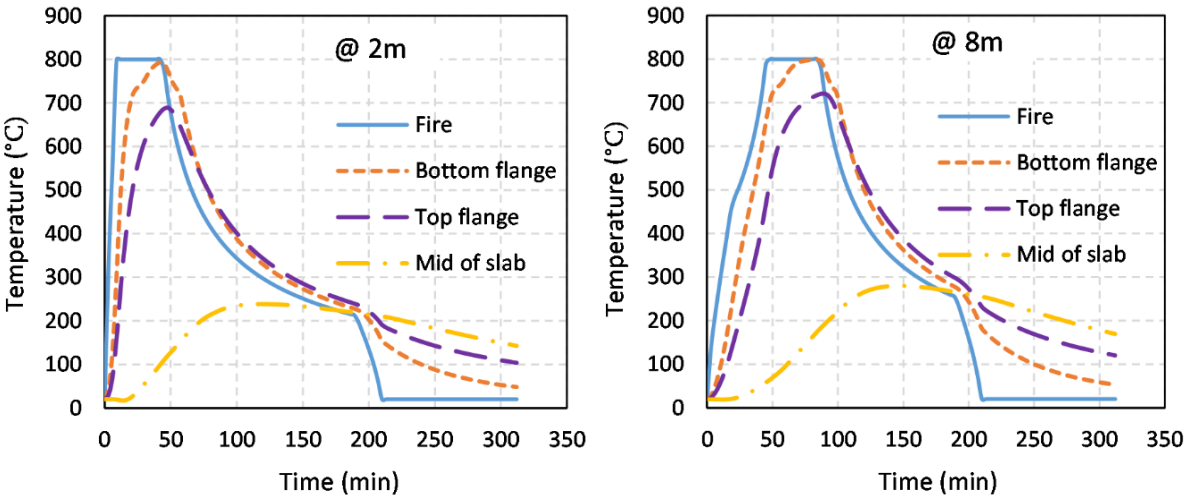

Figure 3.19. Temperature time history of the travelling fire and composite beam at 2 m and 8 m from the left edge of the compartment.

Figure 3.20 shows the beam displacement response for the different number of beam elements considered. It can be observed from Figure 3.20 that the displacement decreases as the number

of beam elements increases. However, the percentage difference also decreases with increasing number of elements per beam. A percentage difference less than 5 % is assumed to represent reasonable estimates of displacement and is considered sufficient for the purpose of this study. Such difference is observed for the 12 and 20 beam elements. As a result, in this thesis, the 9 m composite beam is modelled with 12 displacement based beam-column elements. This level of discretization is assumed as a good compromise between computational effort and accuracy of the structural response. Composite beams of longer length are modelled with proportionally larger number of beam elements in consistency with the sensitivity study carried out.

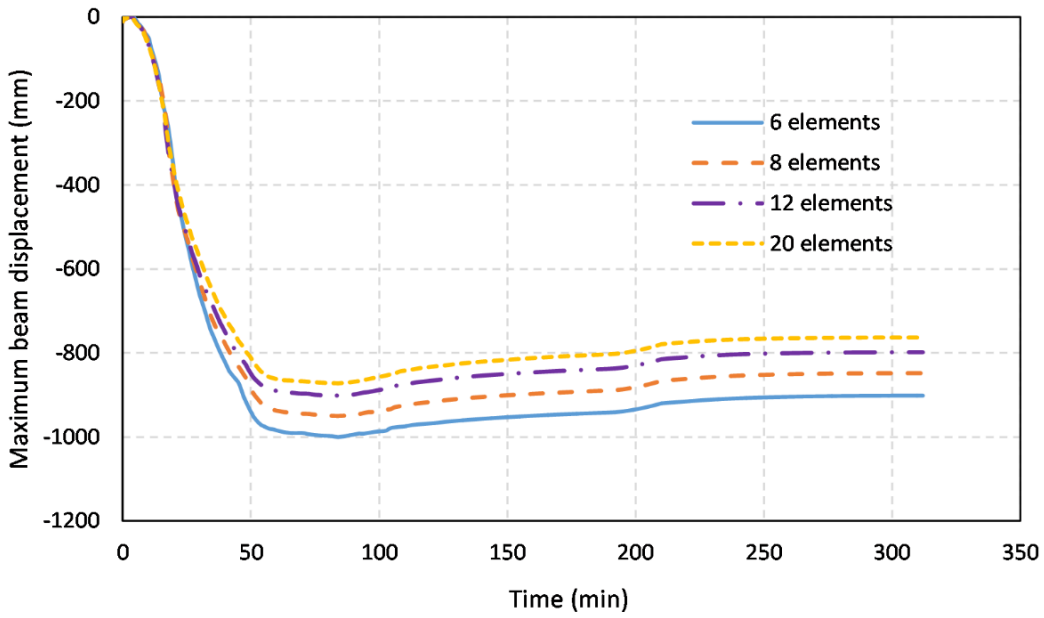

Figure 3.20. Vertical displacement at mid span of the 9 m composite beam for increasing number of elements.

3.6 Conclusions

The capability of OpenSees has been verified with regards to its suitability for blast and fire actions earlier in this chapter and it was found to agree well with results of previous studies. As a result, it can be concluded that OpenSees is suitable for analysing structures under fire, blast and post-blast fire actions. The numerical analyses carried out and the numerical model for this research have also been presented. Moreover, the sensitivity analyses performed determined the optimum number of beam elements suitable for the composite beam in the model. The results demonstrate that 12 beam elements are suitable for the 9 m composite beam and other beam lengths can be modelled in proportion to the results of the sensitivity analyses.

Chapter 4
Assessment of Efficiency of Travelling Fire Intensity Measures for Performance-based Assessment

4.1 Introduction

It is important that structural fire design is carried out considering all possible design scenarios that may affect the structure. In this context, the effect of travelling fires will also need to be considered, especially for large building compartments. Moreover, as a result of the uncertainty associated with some fire parameters in structural fire design, it is sensible to use a performance-based design framework such as the one developed by Cornell & Krawinkler (2000) called the PEER framework to access structures under the effect of travelling fires. This assessment will require the use of an adequate intensity measure able to describe the severity of the travelling fire. Choosing an adequate intensity measure also helps to determine the fire parameter that has the most significant influence on the thermo-mechanical response of the structure. This will be beneficial for the chapters that follow as it will allow a reduction in the number of fire parameters accounted for in the parametric analyses without significant loss of generality or precision.

This chapter assesses the efficiency of several travelling fire parameters in order to determine the most suitable intensity measure for performance-based travelling fire design. Several fire and structural parameters are considered when determining the response of the steel frames described in the previous chapter. This is followed by a comparative assessment on the benefits of using a Vector intensity measure over the scalar approach usually employed in typical engineering practice. To this end, univariate and multivariate regression models were employed and the efficiency of each intensity measure or combination of intensity measures was used to determine their suitability to characterize travelling fire scenarios. Only the first two stages of the PEER performance-based design framework are considered and the effect of high correlation between intensity measures is demonstrated based on the probability of exceedance of the selected engineering demand parameters.

4.2 Structural and fire parameters

Different values of structural and fire parameters are considered in this study in order to have a large database of structural response for different travelling fire scenarios based on a number of selected structural configurations. The numerical model for this study is the same as that which was previously discussed in Chapter 3. Buildings with 10, 12 and 14 storeys are considered in this study. However, only the first seven storeys have been considered in the numerical model. To this end, axial loads are applied at the top of the seventh storey column representing extra loads from the upper floors. The three composite beam lengths denoted by 'L' in Figure 3.16 are also considered in this chapter. The sections for the different structural configurations have been presented in Table 3.2.

The temperature-time history for the travelling fire at the desired locations in the compartment are determined using the equations proposed by Rackauskaite et al. (2015). The input parameters for these equations are the near field temperature which is the maximum compartment temperature, the heat release rate, the fuel load density and the fire size (see Equations 2.4 to 2.8). The near field temperature is assumed to range from 800 °C to 1000 °C which is typical of large fires in buildings. The fire size which is the percentage of floor area engulfed in fire, is an important part of the Travelling Fire Methodology and a range of fire sizes between 5 and 50 % was adopted for the present study.

The range of values adopted for the fuel load density from 360 to 600 MJ/m^2 is based on the recommendations from Eurocode 1 (BSI, 2002) which follows the Gumbel distribution. The values for the heat release rate per unit area are determined considering the combustion of cellulose fuels and the mass burning rate of office fuels (Jiang et al., 2013). The burning rate of office fuels considered is between 20 and 40 g/m^{2}s (Milke et al., 2002) while the heat of combustion of cellulose fuels is 16 kJ/g (Drysdale, 2011). This results in heat release rates per unit area between 368 and 640 kW/m^2. Table 4.1 summarizes the range of values for the different parameters used in the study.

It should be noted that the temperature-time history of each travelling fire scenario was determined considering a range of values for the parameters. The random number generator in MATLAB was used to produce random values for the parameters within the specified range in Table 4.1. This approach is considered adequate as no realistic fire parameter values could be

obtained from previous accidental or experimental travelling fires. Nevertheless, it is expected that realistic fires will fall within the range of values considered herein.

Table 4.1. Range of values of structural and fire parameters considered in this study.

Beam Length (m)	Total number of storeys	Range of Near field temperatures (°C)	Range of Fire sizes (%)	Range of Heat release rates (kW/m^2)	Range of Fuel load densities (MJ/m^2)
9	10	820 - 1000	5 - 50	368 - 640	360 - 600
	12	820 - 1000	5 - 50	368 - 600	375 - 570
	14	820 - 1000	5 - 35	368 - 600	375 -525
12	10	820 - 1000	5 - 50	368 - 640	360 - 600
	12	820 - 950	5 - 35	368 - 600	375 - 525
	14	820 - 900	5 - 30	368 - 600	390 - 525
15	10	820 - 1000	5 - 50	368 - 640	360 - 600
	12	820 - 900	5 - 30	368 - 600	390 - 525
	14	820 - 900	10 - 30	368 - 544	390 - 525

The fourth storey of the numerical model in Figure 3.17 is assumed to be the location of the fire. This was done since the fourth storey represents the middle of the numerical model and simulates a floor compartment surrounded by floors above and below that can help to distribute the forces from the fire action. The fire is assumed to travel along the compartment in the horizontal direction from the left edge of the compartment to the right edge as illustrated in Figure 3.18. As a result, the temperature loading is applied to the structural members in the fourth storey based on the results of the heat transfer analyses.

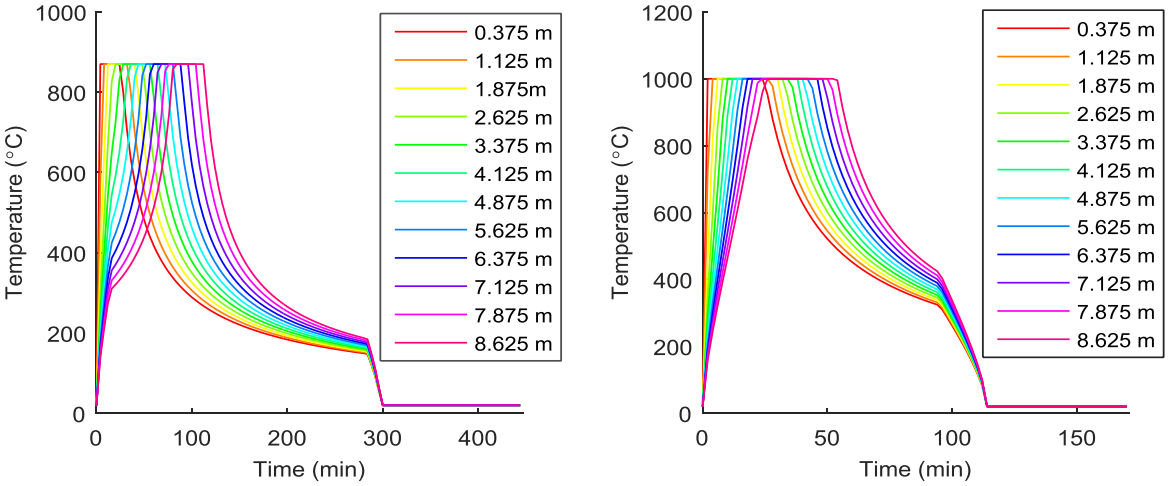

(a) 5 % fire size

(b) 20 % fire size

Figure 4.1. Temperature-time curves at different locations in a 9 m beam.

The third floor beam is assumed to be naturally shielded by the concrete slab and thus, remain at ambient temperature conditions. The numerical models are first analysed under dead and imposed floor actions in OpenSees. Temperature loads from different travelling fire scenarios are applied in a subsequent stage. The structural response is then recorded for different engineering demand parameters. Typical temperature-time curves of the travelling fire scenarios employed are illustrated in Figure 4.1 which shows the temperature history at different locations on a 9 m beam for 5 % and 20 % fire size. The figure also shows that the total fire duration increases with increasing fire size and that the beam is subjected to repeated heating and cooling as the fire travels across the compartment.

Stochastic models were used to model the input variables for the temperature-time histories based on random selection of parameter values between the specified range in Table 4.1 as discussed earlier. However, the resulting structural response values are deterministic based on results of the nonlinear finite element analyses.

4.3 Regression analyses

In order to determine the most suitable intensity measure for the performance-based assessment, regression analyses are usually carried out. These analyses help to determine the relationship between selected intensity measures and the engineering demand parameters of interest. The following sections will explain the implementation of the regression analyses conducted in this study. Moreover, the intensity measures and engineering demand parameters adopted in the study are presented in the next section.

4.3.1 Intensity measures and Engineering demand parameters

Intensity measures (IM) in the context of this thesis, are parameters that describe the severity of a hazard or action. Table 4.2 summarizes the IMs used in this study. The IMs were chosen based on their effect on the thermal and structural response as observed in preliminary studies. The IMs include the fuel load density which is the amount of fuel present in combustible materials in the compartment while the heat release rate is the amount of heat energy released in the compartment as a result of the fire. Other IMs considered in the study include the fire spread rate which is the velocity the fire uses to travel across the compartment while the fire size is the area occupied by the fire expressed as a percentage of the floor area.

On the other hand, engineering demand parameters (EDP) describe the response of the structure to the hazard or loading scenario, in this case travelling fires. Eight IMs and seven EDPs are considered in this study. The EDPs adopted for the study are shown in Table 4.3 and they are known to sufficiently represent the response of structures under temperature loading from fire scenarios. It should be noted that the values of the EDPs are normalized according to the structural configurations.

Table 4.2. Intensity measures considered in this study.

Intensity measure	Description	Unit
T_{max}	Maximum compartment temperature	^oC
L_f	Length of fire	m
t_b	Burning duration	min
T_{tot}	Total fire duration	min
FLD	Fuel load density	MJ/m^2
HRR	Heat release rate	kW/m^2
FS	Fire size	% of total floor area
S	Fire spread rate	m/min

Table 4.3. The engineering demand parameters adopted in this study.

Engineering demand parameter	Description
MBD	Maximum relative beam displacement
MBC	Maximum relative beam compressive force
MBT	Maximum relative beam tensile force
MCD	Maximum relative column lateral displacement
MJD	Maximum relative joint horizontal displacement
MJR	Maximum relative joint rotation
IAC	Increase in base column axial force due to fire

4.3.2 Univariate regression

As stated earlier in this chapter, it is important to assess the suitability of various IMs so that the most efficient IM is used for the performance-based design and assessment process. The efficiency of an IM is an important characteristic that can be used to determine the most adequate IM (Bray & Travasarou, 2003; Buratti (2012); Modica & Stafford, 2014). To evaluate it, regression analyses are carried out to determine the relationship between the IMs and EDPs. For the univariate regression analyses involving one IM, the natural logarithm of each EDP is

plotted against the natural logarithm of each IM in this study and the regression models are evaluated using Equation 4.1. It should be noted that the lognormality of each IM was tested to ensure that a lognormal distribution could be used to model each IM.

$$\ln EDP|IM = \alpha_0 + \alpha_1 \ln IM + e \tag{4.1}$$

where α_0 and α_1 are regression coefficients and e is the standard error which is a normally distributed variate with zero mean (Cornell et al., 2002). Equation 4.1 is used to represent a simple relationship between the IMs and EDPs and appear to capture the main trends between the variables. It is understood that more accurate equations might be used to establish the relationship between the IMs and EDPs. However, due to the complexity of the underlying process, simple empirical forms are employed in this study. The IMs and EDPs are assumed to follow a lognormal distribution based on initial assessment of the histogram of the data using fitting techniques. Moreover, the efficiency of the IMs are determined based on the values of the standard deviation which can be evaluated using Equation 4.2.

$$\sigma_{EDP|IM} = \sqrt{\frac{\sum_{i=1}^{n}(\ln EDP_i - \ln EDP|IM_i)^2}{n-1}} \tag{4.2}$$

where $\sigma_{EDP|IM}$is the standard deviation for an EDP given a particular IM and n is the number of records. According to Brav & Travasarou (2003), the most efficient IM is the one with the lowest standard deviation for a particular EDP.

4.3.2.1 Results and discussions

Scatter plot matrices are presented in Figure 4.2 and Figure 4.3 which show the regression curves that describe the relationship between the IMs and EDPs examined. Table 4.4 presents the standard deviation values of the IMs for each EDP. The EDP values are normalized to make models with different beam lengths and section sizes, considered in the study comparable. As a result, beam tensile and compressive forces are normalized against the axial capacity of the beams while displacements are normalized against their corresponding beam and column lengths.

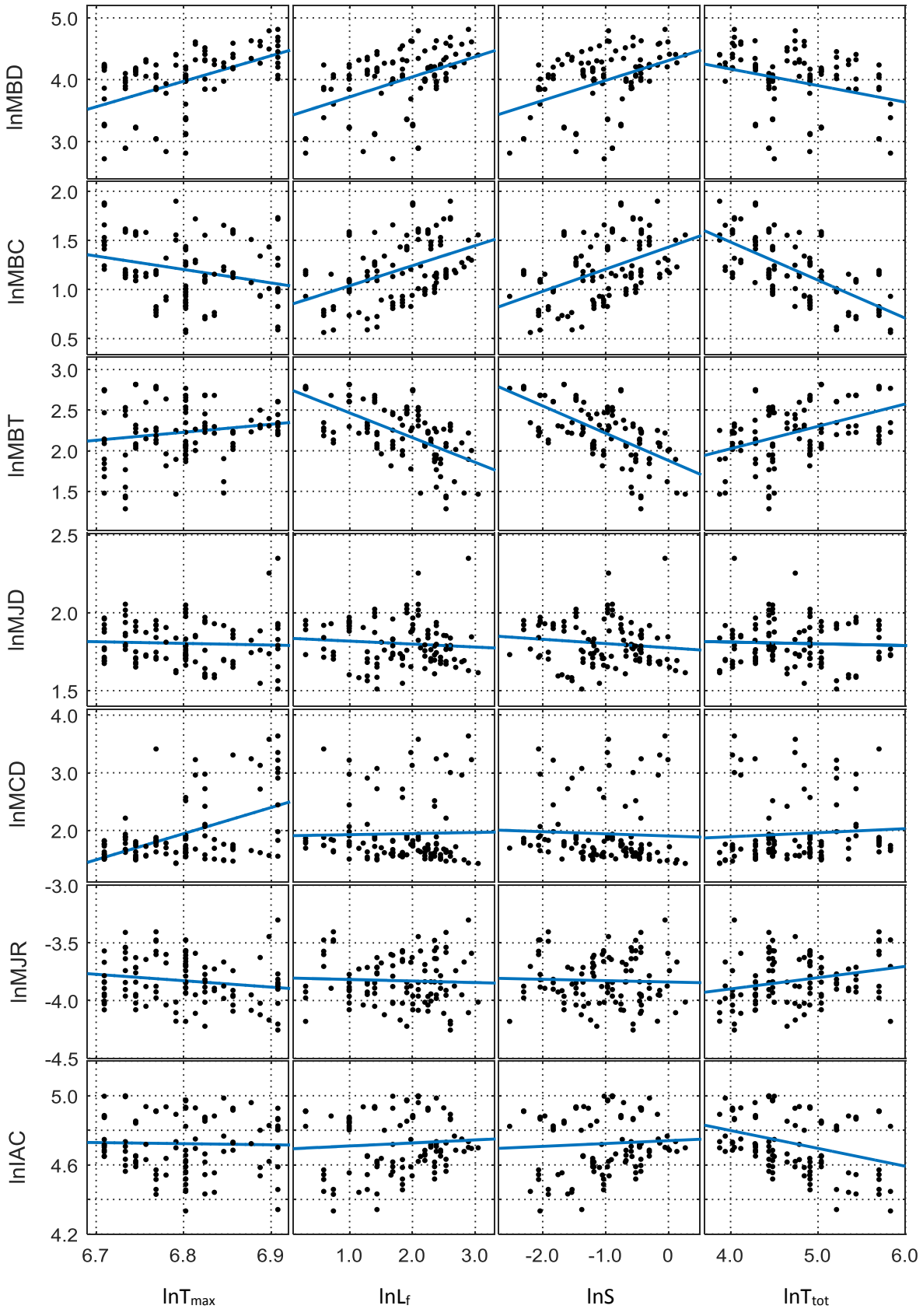

Figure 4.2. Scatter plot matrix showing the regression models of the natural logarithm of the EDPs against the natural logarithm of T_{max}, L_f, S and T_{tot}.

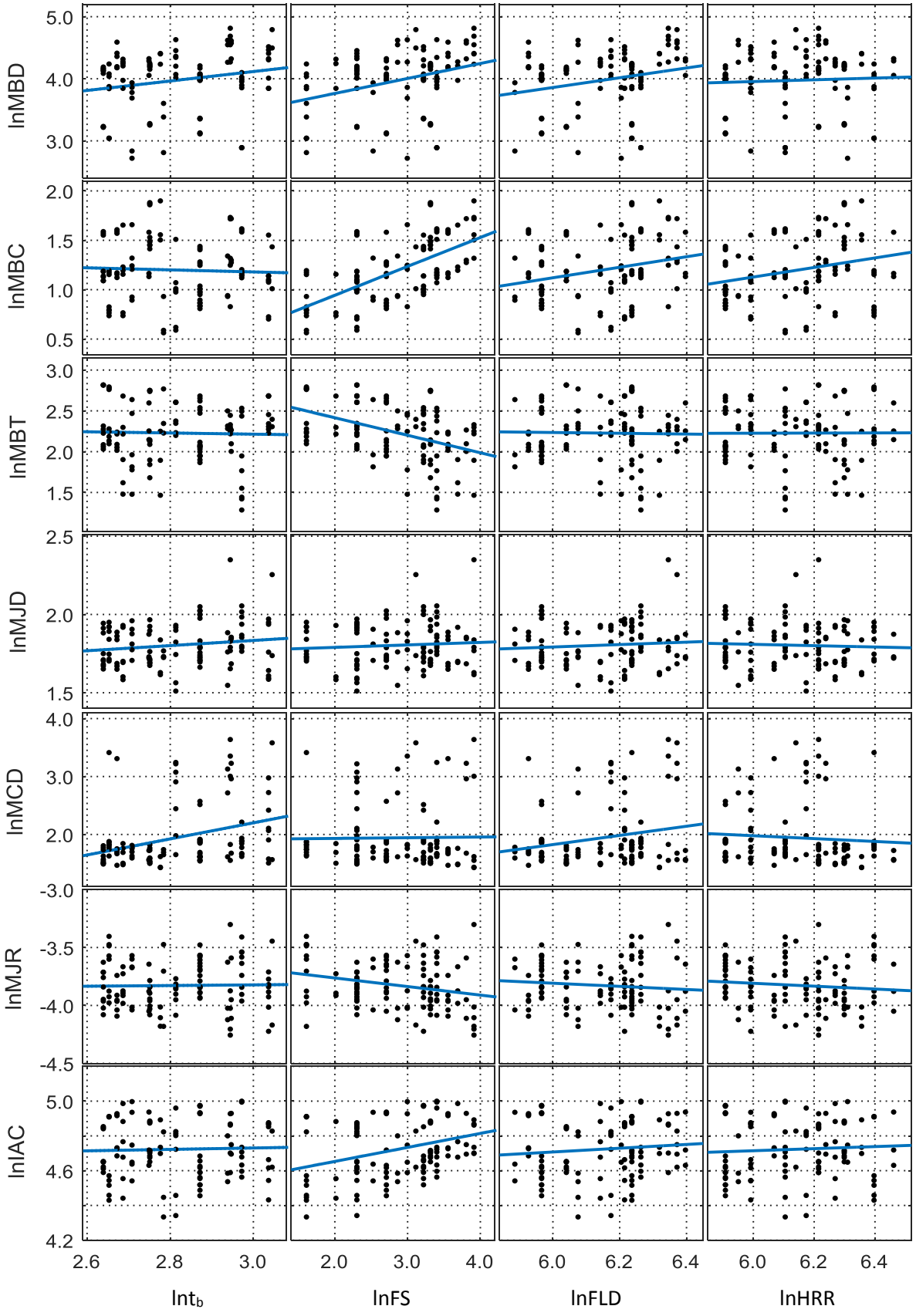

Figure 4.3. Scatter plot matrix showing the regression models of the natural logarithm of the EDPs against the natural logarithm of t_b, FS, FLD and HRR.

Table 4.4. Standard deviation of the IMs based on the selected EDPs.

	Standard deviation, $\sigma_{EDP\|IM}$							
EDP	**T_{max}**	**HRR**	**FLD**	**t_b**	**T_{tot}**	**FS**	**S**	**L_f**
MBD	0.438	0.503	0.490	0.494	0.482	0.477	0.457	0.451
MBC	0.308	0.309	0.310	0.319	0.242	0.366	0.283	0.286
MBT	0.348	0.353	0.352	0.352	0.321	0.323	0.275	0.282
MJD	0.144	0.144	0.143	0.142	0.144	0.143	0.143	0.143
MCD	0.554	0.602	0.595	0.580	0.603	0.604	0.603	0.600
MJR	0.204	0.206	0.207	0.207	0.201	0.202	0.207	0.207
IAC	0.169	0.169	0.168	0.169	0.160	0.160	0.169	0.168

From Figure 4.2 and Figure 4.3, it can be observed that some of the IMs are well correlated with the EDPs. For example, increasing levels of length of fire (L_f) and fire spread rate (S) result in an increase in the maximum relative beam displacement (MBD) and maximum relative beam compressive force (MBC). Also, an increase in the maximum compartment temperature (T_{max}) leads to an increase in MBD, which is expected since increasing temperatures reduce the ductility of structural members and result in increasing levels of deformation. However, an increase in the total fire duration (T_{tot}) is associated with a decrease in MBD and MBC, but an increase is observed for the maximum relative beam tensile force (MBT). Also, increasing values of L_f and S result in a decrease in MBT. Nevertheless, no significant correlation was observed for the maximum relative joint horizontal displacement (MJD). Note that the regression curves are only applicable to the range of values of IMs and the structural configurations considered, and may not apply to other structures.

A closer observation of Figure 4.2 reveals that sometimes increasing values of some IMs for example maximum compartment temperature, might not necessarily result in an increase in an EDP such as MBD. This can affect the regression coefficients and increase the value of standard deviation thereby affecting the accurate prediction of the structural response. For example, a travelling fire scenario with a T_{max} of 880 °C (6.75 in Figure 4.2) yields a value of MBD of 20.91 (3.04 in Figure 4.2) while a lower temperature of 850 °C results in a higher value of MBD. This is contrary to expectation as displacements are normally assumed to increase with increasing temperatures. However, due to the other factors (such as burning duration, fire size etc.) at play in the travelling fire scenario, higher temperatures might not always lead to higher displacements. As a result, it may be that a decrease in the fire size (FS) with a slight decrease in burning duration (t_b) results in a decrease in MBD when T_{max} increases based on the effect

of FS and t_b on the response of the structure. Therefore, there is a possibility that low values of MBD may be obtained for travelling fire scenarios with T_{max} between 800 °C and 900 °C and FS between 5 % and 15 %. On the other hand, the plot of lnMJD against $\ln T_{max}$ shows that high values of T_{max} and t_b can result in high values of MJD.

Eliminating some data values to improve the model can result in a substantial difference in the standard deviation. For instance, when the lower lnMBD data values for the plot of lnMBD vs. $\ln L_f$ are removed, the standard deviation reduces from 0.451 to 0.237 which is a percentage decrease of about 47 %. Figure 4.4 demonstrates the influence of the removed data values on the slope of the regression line. This shows that better structural response predictions can be obtained when a smaller range of IM values or specific structural configurations are considered. In what follows, all fire scenarios are considered and all values of the structural response parameters are used in the regression analyses for simplicity.

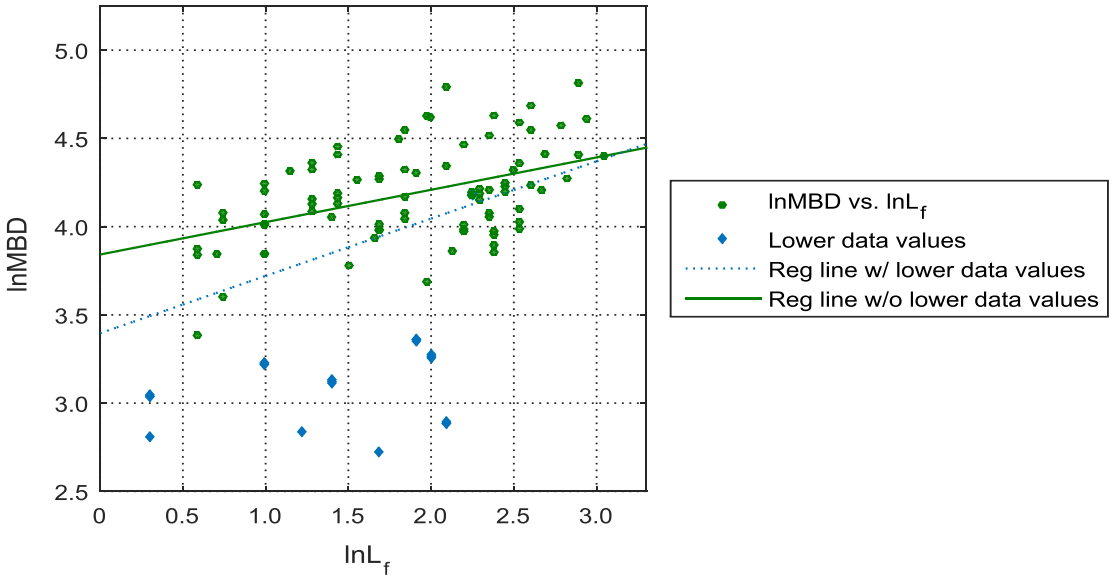

Figure 4.4. Plot of natural log of maximum relative beam displacement against natural log of length of fire showing the regression line with and without the lower lnMBD data values.

4.3.3 Efficiency of intensity measures

As stated earlier, the most efficient IM is essentially the one with the lowest value of standard deviation. Therefore, Table 4.4 demonstrates that the most efficient IM for the maximum relative beam compressive force is the total fire duration followed by the fire spread rate and length of fire. Also, the fire spread rate is the most efficient IM followed by the length of fire and total fire duration when considering the maximum relative beam tensile force. This shows

that beam axial forces can be estimated using the total fire duration, length of fire and fire spread rate. This also means that provided this information is available, compartments can be designed to ensure that compressive and tensile forces in the structural members do not exceed their capacities when subjected to travelling fires.

Considering the maximum relative beam displacement, the most efficient IM is the maximum compartment temperature followed by the length of fire and then the fire spread rate. This is as expected and it shows the effect of temperatures on the displacement of structural members in the event of a travelling fire. Also, measures can be taken in the design stage to avoid temperatures, lengths of fire or fire spread rates that can cause excessive displacements of structural members. For the maximum relative column lateral displacement, the most efficient IM is the maximum compartment temperature followed by the burning duration. This demonstrates the effects of maximum temperatures and fire burning durations on column displacements and can be used to ensure that column displacements are minimized to avoid instability or collapse of the structural frame.

The most efficient IM for the maximum relative joint horizontal displacement is the burning duration followed by the fire spread rate. This means that burning durations and fire spread rates can be used to predict the lateral stability of the frame under elevated temperatures. For the increase in base column axial force, the total fire duration is the most efficient IM followed by the fire size. This is important in foundation design as it shows that this EDP can be estimated with knowledge of expected total fire duration, which can ensure that foundations are properly designed for increased compression forces as a result of travelling fires. Finally, the most efficient IM for the maximum relative joint rotation is the total fire duration followed by the fire size. This can be helpful when designing connections to ensure that maximum rotations are not exceeded as a result of travelling fires.

From the above discussion, it is possible to identify the IMs that have a greater influence on the EDPs considered. However, it is necessary to have a more general IM that can be used to predict the EDPs and this is referred to as the most efficient IM overall. To determine this, the IMs are ranked based on the mean values of standard deviation for all the EDPs considered as shown in Table 4.5. The ranking is performed with 8 being the least efficient IM and 1, the most efficient IM. Considering the mean standard deviation value of the fire spread rate (S) and the length of fire (L_f) in Table 4.5, it can be deduced that they are the most efficient IMs for performance-based travelling fire design and assessment based on the structural configurations

and EDPs considered in the study. This validates the preliminary result presented in Teslim-Balogun et al. (2017).

Table 4.5. Ranking of IMs based on the mean standard deviation.

Intensity measure	Mean σ	Rank
Fire spread rate (S)	0.305	1
Length of fire (L_f)	0.305	2
Total fire duration (T_{tot})	0.307	3
Maximum compartment temperature (T_{max})	0.309	4
Burning duration (t_b)	0.323	5
Fuel load density (FLD)	0.324	6
Fire size (FS)	0.325	7
Heat release rate (HRR)	0.326	8

When EDPs such as the maximum relative beam compressive force, beam displacement, column lateral displacement and joint horizontal displacement are considered, the fire spread rate and length of fire remain the most efficient IMs. This check is necessary as these EDPs are the most widely used structural response parameters in structural engineering. The study also reveals the importance of other IMs like the maximum compartment temperature and the total fire duration as they are efficient IMs for particular EDPs. Realistically, it is impractical to assume that the most efficient IMs identified in this section can be used alone as a measure of fire intensity since all fire parameters are naturally linked. This means that in a practical sense, it is preferable to consider two or more IMs for performance-based travelling fire design and assessment. This will require that a multivariate regression analysis is first carried out.

4.3.4 Multivariate regression

Due to the nature of travelling fires and the correlation between fire parameters, it may be necessary to consider more than one IM for a better performance-based structural assessment. A lower standard deviation value is expected when two or more IMs are combined which will result in an increase in the efficiency of the estimation. However, it is important that the chosen IMs for combination are adequate. This can be determined by plotting the residual of an IM against another. A significant correlation in the plot will point towards the suitability of the IMs to provide a better description of the travelling fire.

The maximum compartment temperature is taken as the first IM in this study and it is combined with each of the other IMs to form a Vector IM. Previous studies have used the maximum compartment temperature as the IM for performance-based structural fire assessment (Lange et. al., 2014) and as a result it is considered as the first IM for combination in this study. For the multivariate regression analyses, the natural logarithm of each EDP is plotted against the natural logarithm of the maximum compartment temperature (IM_1) and a secondary intensity measure (IM_2), and regression functions are determined using Equation 4.3.

$$\ln EDP_i|IM = \beta_0 + \beta_1 \ln IM_1 + \beta_2 \ln IM_2 + e \tag{4.3}$$

where β_0, β_1 and β_2 are regression coefficients and e is the residual error of regression. The standard deviation values of the Vector IMs for each EDP are determined and the residuals of the EDPs for the maximum compartment temperature are plotted against the secondary intensity measure. A significant correlation in the plot shows that the second IM can be combined with the maximum compartment temperature to form a suitable Vector IM, which is more efficient compared to when Scalar IMs are considered. The standard deviations of the Vector IMs for each EDP are shown in Table 4.6 while Figure 4.5 shows the plot of the residuals of three of the EDPs for the maximum compartment temperature against the maximum compartment temperature, length of fire and fire spread rate.

Table 4.6. Standard deviation of the Vector IMs.

EDP	Standard deviation of Vector IMs						
	T_{max}, HRR	**T_{max}, FLD**	**T_{max}, t_b**	**T_{max}, T_{tot}**	**T_{max}, FS**	**T_{max}, S**	**T_{max}, L_f**
MBD	0.428	0.419	0.439	0.416	0.416	0.379	0.382
MBC	0.304	0.301	0.310	0.228	0.234	0.274	0.274
MBT	0.349	0.349	0.348	0.318	0.317	0.269	0.272
MCD	0.144	0.144	0.142	0.144	0.144	0.143	0.144
MJD	0.556	0.544	0.547	0.556	0.557	0.555	0.554
MJR	0.203	0.204	0.205	0.198	0.200	0.205	0.205
IAC	0.169	0.170	0.169	0.160	0.161	0.169	0.169

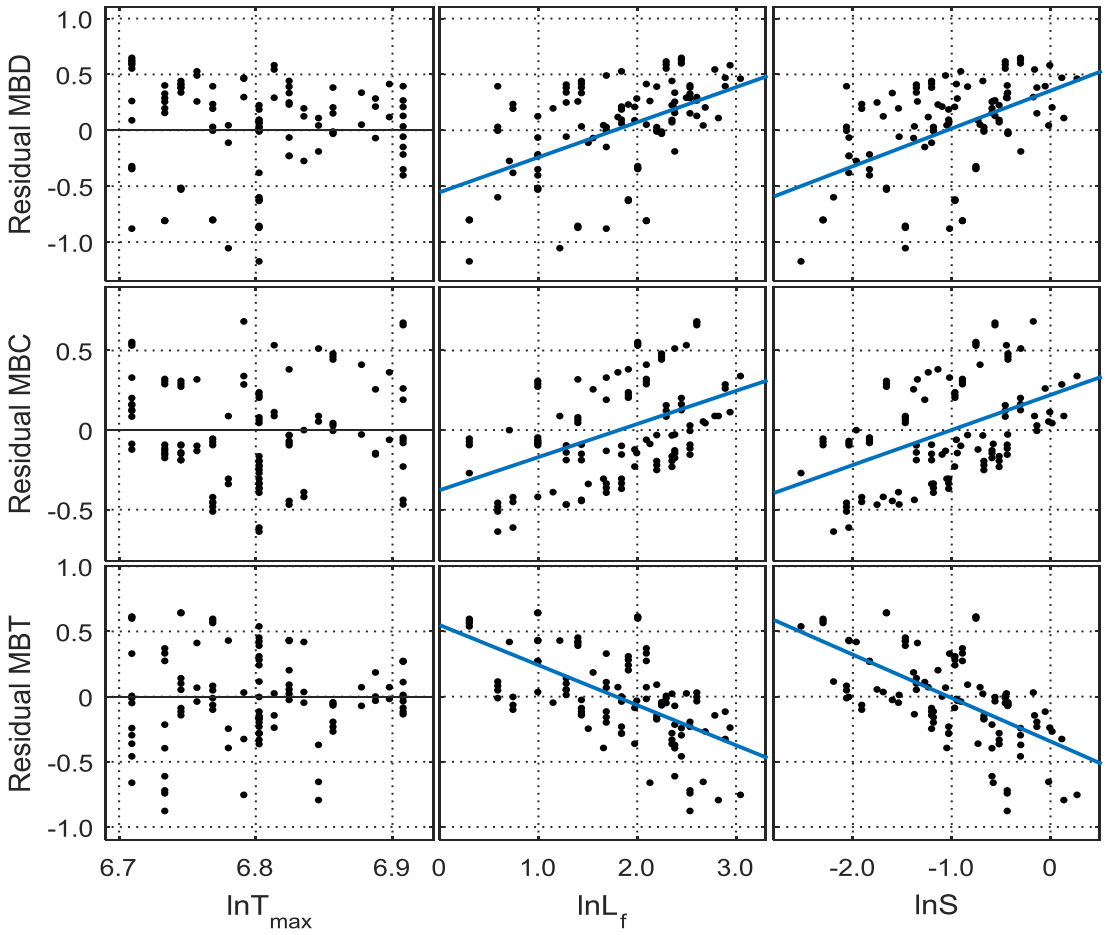

Figure 4.5. Scatter plot matrix for residuals of natural log of MBD, MBC and MBT for T_{max} against natural log of T_{max}, L_f and S.

It can be observed from Table 4.6 that the combination of two IMs results in a lower standard deviation when compared to Scalar IMs for the EDPs considered. This is also evident in Figure 4.5 since the residual plots for the maximum compartment temperature show good correlation with the length of fire and fire spread rate. The most efficient Vector IM for each EDP is considered to be the Vector IM with the lowest value of standard deviation.

The efficiency of the IM is expected to improve with the use of a Vector IM. However, in the case where the EDP does not have significant correlation with the IMs, a Vector IM may not be required as there will be little difference between the standard deviation of the Vector IM and the Scalar IMs. Nevertheless, ranking the Vector IMs based on the mean values of the standard deviation for the EDPs as in the case of the Scalar IM will result in the most efficient Vector IM for performance-based travelling fire assessment as demonstrated in Table 4.7.

Table 4.7. Ranking of Vector IMs.

Vector IM	Mean σ	Rank
T_{max},S	0.285	1
T_{max},L_f	0.286	2
T_{max},T_{tot}	0.289	3
T_{max},FS	0.290	4
T_{max},FLD	0.304	5
T_{max},HRR	0.308	6
T_{max},t_b	0.309	7

Based on the mean standard deviation values in Table 4.7, the combination of the maximum compartment temperature and either the length of fire or fire spread rate can be used as a Vector IM within a performance-based travelling fire framework for the structural configurations considered. This is because they represent the most efficient intensity measures that can be used to represent the severity of the travelling fire. This also strengthens the justification for considering travelling fires in building compartments since the length of fire and fire spread rate are important parameters of the Travelling Fire Methodology.

4.4 Performance-based travelling fire assessment

Several intensity measures have been accessed for their efficiency and suitability for use within a performance-based framework in the previous section. It was shown that Vector IMs consisting of the maximum compartment temperature and the length of fire or fire spread rate are the most efficient IMs for the framework. In this section, a performance-based framework for travelling fires is formulated and used to justify the importance of the Travelling Fire Methodology using the EDP and IM values examined in the previous section. The first two parts of a performance-based framework – hazard and structural analyses are developed in this study and the probability of exceeding the engineering demand parameter for the selected intensity measures is determined.

4.4.1 Hazard analysis

This is the first part of a performance-based design framework. Here, the intensity measures are selected and the annual rate of exceeding the IM is evaluated. In this section, maximum compartment temperature (T_{max}) and length of fire (L_f) are chosen as the IMs based on the

results of the assessment carried out in the previous section and both IMs are assumed to follow a lognormal distribution based on an initial assessment of the data by considering the suitability of various distributions. The hazard analysis is carried out considering Scalar IMs and a Vector IM of T_{max} and L_f. Equation 4.4 is used to evaluate the annual rate of exceeding the IMs (λ_{IM}) while the probability of exceeding the Scalar IMs, $P(IM)$ is determined based on the CDF of the lognormal distribution.

$$\lambda_{IM} = \lambda_E P(IM) \tag{4.4}$$

where λ_E is the annual rate of occurrence of an event, which in this case is a travelling fire. In probabilistic structural fire design, the annual rate of a structurally significant fire is usually obtained as the product of the probability of occurrence of fires per m^2 for the occupancy, the probability of flashover occurring, the area of the compartment and reduction factors based on active fire protection systems in the building and/or fire brigade response (Sleich et al., 2002). Assuming the floor area is divided into two compartments of area 378 m^2, the annual rate of a structurally significant fire in each compartment is 1.18e-6 based on a probability of fire occurrence of 2e-7 m^2/year and reduction factors of 0.0625 and 0.25 for smoke alarms system and remote monitoring by the fire brigade respectively. For simplicity, λ_E is taken as 1 since the study only compares the differences between the exceedance rates of the EDPs. Also, there is inadequate information about the rate of occurrence of travelling fires. Therefore, this study only evaluates the probability of exceedance of the EDP and not the annual rate of exceedance. For the Vector IM, the joint probability distribution is determined using Equation 4.5:

$$f(X, \mu, \Sigma) = (2\pi\sqrt{|\Sigma|})^{-1}\exp(-\frac{1}{2}(X-\mu)\Sigma^{-1}(X-\mu)^T) \tag{4.5}$$

where μ and X are vectors of the mean and variables respectively, and Σ is the covariance matrix. The covariance matrix consists of the variance of each variable on the diagonal and the covariance between variables, which is a function of the correlation (ρ) between the variables. The probability of exceedance is G(X) which is 1 – CDF value, and the plot is known as the hazard curve.

In this study, the probability of exceedance of the Vector IM is evaluated for three values of correlation between T_{max} and L_f which are ρ = 0, 0.8 and -0.8. They represent zero correlation, high positive correlation and high negative correlation between the two IMs respectively. These values of correlation are chosen because it is possible that during the random selection of

parameter values for the travelling fire scenarios, some information might have been lost regarding the actual correlation between the IMs. It is expected that the actual correlation value will fall within the values chosen and the correlation between both IMs is expected to differ based on configuration of the compartment and amount of heat energy released as a result of the fire.

The Probability distribution function (PDF) and Probability of exceedance (POE) curves for Scalar IMs – T_{max} and L_f are shown in Figure 4.6. The Joint Probability of exceedance of the Vector IM is illustrated in Figure 4.7 while the PDF contour and surface plots for the Vector IM are presented in Figure 4.8.

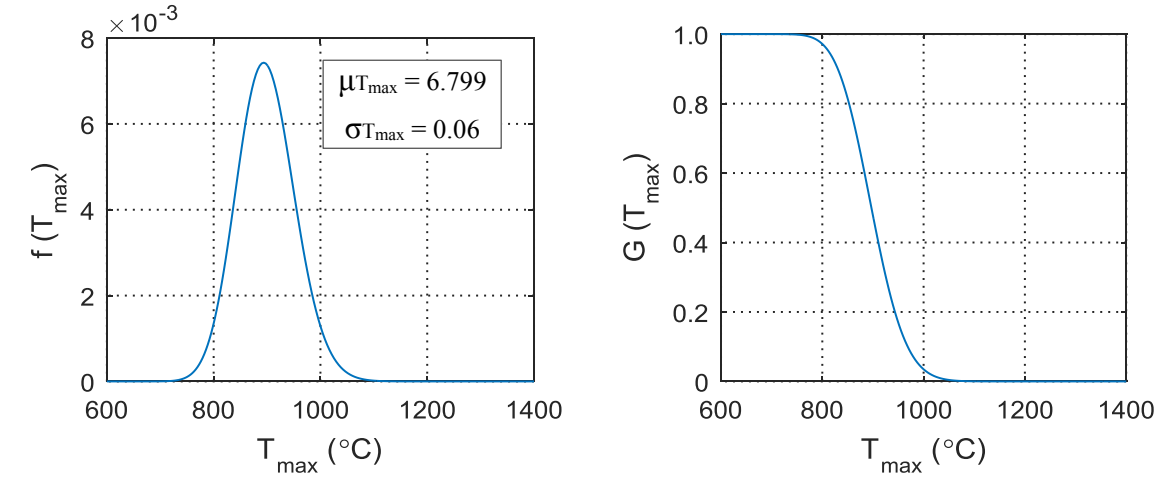

(a) PDF of T_{max}

(b) POE of T_{max}

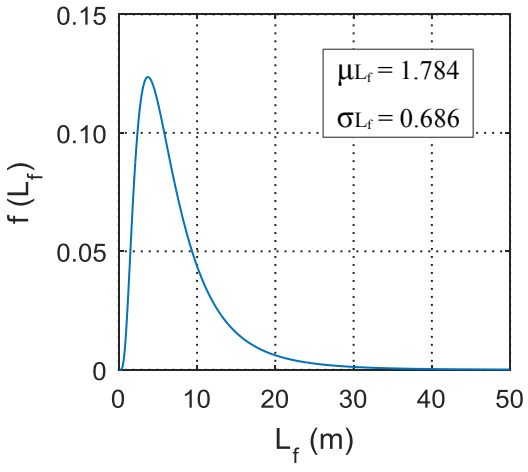

(c) PDF of L_f

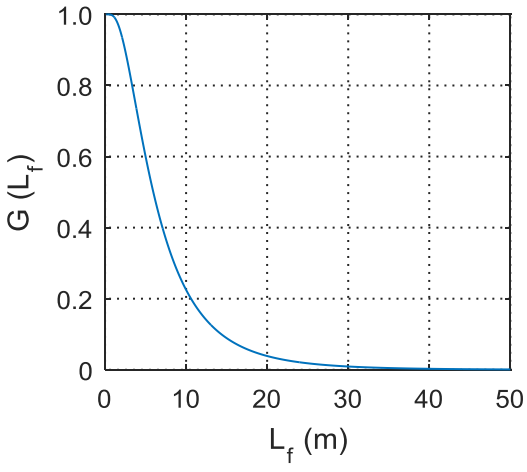

(d) POE of L_f

Figure 4.6. PDF and POE curves of maximum compartment temperature and length of fire.

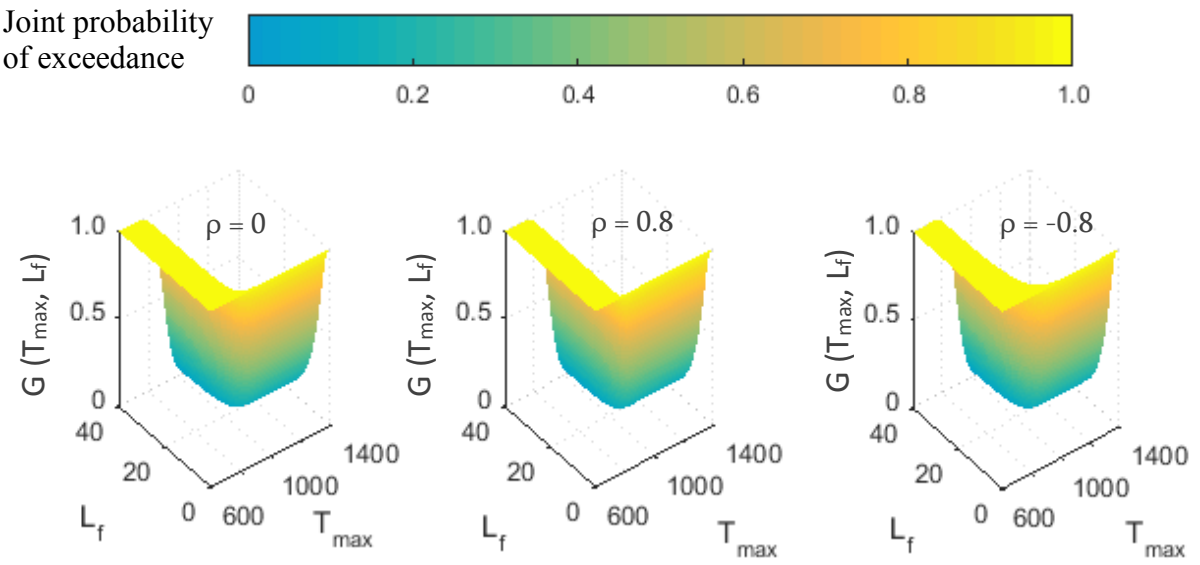

Figure 4.7. Joint POE of maximum compartment temperature and length of fire.

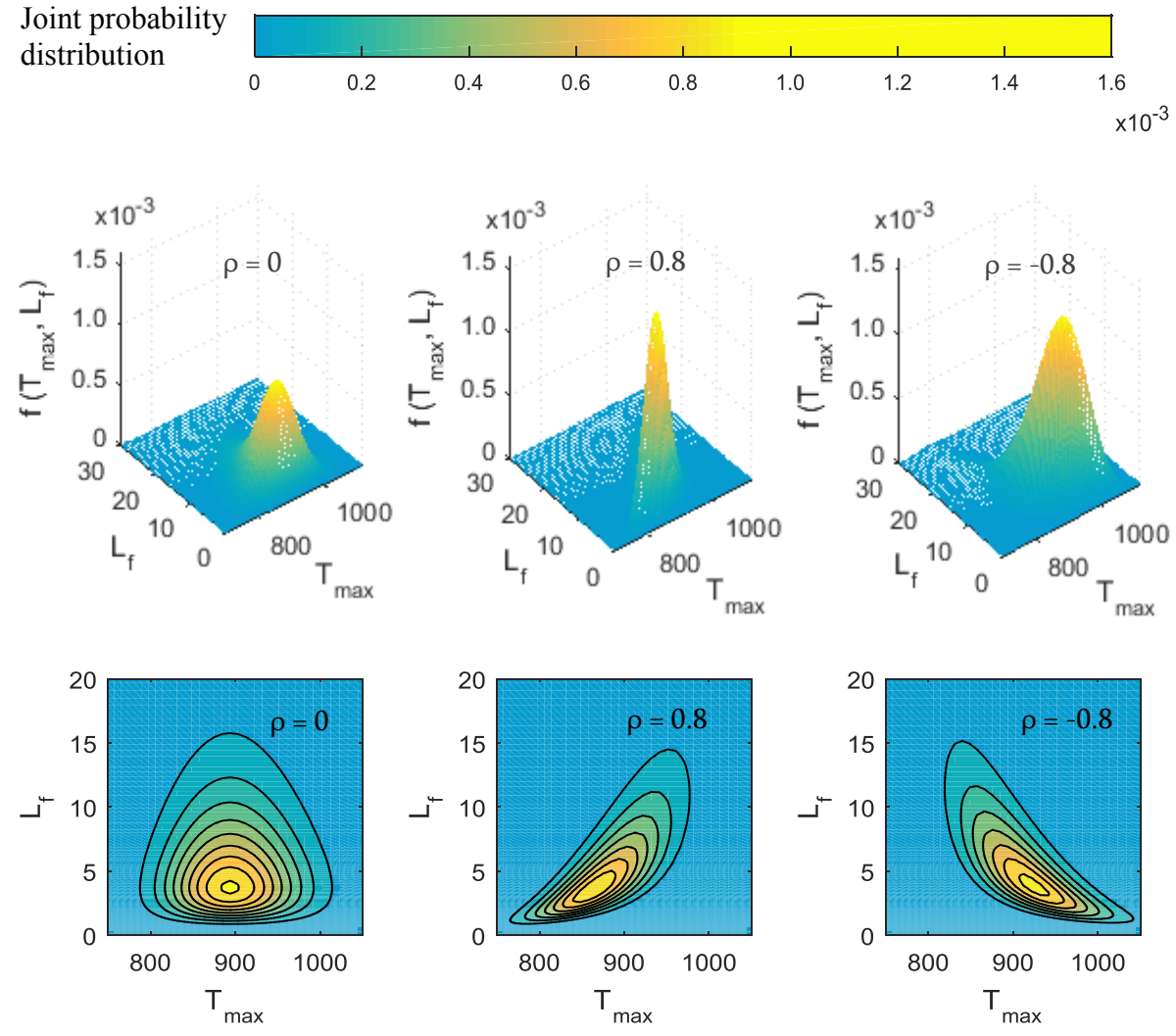

Figure 4.8. Joint PDF of maximum compartment temperature and length of fire (surface and contour plots).

4.4.2 Structural analysis

The second part of a performance-based framework is the structural analysis. Here, non-linear structural analyses are carried out on the numerical model and values of the engineering demand parameters (EDP) are recorded. The EDPs chosen for the study are Maximum relative beam displacement (MBD) and Maximum relative beam compressive force (MBC) as they were found to have good correlations with the IMs based on the assessment carried out earlier in this chapter. This part of the framework is used to determine the annual rate of exceeding the EDP (λ_{EDP}) which is integrated numerically using Equation 4.6 below:

$$\lambda_{EDP} = \int P\,(EDP|IM)|d\lambda_{IM}\,| \tag{4.6}$$

where $P\,(EDP|IM)$ is the probability of exceeding a value of EDP given a value of IM and λ_{IM} is the annual rate of exceeding the IM. Figure 4.9 shows the PDF of MBD considering the Scalar IMs and the Vector IM while Figure 4.10 shows that of MBC. Based on initial assessment of the data by comparing various distributions, a lognormal distribution was adopted for MBD and MBC. For the Vector IM, $P\,(EDP|IM)$ is integrated over the whole IM hazard curve considering all combinations of both IMs for the range of values of each IM. A check that $d\lambda_{IM}$ sums up to 1 is then conducted to determine if the number of values of each IM is sufficient. The Probability of exceedance of MBD for the Vector IM considering the three values of correlation and the Scalar IMs are illustrated in Figure 4.11 while that of MBC is shown in Figure 4.12.

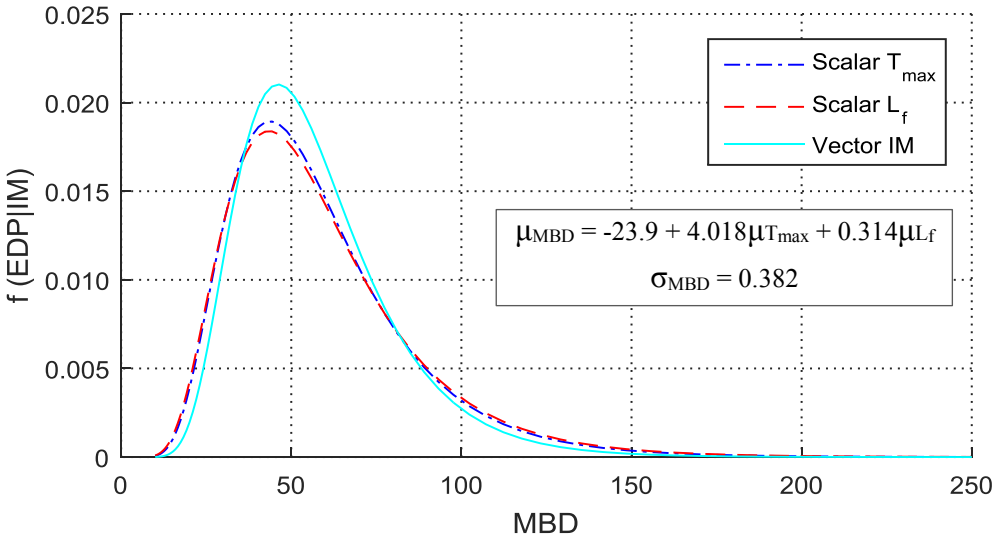

Figure 4.9. PDF of maximum relative beam displacement given the IMs.

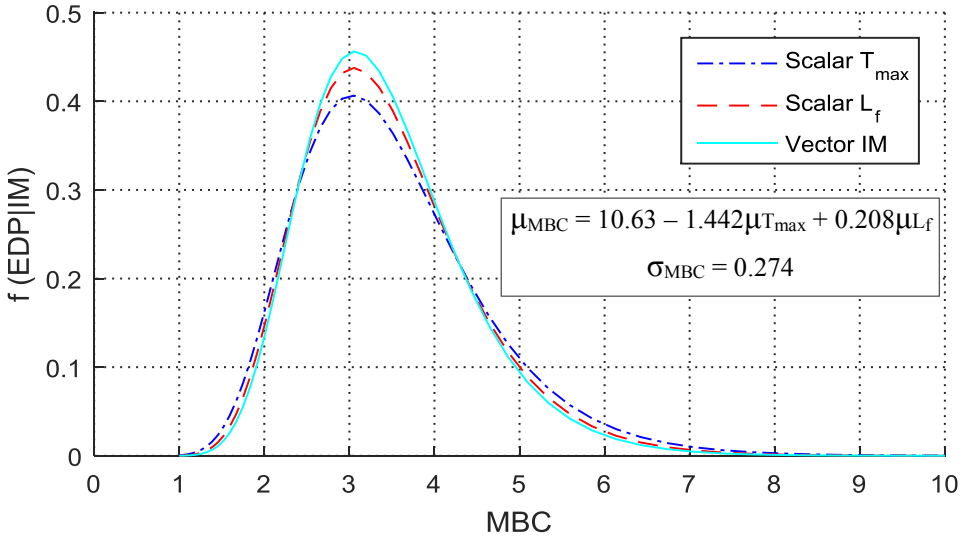

Figure 4.10. PDF of maximum relative beam compressive force given the IMs.

Figures 4.9 and 4.10 were determined based on the equations of the regression models as there was a good correlation between the IMs and the EDPs. An initial assessment of the distribution of the structural analysis results shows that they fit well with the lognormal distribution of the EDPs adopted in the study, especially when the Vector IM is considered.

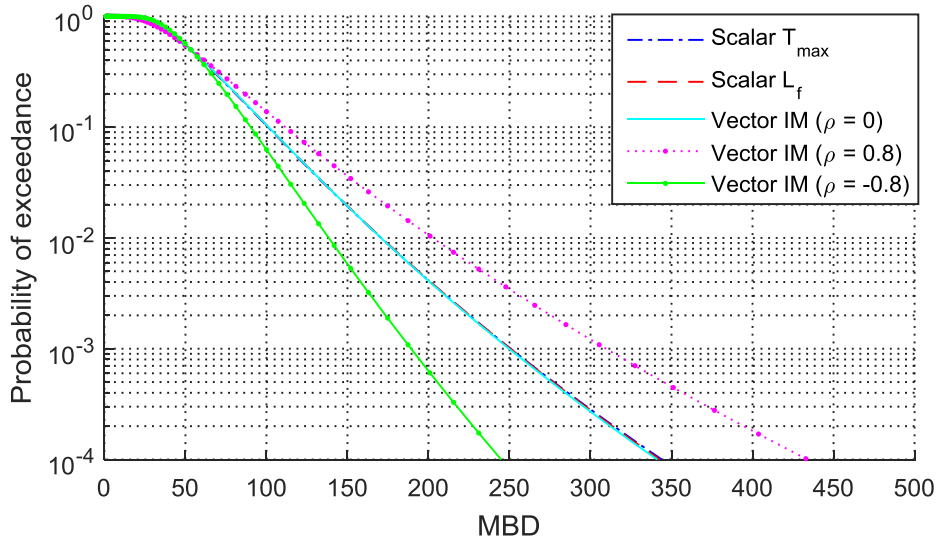

Figure 4.11. Probability of exceedance of maximum relative beam displacement.

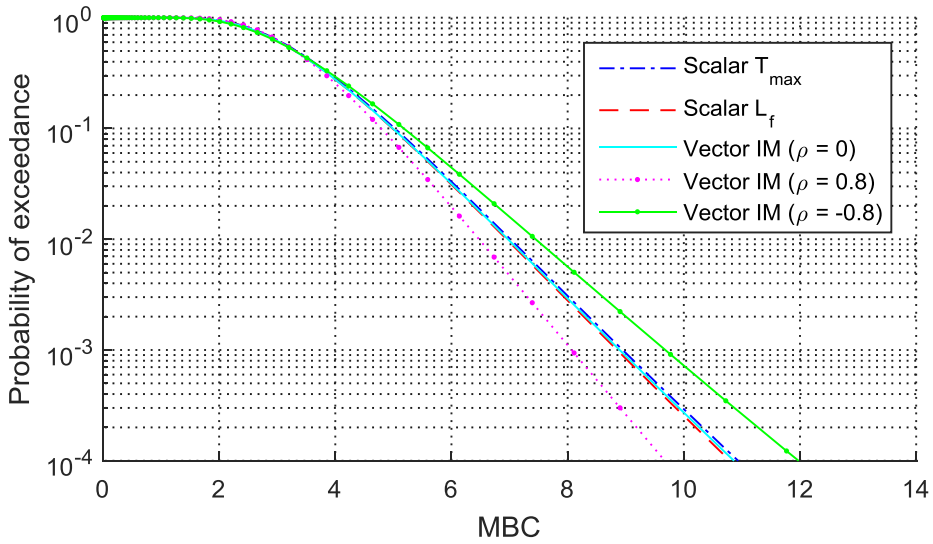

Figure 4.12. Probability of exceedance of maximum relative beam compressive force.

4.4.3 Discussion

It can be observed from the results presented above that the PDF values are higher for the high positive and negative correlation case compared to that of zero correlation as seen in Figure 4.8, which in turn has an effect on the Joint probability of exceedance. Also, comparing the PDF of the EDPs for the Scalar IMs with that of the Vector IM in Figure 4.6, it can be observed that, as expected, the standard deviation for the Vector IM is lower with higher values of PDF compared to the Scalar IMs. The PDF also shows the effect of the Vector IM especially in the case of MBD. Although this is quite well known, the above observations have been stated to show that the selected IMs reduce the variability and are well suited to describe the response of the structure under the travelling fire scenarios.

The effect of the different correlation values is demonstrated in Figure 4.11 for MBD and Figure 4.12 for MBC, which show the Probability of exceedance plots of the EDPs with the y-axis in log scale. The plots show that the POE is similar for the zero correlation case of the Vector IM and the Scalar IMs, which means that a Vector IM is unnecessary if there is no correlation between the IMs. The figures also demonstrate that for very low values of POE, there is a significant difference in the EDP values when there is a high level of correlation between the IMs. In Figure 4.11, which is the POE plot of MBD, this difference is even more evident. The percentage difference between the high correlation plots and the zero correlation case is depicted in Figure 4.13 for MBD and Figure 4.14 for MBC.

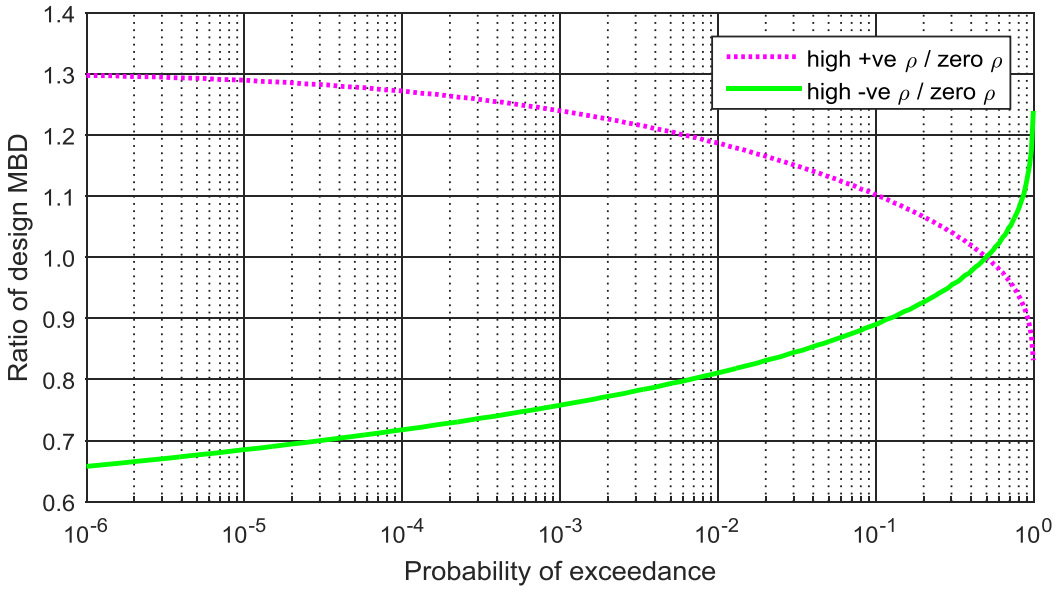

Figure 4.13. Ratio of maximum relative beam displacement for the high positive and negative correlation to the zero correlation case for different probabilities of exceedance.

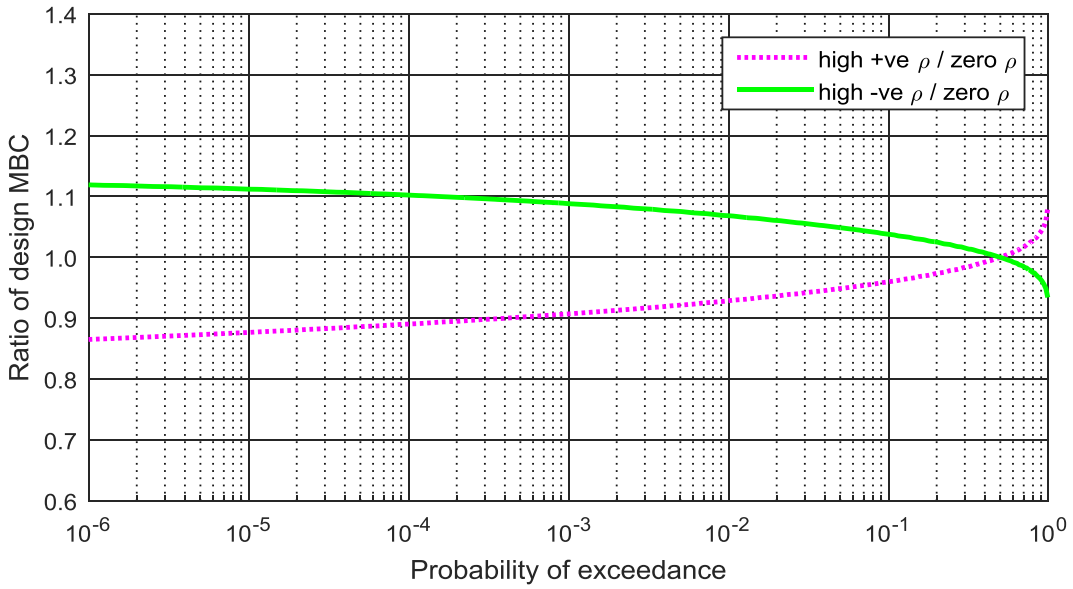

Figure 4.14. Ratio of maximum relative beam compressive force for the high positive and negative correlation to the zero correlation case for different probabilities of exceedance.

Plots of the ratio of the EDPs for the positive and negative correlation case to that of zero correlation for different values of probabilities of exceedance are shown in Figure 4.13 for MBD and Figure 4.14 for MBC. Figure 4.13 demonstrates that MBD can increase or decrease by about 30 % when there is high correlation between the IMs for very low probabilities of

exceedance while Figure 4.14 shows that MBC can increase or decrease by about 10 % when low probabilities of exceedance are expected. However, the actual percentage difference between the high correlation and zero correlation case will depend on the annual rate of occurrence of the travelling fire which is assumed to be 1 in this study.

High positive correlations between the length of fire and maximum compartment temperature may be expected in large open plan compartments such as in large office buildings, which can therefore potentially increase the expected value of beam displacements based on the interaction between the length of fire and the maximum compartment temperature. As a result, it is essential that performance-based techniques are used to design or access structures for structural fire resistance in order to ensure that all possible scenarios are properly taken into consideration and a reasonable risk level is chosen.

4.5 Conclusions

From the study, it can be concluded that a Vector IM of the maximum compartment temperature and length of fire or fire spread rate is adequate for a performance-based travelling fire framework for the EDPs and structural configurations considered. This study also shows the importance of using a Vector IM to achieve a better prediction of the EDP and the probability of exceedance, as Scalar IMs might underestimate or overestimate EDP values when there is significant correlation between the IMs for low probabilities of exceedance.

As a result, the study demonstrates that maximum compartment temperature alone cannot be used to describe the severity of a fire as is the case with current design methods and other fire parameters such as the length of fire should be considered as well, which makes it important for travelling fires to be considered in structural fire design.

Chapter 5
Effects of Blast and Travelling Fires on Steel Frames

5.1 Introduction

The past studies on explosions reviewed in Chapter 2 have shown that there is a likelihood of a fire occurring after a blast event and that this fire is likely to travel especially in larger compartments. This makes it necessary to study the behaviour of structures under the effect of such multi-hazard conditions. In this chapter, parametric analyses are carried out to determine the effects of blast pressure, fire size, maximum compartment temperature and direction of travel on the structural performance of steel frames. An initial study is first performed to determine the most vulnerable floor when the fire from the blast event is: (i) a horizontally travelling fire on one floor, (ii) a multi-floor horizontally travelling fire burning simultaneously or (iii) a vertically travelling fire. These studies are carried out in order to have a better understanding of the performance of steel structures when subjected to blast and travelling fires which will inform the latter parts of this thesis.

5.2 Blast and fire parameters

The numerical model with the 9 m composite beam presented previously in Figure 3.17 is used for this study. An axial load that corresponds to 5 extra floors is applied at the top of the column. Random values for suitcase bombs ranging from 10 kg to 50 kg occurring at different locations in the compartment are generated for the blast. This is used to calculate the scaled blast parameter Z. Subsequently, the corresponding blast pressures and time durations of the blast are evaluated in accordance with US DoD (2008).

A triangular pressure-time history with a fictitious positive time duration can be used in design to represent the blast history based on the value of the reflected blast pressure and impulse (Ngo et al., 2007). As a result, negative pressures are not considered herein. In this study, 5 blast pressures were selected for the parametric analyses and they were found to provide an adequate range of pressures that can affect the structural response significantly. The blast pressures are applied on the structural members in the affected compartment.

Three maximum compartment temperatures and fire sizes are considered in this study noting that the temperature in the compartment is mainly a function of the fuel loads, heat release rate

and compartment configuration. The travelling fire is assumed to occur in the region adjacent to the location of the blast and two directions of travel are considered. A heat release rate per unit area of 500 kW/m^2 and a fuel load density of 570 MJ/m^2, recommended for office buildings in BSI (2002), are assumed herein. Figure 5.1 illustrates a potential blast location and the directions of travel for a subsequent fire of 10 % of the floor area. Table 5.1 shows the blast parameters in the study while Table 5.2 shows the fire parameters adopted in the study.

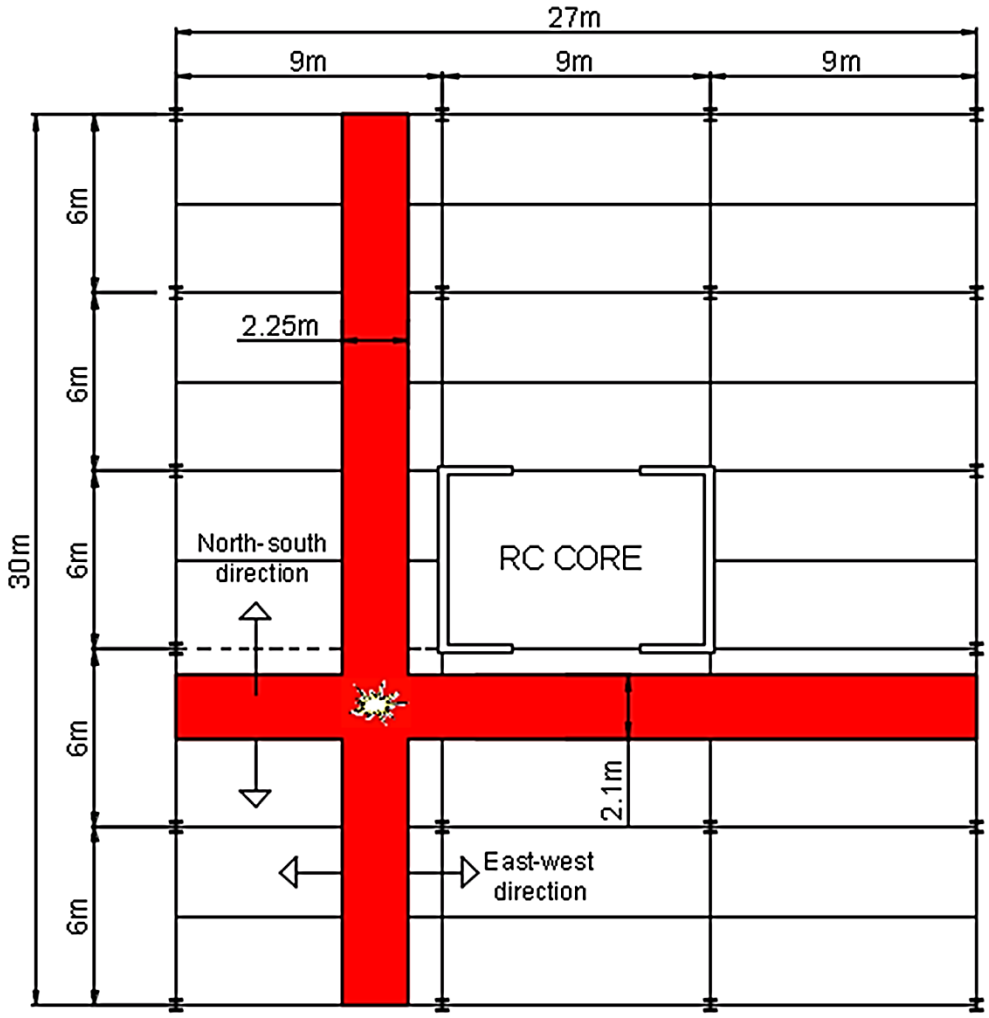

Figure 5.1. Position of a blast source from the centre of the beam (in dotted lines) and directions of travel for a travelling fire of 10 % of the floor area.

Table 5.1. Blast parameters.

Charge weight (kg)	Distance (m)	Scaled parameter Z	Reflected pressure (kPa)	Reflected impulse (kPa-ms)	Fictitious duration (msec)	Blast load on beam (kN/m)	Blast load on column (kN/m)
10	10.0	4.65	117	293.21	5.03	350	700
20	11.9	4.37	133	396.20	5.94	400	800
30	12.9	4.14	150	481.75	6.42	450	900
40	13.5	3.95	167	558.81	6.71	500	1000
50	14.0	3.79	183	630.52	6.88	550	1100

Table 5.2. Travelling fire parameters.

Parameter	Range of values
Max compartment temperature	800, 900 and 1000 °C
Fire size	10, 25 and 50 % of floor area
Direction of travel	North-south and East-west
Heat release rate	500 kW/m^2
Fuel load density	570 MJ/m^2

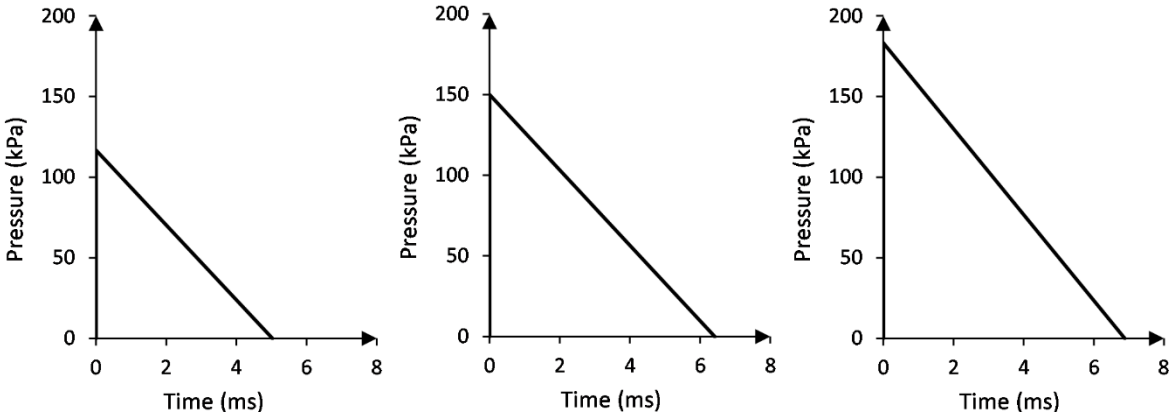

Figure 5.2. Typical pressure-time histories of the blast loads.

Figure 5.2 shows the pressure-time histories of some of the blast loads. Shear failure of the connection can occur before flexural failure of the beam occurs. However, shear failure of connections was not considered in this study due to the assumption of fully rigid connections between the beam and column. The tributary area considered for the beam is the length of the beam multiplied by the spacing of the beam taken as 3m in this study while the tributary area of the column considered is the height of the column multiplied by the column spacing of 6m.

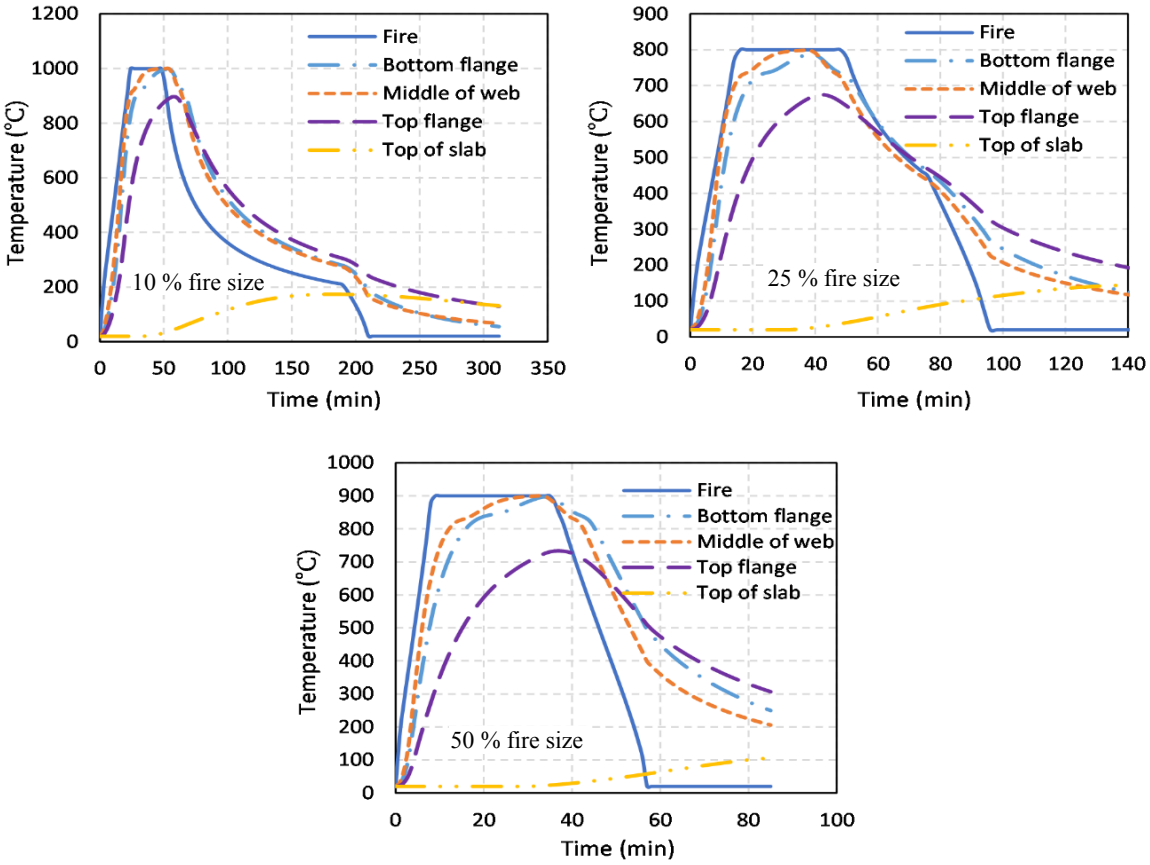

Figure 5.3. Typical temperature-time curves of the travelling fire scenarios.

Figure 5.3 shows the temperature-time curves of some of the travelling fire scenarios and illustrates the evolution of temperatures at different locations in the beam section. Analyses were initially carried out for different blast and travelling fire scenarios to determine the most vulnerable floor before performing the parametric analyses. The preliminary analyses carried out are discussed in the next section.

5.3 Preliminary studies

Initial studies were carried out to determine the most critical floor in the steel frame as discussed below. The blast pressure used in the analyses is the 30 kg blast that resulted in a reflected pressure of 150 kPa. Also, a maximum compartment temperature of 800 °C and a fire size of 25 % of the floor area is assumed for the travelling fire. Only one direction of travel is considered (north-south direction). Maximum mid-span beam displacement, maximum column lateral displacement at mid-height and maximum total beam axial force increment (i.e., force due to blast and travelling fire only) are used to compare the structural response at different

floor levels. The displacements are normalized against member lengths while the beam axial forces are normalized against the axial capacity of the beam.

5.3.1 Blast and horizontally travelling fire

In this study, the steel frame is analysed for a blast and horizontally travelling fire on a single floor of the building. The analysis is carried out for all the floor levels in order to determine the most critical floor beams and columns in the frame under both actions. Table 5.3 shows the maximum displacements and axial forces of the beam and column in each storey subjected to the blast and horizontally travelling fire. Figure 5.4 illustrates the deformation of the frame when each storey is subjected to the blast action while Figure 5.5 shows the deformation of the frame when each storey is subjected to the subsequent fire action.

From the results, the highest beam displacement is observed when the first storey is subjected to the blast and travelling fire. The second highest beam displacement is observed when the fifth storey is subjected to both actions while the lowest beam displacement is observed when the sixth storey is subjected to the loading scenarios. This shows that in the event of a blast and travelling fire happening on a single floor, the ground floor beam is likely to experience higher values of beam displacements. This is due to the structural configuration of the first storey which has a lower number of elements to absorb the impact of the actions in comparison to other storeys. However, Table 5.3 shows that the maximum beam displacements values are very similar. The results also show that the highest column displacement occurs in the seventh storey column when the seventh storey is subjected to both actions and the maximum column displacement decreases as the floor number decreases. This can be due to non-linearity such as P-Δ effects which can cause upper floor columns to experience higher values of column displacement under blast and travelling fires since the resistance to loads from floors above is reduced.

Examining the results of the maximum beam axial force show that the compressive force decreases as the floor number increases so that the highest normalized compressive force occurs in the first floor beam when the first storey is subjected to the blast and travelling fire. However, the highest tensile force occurs in the seventh floor beam when both actions are applied at the seventh storey. The high compressive force in the first floor beam is expected to be as a result of reduced redistribution of forces since there are no beams below it that can absorb some of the forces.

Table 5.3. Structural response when individual storeys are subjected to blast and travelling fire.

Affected storey	Maximum beam displacement in affected storey (% of beam length)	Maximum column displacement in affected storey (% of column height)	Maximum beam axial force increment in affected storey	
			Compression (% of axial capacity)	Tension (% of axial capacity)
1st	4.359	0.409	32.903	17.604
2nd	4.057	0.735	-26.319	18.955
3rd	4.102	0.737	-26.391	18.548
4th	4.110	0.728	-25.847	18.679
5th	4.220	0.736	-26.473	17.924
6th	3.993	0.758	-24.116	16.927
7th	4.134	0.939	-8.829	19.459

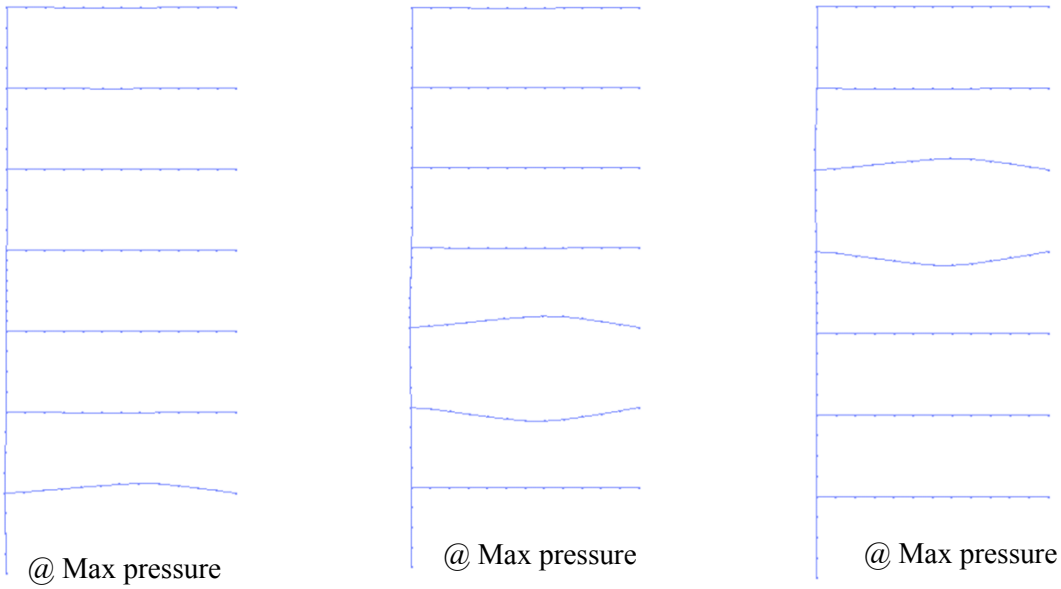

Figure 5.4. Deformation of the frame when the 1st, 3rd and 5th storeys are subjected to the blast load (5x magnification of displacements).

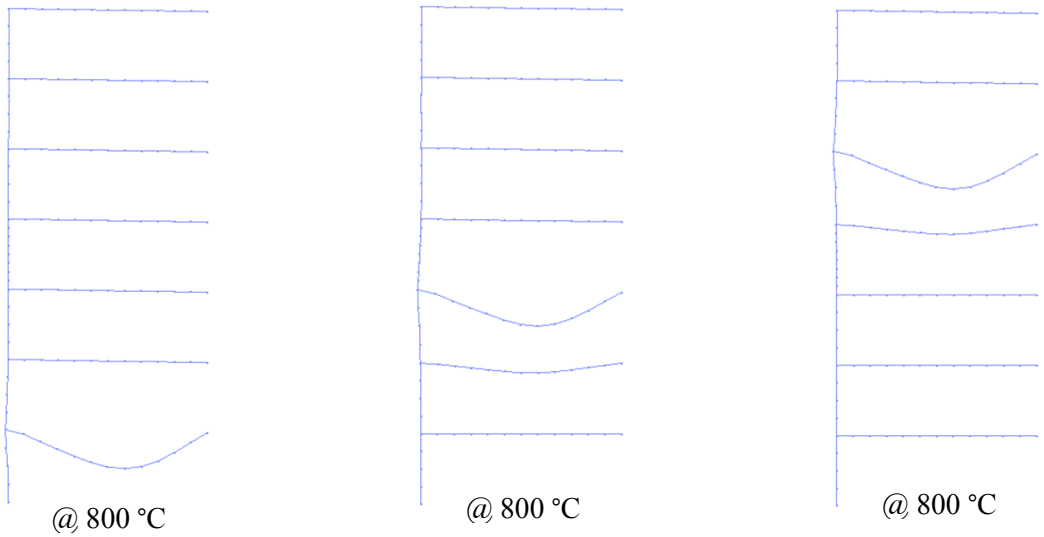

Figure 5.5. Deformation of the frame when the 1st, 3rd and 5th storeys are subjected to the subsequent travelling fire (5x magnification of displacements).

5.3.2 Blast and multi-floor horizontally travelling fire

In this study, the response of the steel frame under the effect of a blast load followed by a horizontally travelling fire burning simultaneously in one or more floors is explored. This study is carried out in order to determine which storey level is most vulnerable to the combined actions under multiple floor fires. The multi-floor fire is modelled assuming that the ignition of the floor subjected to the blast load causes fire to burn in more than one floor at the same time (i.e. on the assumption that fire spread is very rapid and instantaneous). The blast load is initially applied at the first storey. Another set of analyses is then performed for the blast occurring in the fourth storey. The storey levels subjected to the travelling fire for each case are denoted by the pink rectangles in Figures 5.6 and 5.7.

Blast load at 1st storey (ground floor compartment)

Figure 5.6 illustrates the structural response at different storey levels when the blast occurs in the first storey and the fire extends to one or more floors. The maximum beam displacement is recorded in the first floor beam when only the first storey is under fire since the blast occurred in the first storey. Also, the highest beam displacement is observed in the first floor beam for most of the cases of multiple floors involved in the fire. However, the lowest beam displacement is observed in the seventh floor beam when all the multiple floor fire scenarios are considered since it is the furthest from the blast load. Also, it is observed that the lowest column displacement occurs in the first storey while the highest column displacement occurs

in the second storey when 3 floors are burning at the same time. Figure 5.6 also shows that the highest compressive and tensile forces occur in the first floor beam since the blast occurred in the first storey. As the number of floors burning at the same time increases, it is observed that the first floor beam still experiences the highest compressive forces while the highest tensile force occurs in the second floor beam. Figure 5.8 illustrates the deformation of the frame due to the blast occurring at the 1st storey and multiple floor travelling fires.

Blast load at 4th storey (third floor compartment)

The structural response when the blast occurs at the fourth storey followed by multiple floor fires is shown in Figure 5.7. It is observed that when the blast occurs at the fourth storey, the fourth floor beam experiences the highest beam displacement overall. This only occurs when the fire in the fourth storey extends to the third storey. However, as the number of floors subjected to fire increases to three or more, other floors are observed to have higher displacements particularly the first, second and fifth floor beams. As a result, a significant reduction in the deformation of the fourth floor beam is observed when the number of floors subjected to fire increases even though the blast occurs in the fourth storey. This means that beams very close to the location of the blast have the tendency to deflect more in the event of a subsequent travelling fire because, part of the energy from the blast is dissipated to the surrounding beams. When all the floors are subjected to the travelling fire, the first floor beam experiences the highest maximum displacement as seen in Figure 5.7.

It is also observed from Figure 5.7 that the column subjected to the blast (fourth storey column) is the most vulnerable. However, surrounding columns such as the columns in the third and fifth storey levels are also observed to have high displacements as the number of floors burning increases. However, the column displacements decrease as the distance from the affected column increases. Figure 5.7 also shows that the fourth floor beam experiences the highest axial force when the fire involves up to 2 floors. However, as the number of floors subjected to fire increases, other floors are subjected to higher compressive and tensile forces. When there are 4 or 5 floors subjected to the travelling fire, the second floor beam sustains the highest compressive force but, when six or seven floors of the building are under fire, the highest compressive force occurs in the first floor beam. Also, when the number of floors subjected to fire is greater than or equal to 3, the fifth floor beam experiences the highest tensile force. The deformation of the frame during the multiple floor fire when the blast occurs at the fourth storey is shown in Figure 5.9.

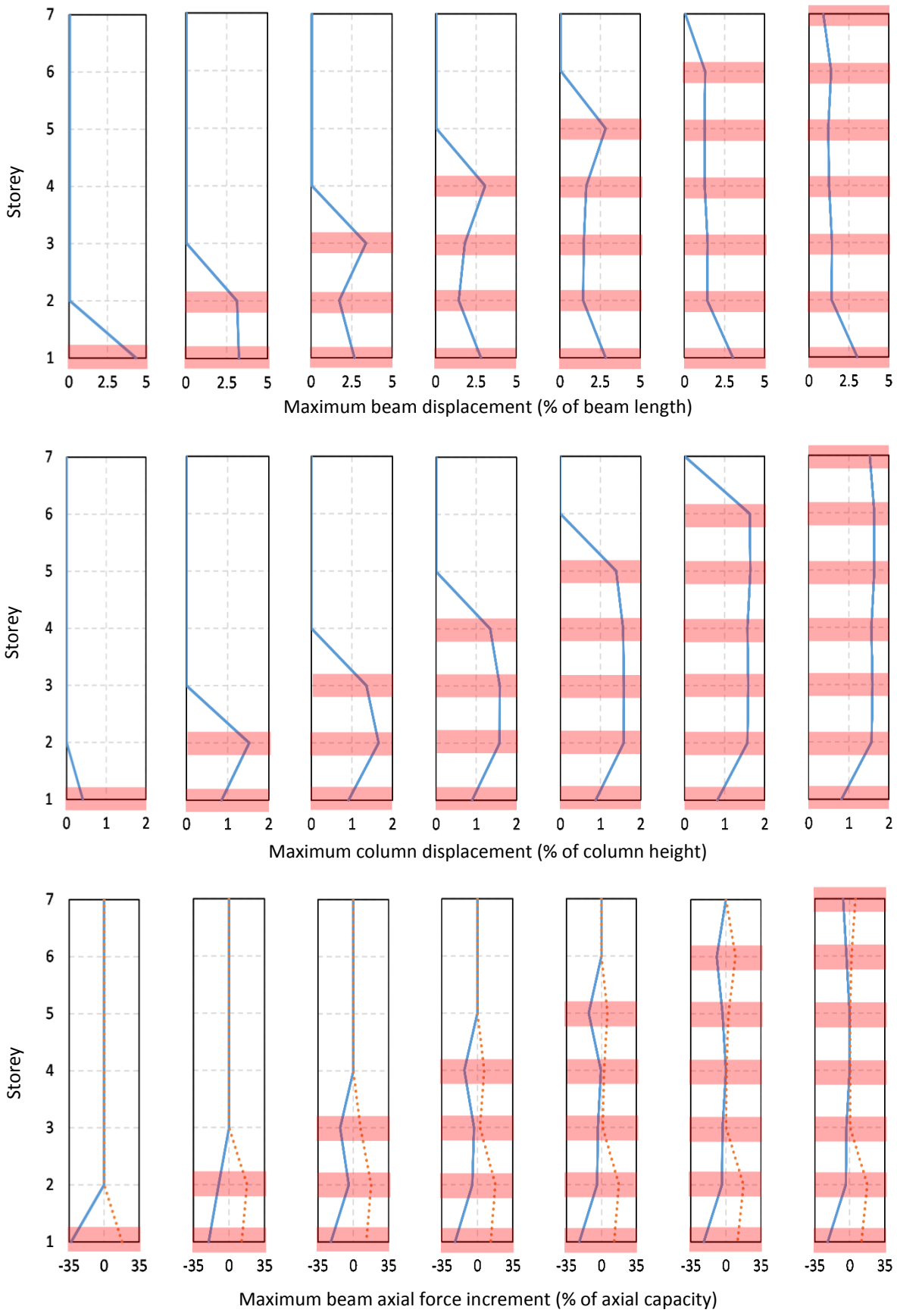

Figure 5.6. Structural response at different storey levels as number of floors under fire increases for blast at the 1st storey (dotted lines represent tension and pink rectangles indicate storeys under fire).

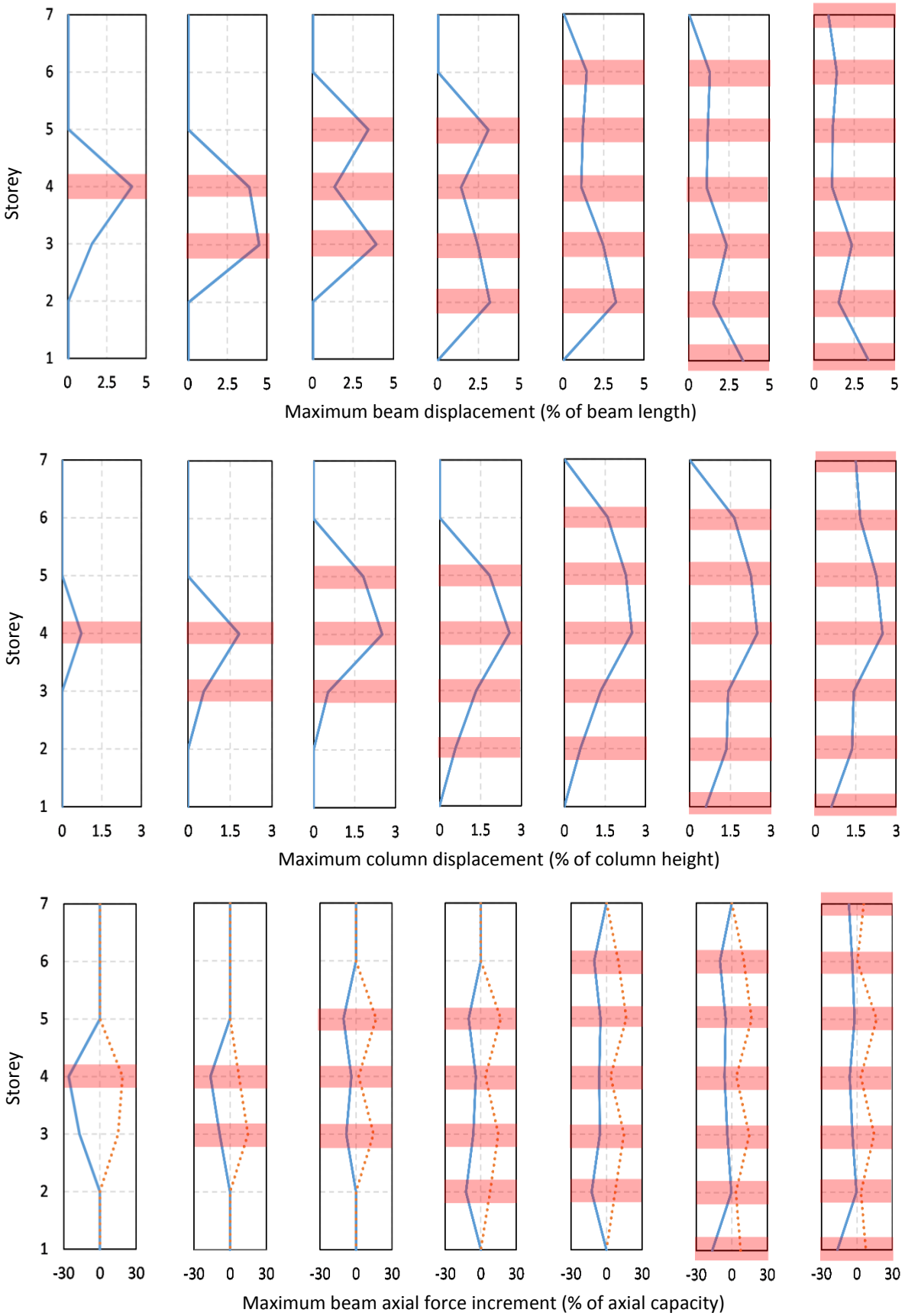

Figure 5.7. Structural response at different storey levels as number of floors under fire increases for blast at the 4th storey (dotted lines represent tension and pink rectangles indicate storeys under fire).

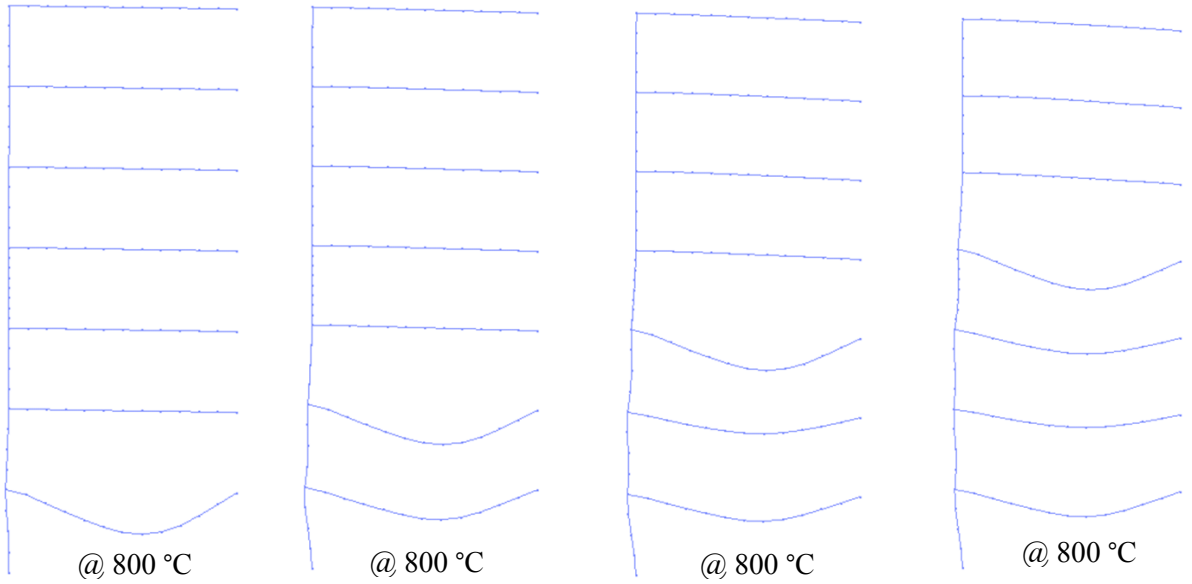

Figure 5.8. Deformation of the frame during multiple floor fires for an initial blast at the 1st storey (5x magnification of displacements).

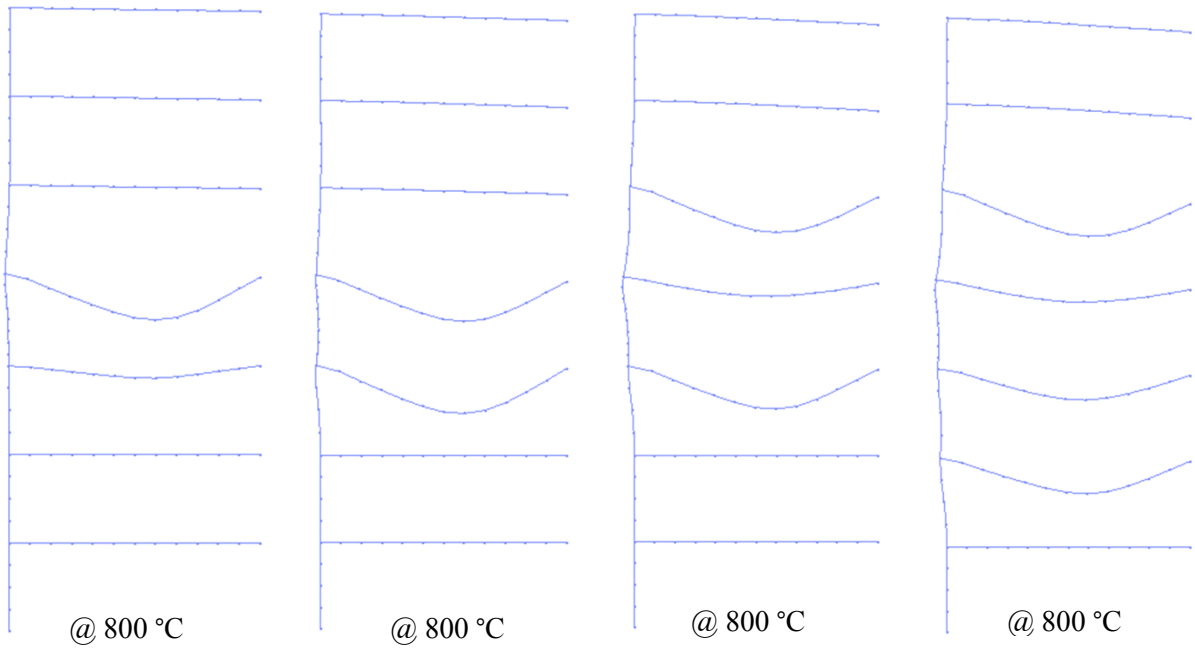

Figure 5.9. Deformation of the frame during multiple floor fires for an initial blast at the 4th storey (5x magnification of displacements).

5.3.3 Blast and vertically travelling fire

This section examines the effects of blast pressures followed by vertically travelling fires on steel frames. To this end, the steel frame under consideration is first analysed for a 30 kg blast load occurring at the first storey followed by a vertically travelling fire which travelled from

the first storey (ground floor) to the seventh storey (sixth floor). Another analysis is then carried out with the blast occurring at the fourth storey followed by a vertically travelling fire which travelled upwards and downwards from the fourth storey as illustrated in Table 5.4. The time delay between the fire spreading to adjacent floors is taken as 15 mins in both cases.

Table 5.4. Ignition pattern of the vertically travelling fire for blast load at the 4th storey.

Time of ignition (min)	Storey
0	4
15	3 & 5
30	2 & 6
45	1 & 7

30kg blast at the 1st storey

Figure 5.10 shows an envelope of the maximum values of the structural response at each storey when the blast occurs at the ground floor. It can be observed from this figure that the first and second floor beams experience higher values of beam displacements compared to the upper floor beams. This is because the blast occurred at the first storey and therefore, higher beam displacements will occur in the beams close to the location of the blast. However, the lowest maximum lateral displacement is observed in the ground floor column while the highest lateral displacement occurs in the sixth storey column. This is due to the fixed connection at the base of the ground floor column which will limit the lateral displacement at this level. It is expected that the ground floor column will experience very high displacements when large explosives are detonated at the first storey.

Under the blast and vertically travelling fire, the highest compressive force occurs in the first floor beam. However, the highest tensile force occurs in the second floor beam followed by the first floor beam. The high values of axial force in the first floor beam are as a result of the proximity to the location of the blast and the stiffness of the ground storey when compared with other storeys in the frame. The deformation of the frame during the vertically travelling fire is illustrated in Figure 5.11.

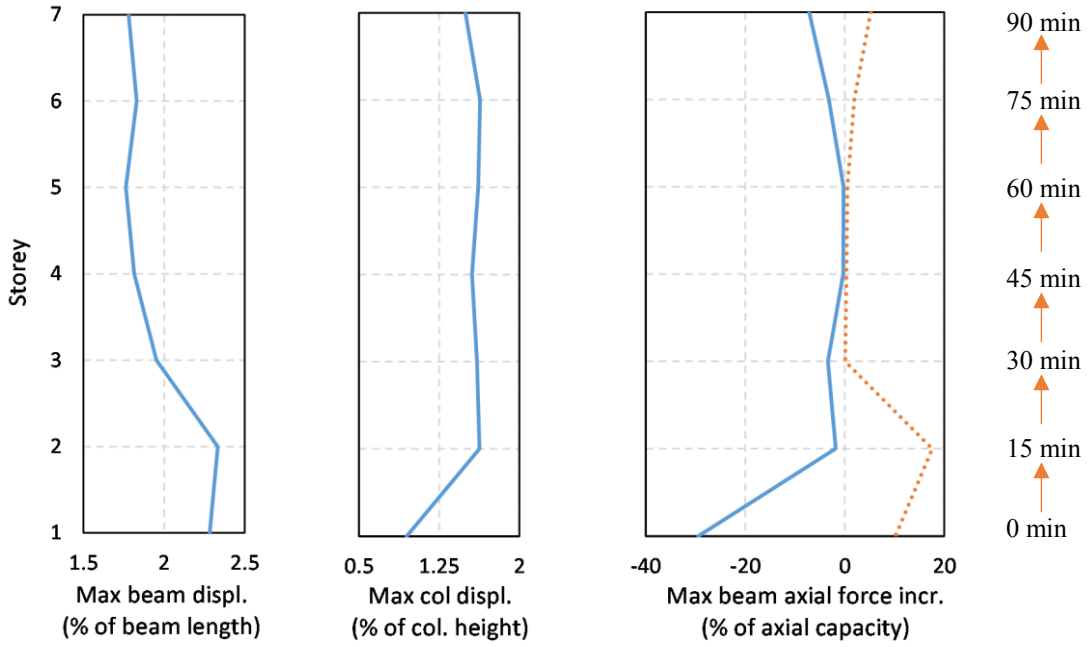

Figure 5.10. Envelope of structural response showing the maximum values at different storey levels for a 30 kg blast at the 1st storey and a vertically travelling fire (dotted lines represent tension and ignition time of each storey is indicated).

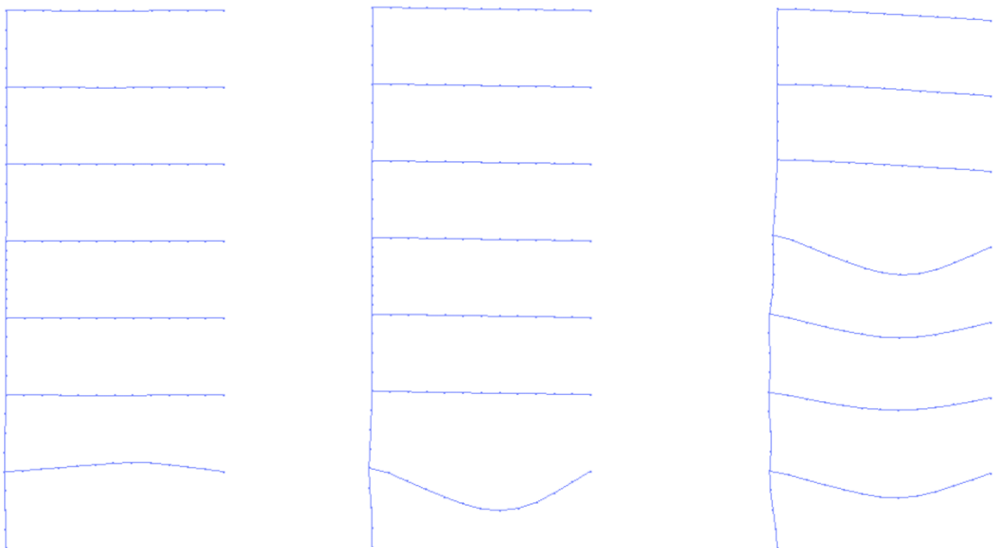

(a) During the blast (b) Ignition of first storey (c) Fire travelling from 1st to 4th storey

Figure 5.11. Deformation of the frame during the vertically travelling fire for an initial blast at the 1st storey (5x magnification).

30kg blast at the 4th storey

The envelope of maximum values of the structural response when the blast occurs in the fourth storey is illustrated in Figure 5.12. As in the case of the blast at the first storey, higher beam

displacements are also observed in the lower floor beams (i.e. first to third) compared to the upper floor beams. This is interesting because it shows that even though the blast did not occur at the first storey, it still experiences the highest beam displacement, making it the most critical floor in the building. Also, as the fire travels from one floor to a lower floor, there is an increase in displacement, but when the travel direction is in the upward direction, a decrease in displacement is observed. This indicates that the fire requires less energy to travel downwards and more energy to travel upwards. As a result, for the same energy level, the impact on the beam is higher when the fire travels downwards.

Figure 5.12 also shows that higher lateral displacements can occur in the upper level columns which is due to the fixed connection at the base of the frame. The figure also shows that the highest compressive force occurs in the first floor beam while the highest tensile force occurs in the fifth floor beam. It is also observed that surrounding floor beams above and below the fourth floor beam are subject to higher tensile forces, but lower compressive forces. This is because the fourth storey being the location of the blast has floors above and below it that help to redistribute the forces and reduce compressive forces in the beam. The high tensile force is due to the beams being located in the region of the blast load. Figure 5.13 illustrates the deformation of the frame during the vertically travelling fire.

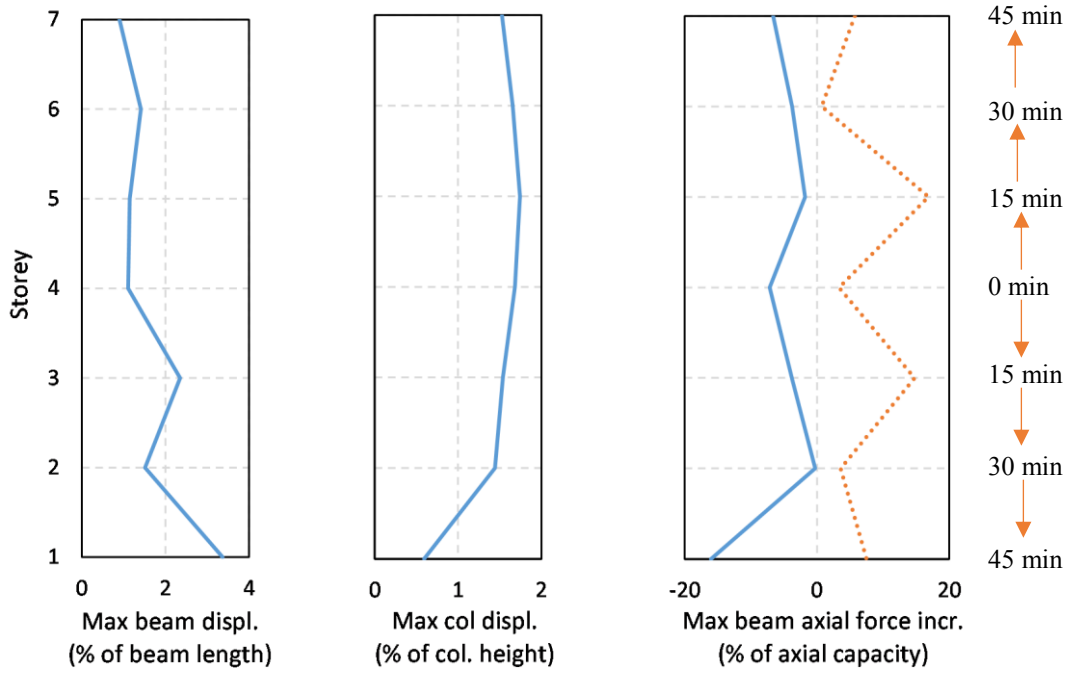

Figure 5.12. Envelope of structural response showing the maximum values at different storey levels for a 30 kg blast at the 4th storey followed by a vertically travelling fire (dotted lines represent tension and ignition time of each storey is indicated).

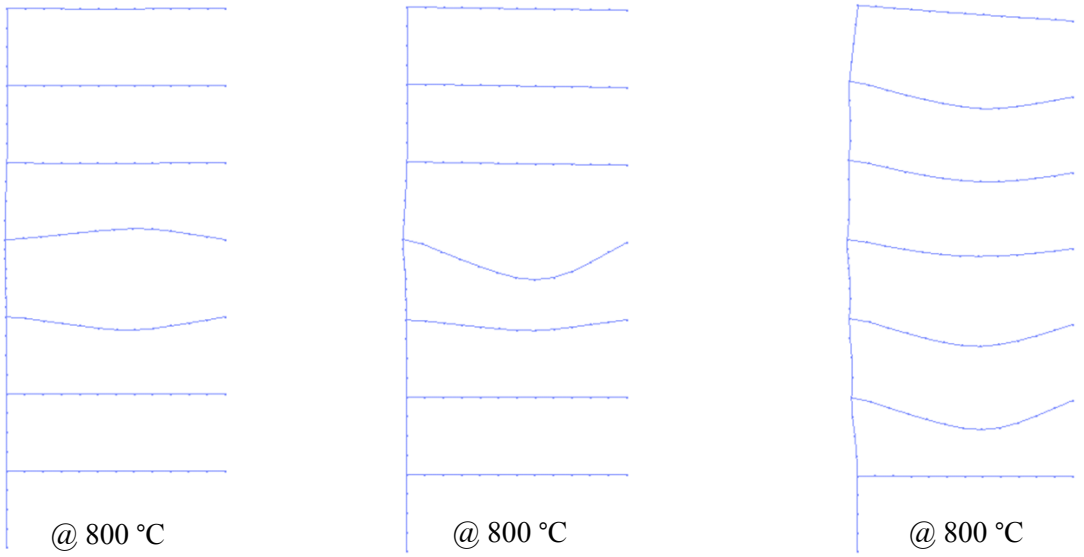

Figure 5.13. Deformation of the frame during the vertically travelling fire for an initial blast at the 4th storey (5x magnification of displacements).

5.3.4 Discussion

The preliminary studies carried out so far have shown that for an initial blast load, the first floor beam will experience the highest displacements and compressive forces under a horizontally travelling fire on a single floor. Also, floor beams in the region of the blast tend to have higher displacements and axial forces under multiple floor horizontally travelling fires. Moreover, the first floor beam will have the highest displacements and axial forces when all the floors are engulfed in fire. Nevertheless, the highest displacement and compressive force under a vertically travelling fire was observed in the first floor beam even when the blast did not occur in the first storey. Upper floor columns were observed to have higher displacements for the three fire scenarios even when the blast occurred at the first floor. It should be noted the column displacements were less than 2% of the column height for the blast load considered. It is however possible to have high displacements in the first storey column if it is exposed to very high blast pressures.

The above discussion shows that the first storey is likely to be the most vulnerable floor in the event of a blast and travelling fire. This means that first floor beams need to be properly protected under these actions. The study also shows that the maximum column displacement did not occur in the ground floor column. However, for large explosives or higher temperatures, this might not be the case. Therefore, ground floor columns also need to be properly sized to avoid excessive displacements under both actions. Based on the results of this study, parametric analyses are then carried out considering the blast and travelling fire parameters presented in

Table 5.1 and Table 5.2 for the blast occurring at the first storey. The parametric studies involve determining the effects of blast pressure, maximum compartment temperature and fire size on the response of steel frames considering 2 different directions of travel of the fire. The results of the study are discussed in the following sections.

5.4 Effects of blast pressures

Finite element analyses are carried out on the numerical model presented in Figure 3.17 considering 5 different blast pressures and horizontally travelling fires occurring at the first storey. To this end, the blast and thermal loading from the travelling fire are applied on the ground floor column and the first floor composite beam. This study is carried out considering a fire size of 25 % of the floor area and a near field temperature (i.e., maximum compartment temperature) of 800 °C. The analyses are performed considering 2 travel directions of the fire (north-south and east-west). The response of the structure is studied using the results of the first floor beam vertical displacement at mid-span, the lateral displacement at mid-height of the ground floor column and the axial force of the first floor beam. The displacements are normalized against member lengths and the beam axial force is normalized against the axial capacity of the beam. The axial capacity of the beam is calculated as 6070 kN. The time is also normalized against the total fire duration.

The results for both travel directions are discussed in the following sections. It is important to note that the response during the fire is based on the shape of the temperature-time curve of the travelling fire scenarios illustrated in Figure 5.3 which shows an increase to maximum compartment temperature from ambient conditions, a constant fire duration when maximum temperature is reached and then a decline back to ambient temperature after the fire burns out. Changes in slope in the curves will also have an effect on the response.

5.4.1 North-south travel direction

Figure 5.14 shows the beam displacement response at mid-span, column lateral displacement at mid-height and beam axial force for the 5 blast pressures indicated in Table 5.1 and a fire travelling in the north-south direction. The maximum temperature region is represented by the light blue rectangle in the figures. The results of the analyses show that the beam deflects upwards during the blast and the displacement increases as the blast pressure increases. Also, there is a residual displacement due to decay of the blast pressure-time history just before the

fire starts. The results also show that the 117 kPa blast did not induce significant displacement in the beam as the beam went back to initial conditions after the decay period of the blast pressure-time history. This is because the 117 kPa blast only resulted in elastic strains in the beam.

Downward deflections are observed as a result of the fire for most of the initial blast pressures except the 183 kPa blast. Increasing the blast pressure from 117 kPa to 150 kPa results in an increase in beam displacement during the fire until when the blast pressure is 167 kPa. The 167 kPa blast produced a downward beam deflection during the fire which is 26 % lower than that of the 150 kPa blast. This is attributed to the higher mechanical strain from the blast which reduced the effect of the fire, preventing it from inducing a larger displacement in the beam. This is also the case for the fire from the 183 kPa blast in which there is a downward deflection for about 9 % of the total fire duration followed by an upward deflection of the beam. It is observed that at a time of about 9 % of the total fire duration, the maximum compressive force occurs in the beam. The maximum strain in the beam due to the fire also occurs at this time. Nevertheless, the high mechanical strains due to the blast resisted the thermal expansion effects from the fire so that residual deflection from the fire is almost the same as after the blast. Figure 5.14 shows that the maximum downward deflection of the beam for fire travelling in the north-south direction for the initial blast pressures studied is about 4.5 % of the beam length while the maximum upward deflection is 5.5 % of the beam length.

As expected, the lateral displacement of the column increases as blast pressure increases as seen in Figure 5.14. A maximum column displacement of 0.2 % of the column length is observed just after the blast. During the fire, the column is observed to have an increase in displacement in the outward direction during the heating phase of the fire. However, as the fire begins to cool down, the displacement begins to decrease and for most of the values of initial blast pressures, the cooling results in an inward lateral deflection of the column. These results show that cooling of the column can have significant effect on the column by reversing the direction of the displacement response. During the fire, the maximum column lateral displacement of 0.8 % of the column length is observed for the initial 167 kPa blast. It should be noted that all responses are based on the shape of temperature-time history. For instance, for the 167 kPa blast, there is an increase in lateral displacement due to increasing temperatures up to about 18 % of the total fire duration. After this point, there is a slower rate of increase in temperature up to the maximum temperature at about 27 % of the total fire duration.

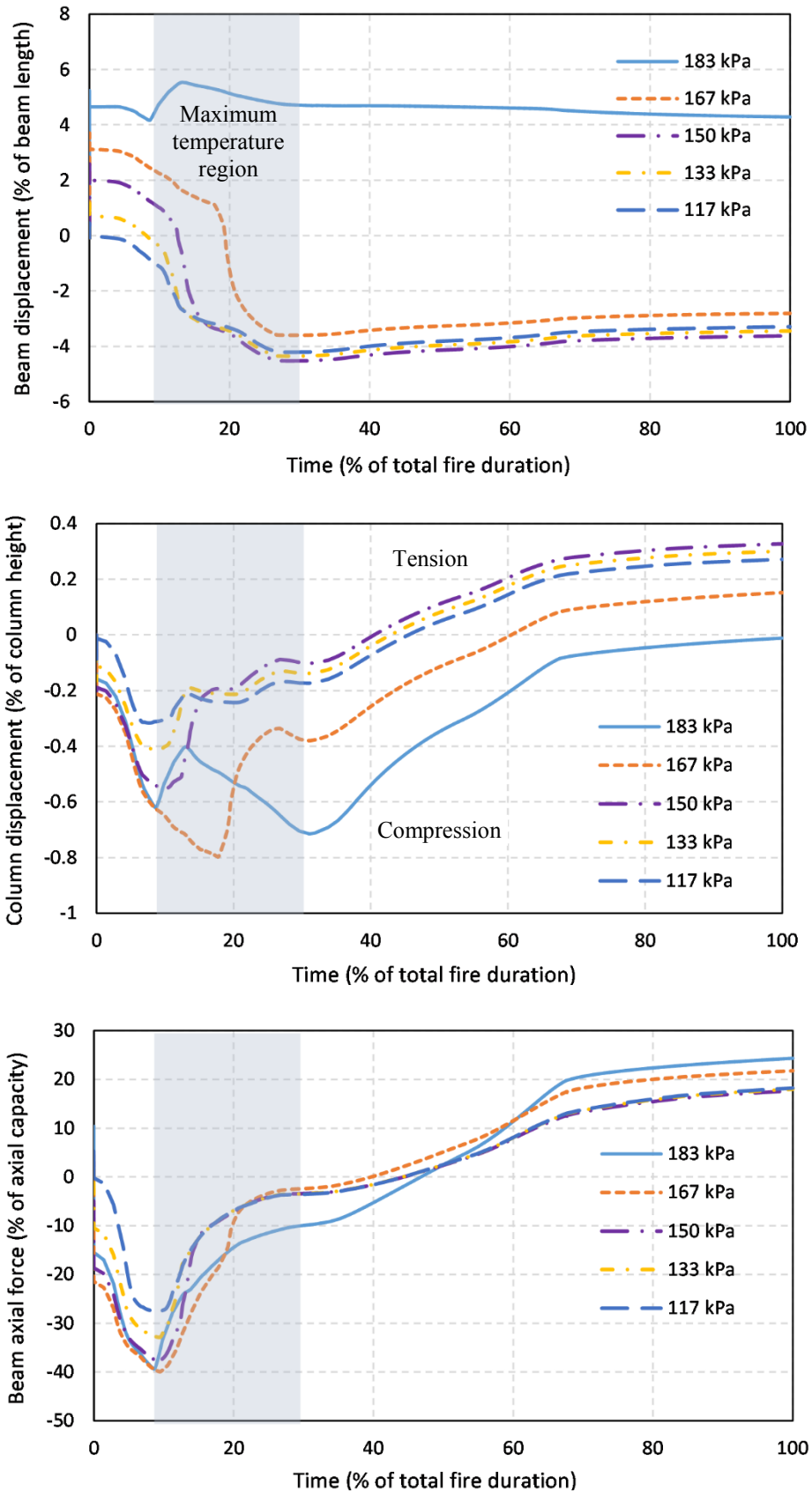

Figure 5.14. Structural response for increasing blast pressures and fire travelling in the north-south direction.

This slow rate of temperature increase up to a time of 27 % of the total fire duration caused the column to recover some of its deflection as it resulted in lower thermal strains in comparison to the strains experienced earlier when there was a faster rate of increasing temperatures. The displacement then continues to reduce due to decreasing temperatures in the column. However, due to the slope of the temperature-time curve, the rate of decrease from cooling is high enough to cause a deflection in the opposite direction. The response due to the 183 kPa blast is a bit different from the others as two peaks during the fire is observed, one at 10 % and the other at 30 % of the total fire duration. Yielding of the column during the fire occurs at the first peak as a result of the damaging effects of the high blast load and, as the slope of the temperature-time curve changes, part of the displacement is recovered. However, as the temperature begins to increase at a faster rate, the displacement increases again up to the point of maximum temperature. The maximum displacement recorded is less than 1 % in all cases.

Figure 5.14 shows that the beam is in tension during the blast and then depending on the amount of blast load, the beam goes into compression during the decay phase of the blast pressure-time history, i.e., just before the fire starts. An increase in the compressive force is observed during the heating phase of the fire. As the beam cools, a decrease in the axial force is observed and it goes into tension at an average time of 43 % of the total fire duration. Increasing blast pressures generally increases the compressive force in the beam during the fire. The 167 kPa blast results in a compressive force during the overpressure higher than that of the 183 kPa blast. This is as a result of the high tensile force of 10 % of the beam axial capacity generated due to the 183 kPa blast. However, the 183 kPa blast pressure results in the highest tensile force at the end of the fire. The higher compressive force due to the 183 kPa blast between 20 % and 40 % of the total fire duration is attributed to the damaging effect of the high blast load which makes the maximum temperature acting during this time induce more forces in the beam. Moreover, the maximum compressive force during the fire is 40 % of the axial capacity of the beam while the maximum tensile force is 23 %.

5.4.2 East-west travel direction

The structural response for the fire travelling in the east-west direction and for increasing blast pressures is shown in Figure 5.15. The beam displacement at mid-span, column lateral displacement at mid-height and beam axial force responses are depicted in this figure. It is important to note that when the fire is travelling in the north-south direction, the longitudinal section of the beam is assumed to be subjected to the same temperature-time history along the

length of the beam. However, when the fire is travelling in the east-west direction, different parts of the beam along its length are subjected to different temperature-time histories. Due to the similarity in the response when compared with the other travel direction, only significant differences between the responses in both travel directions will be discussed.

Comparing the results with that of the north-south direction show that the beam displacement response due to the 167 kPa blast results in an upward displacement which is 29 % less than that of the 183 kPa blast. Also, there is a 4 % decrease in the downward beam displacements due to the 117 kPa and 133 kPa blast pressures, and about 15 % increase in the upward displacement from the 183 kPa blast when the response is compared with that of the north-south travel direction. The peak points in the graph represent the point of maximum axial force and maximum strain in the beam. The response shows that for smaller blast pressures, the beam displacements might be lower in the east-west travel direction while for larger pressures, beam displacements may be higher.

Moreover, the column displacement response shows a similar trend to that of the north-south travel direction except that the maximum displacement recorded is 0.62 % of the column length compared to the maximum value of 0.8 % in the north-south travel direction. Also, at 30 % of the total fire duration, a difference of 0.4 % is noticed in the north-south travel direction between the response due to the 167 kPa and 183 kPa blast pressures while a difference of 0.17 % is observed in the east-west travel direction. All these indicate that in the north-south travel direction, the effect of blast pressures on the column might be higher compared to the east-west travel direction.

Nevertheless, the maximum beam axial force in this travel direction is found to be slightly lower than that of the north-south travel direction. The maximum compressive force is observed to be about 38 % of the beam axial capacity while the maximum tensile force is 22 %. Another importance difference between both travel directions is the time it takes for the axial force to change to tension which is about 50 % of the total fire duration when the fire travels in the east-west direction. However, it took an average of 43 % for the fire travelling in the north-south direction. This is due to the effect of different thermal stresses on different parts of the beam which can reduce the rate at which the axial force decreases so that it takes longer for the beam to go into tension. Figure 5.16 shows the deformation of the frame during the blast and during the fire.

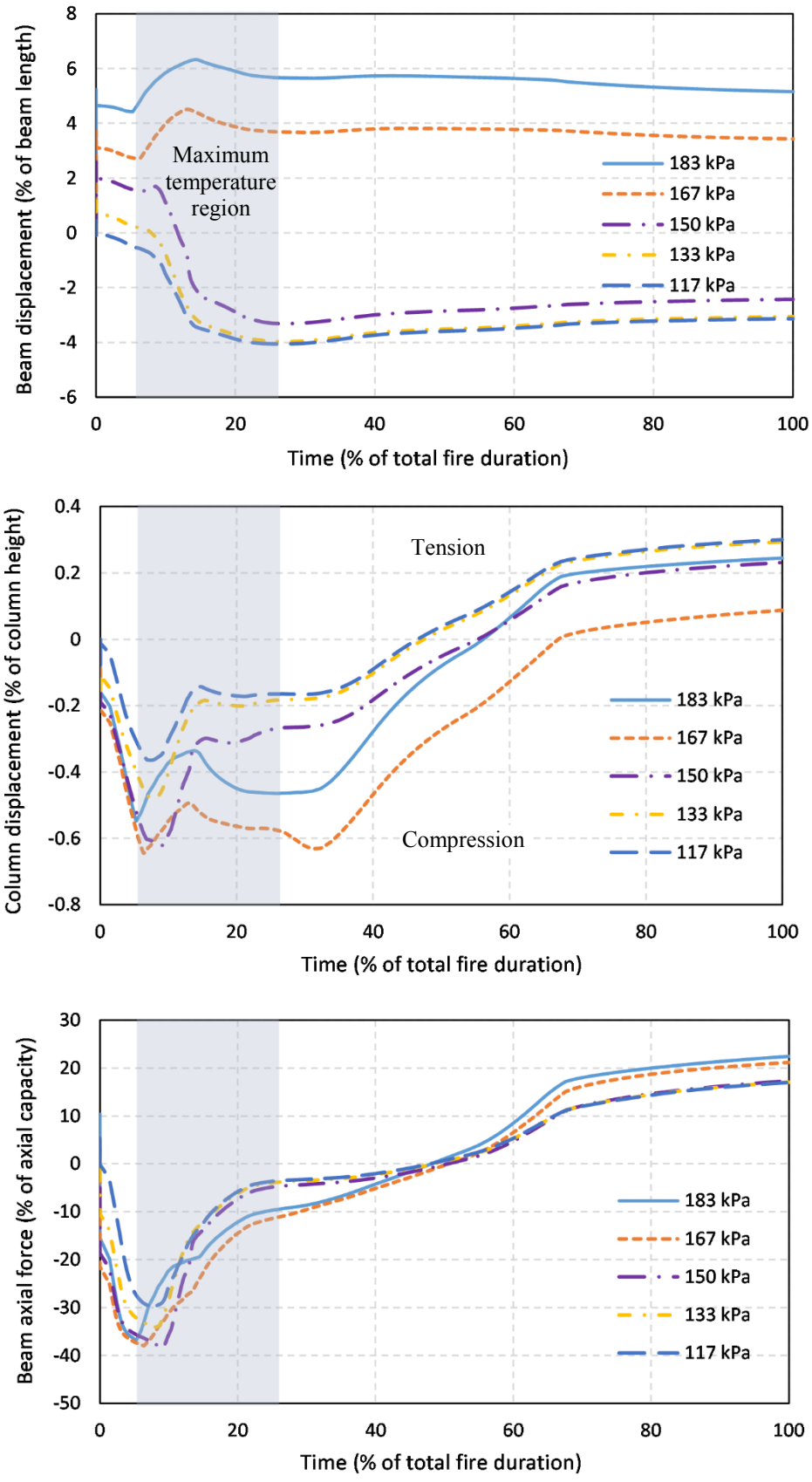

Figure 5.15. Structural response for increasing blast pressures and fire travelling in the east-west direction.

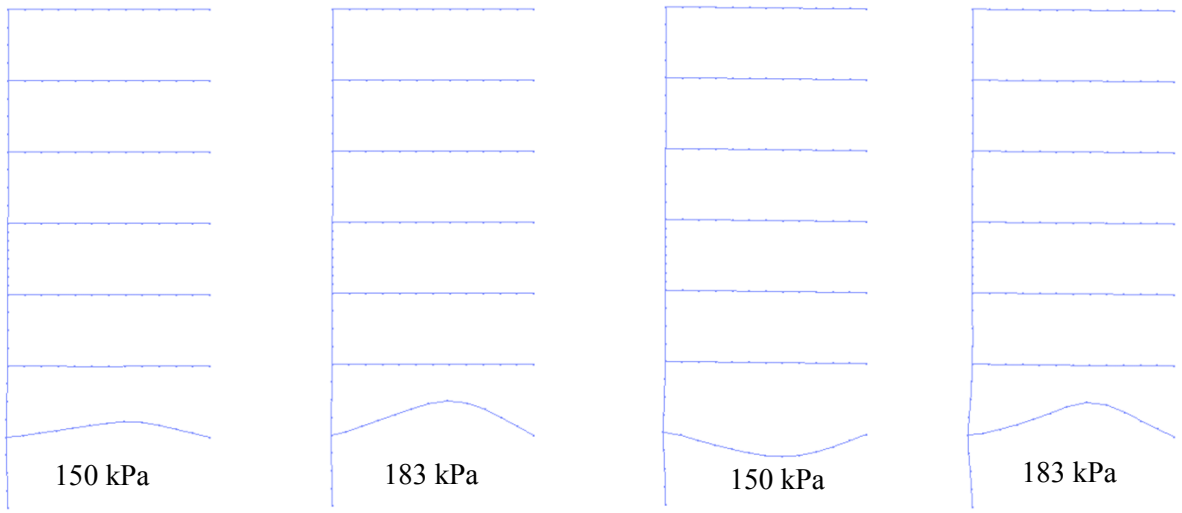

(a) During the blast (b) During the fire (at maximum temperature)

Figure 5.16. Deformation of the frame during the blast and during the fire (4x magnification of displacements).

5.5 Effects of maximum compartment temperature

The effect of increasing maximum compartment temperatures on the steel frame is studied in this section considering the 133 kPa and 183 kPa blast pressures applied at the ground floor followed by a horizontally travelling fire with maximum compartment temperatures of 800 °C, 900 °C and 1000 °C. The analyses are carried out to determine how increasing temperatures in the compartment affect the response of the structural members under both actions. The structural response is recorded using the structural parameters employed before.

5.5.1 North-south travel direction

The structural response for the fire travelling in the north-south direction for the two blast pressures and increasing maximum compartment temperatures is shown in Figure 5.17. For an initial 133 kPa blast pressure, increasing maximum compartment temperatures of the subsequent fire result in an increase in beam displacement, as expected, with each 100 °C increase in temperature leading to an increase in deflections of 2 % of the beam length. For the higher blast pressure of 183 kPa, only the analysis with the 800 °C maximum compartment temperature got to the end of the fire duration while the analyses with the 900 °C and 1000 °C fire stopped at 23 % and 15 % of the total fire duration, respectively. The analyses failed to converge at these times after several attempts. These convergence issues arose due to the high blast pressure which decreased the resistance of the beam, weakening its response under very high temperatures and leading to accumulation of excessive strains as a result of the fire.

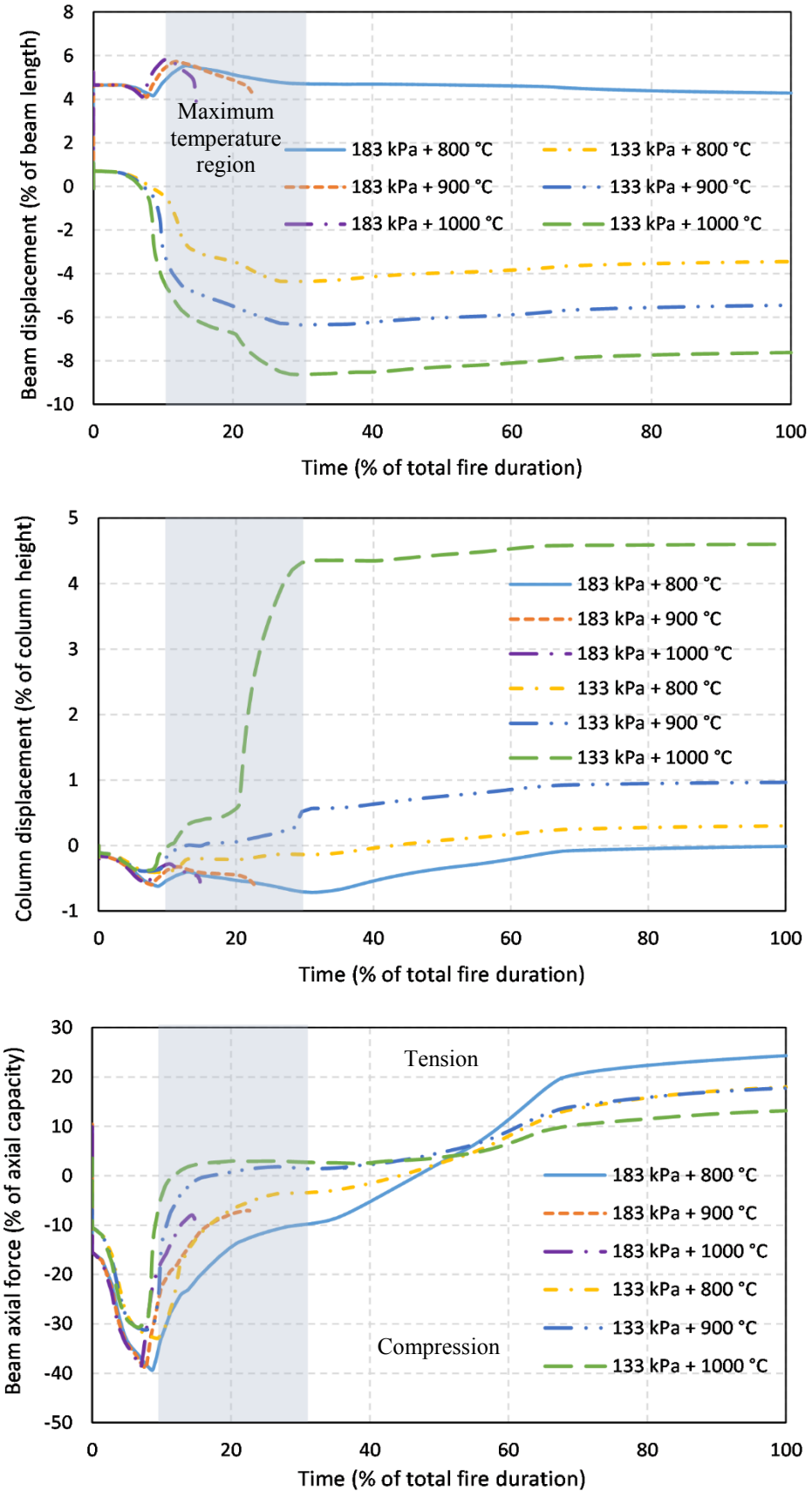

Figure 5.17. Structural response showing the effect of increasing maximum temperatures for fire travelling in the north-south direction.

However, Figure 5.17 also shows that the maximum beam displacement increases with increasing temperature for the initial 183 kPa blast, however, the increase in deflections from one temperature level to the other is about 0.15 % of the beam length. The column lateral displacement also increases with increasing maximum compartment temperatures especially for the initial 133 kPa blast. It is interesting to note the high column displacement of 4.5 % of the column length due to the 1000 °C fire. This is due to buckling of the column as a result of excessive temperature at about 20 % of the total fire duration. Nevertheless, for the 900 °C fire, the stiffness and yield strength of the column are enough to avoid excessive displacements. For the 183 kPa blast, it is difficult to ascertain how increasing temperatures affect the column lateral response since the analyses with the higher temperatures did not converge, as explained earlier. However, it shows that the resistance of the column is greatly reduced under excessive temperatures after a high initial blast load.

The beam axial force response due to increasing temperatures is also illustrated in Figure 5.17. The figure shows that for the 133 kPa blast, increasing temperatures will decrease the time it takes for the axial force in the beam to change from compression to tension. This decrease is more significant when the response of the 900 °C fire is compared with that of the 1000 °C fire. This is because the change in type of axial force for the smaller temperatures occurs before 20 % of the total fire duration while that of the 1000 °C fire occurs at about 45 % of the total fire duration. This is expected since higher temperatures will cause faster significant changes to the material property of structural members. Nevertheless, the maximum axial force decreases with increasing temperatures. For the initial 183 kPa blast, the maximum compressive force is also observed to decrease as the maximum temperature increases.

5.5.2 East-west travel direction

Figure 5.18 shows the structural response of the frame for increasing temperatures of fire travelling in the east-west direction. Comparing the effects of increasing temperatures for both travel directions show that as maximum temperature increases, the maximum beam displacement is slightly lower in the east-west travel direction for the initial 133 kPa blast, but slightly higher for the 183 kPa blast. However, in this travel direction, an increase of 2 % of the beam length is observed between two temperature levels for the initial 133 kPa blast whereas a percentage increase less than 0.05 % of the beam length is observed for the 183 kPa blast. This shows that the blast pressure governs the response even under very high temperatures when the blast load is relatively high.

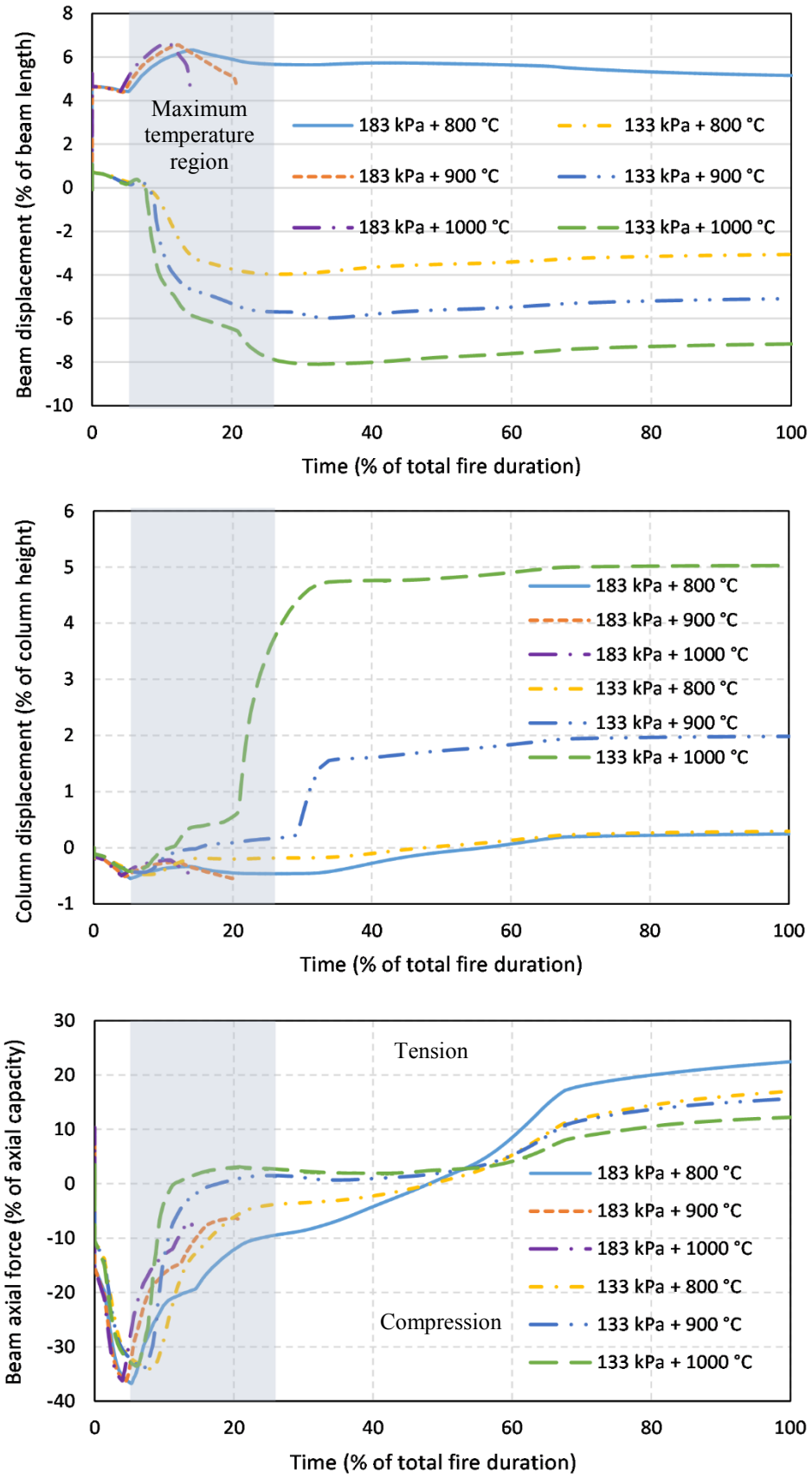

Figure 5.18. Structural response showing the effect of increasing maximum temperatures for fire travelling in the east-west direction.

Considering the effects of increasing temperatures on the column lateral displacement in the east-west direction shows that the maximum column displacement for the initial 133 kPa blast is higher than the displacement in the north-south travel direction. This difference is about 1 % of the column length for the 900 °C fire and 0.5 % of the column length for the 1000 °C fire. The continuous heating and cooling of different parts of the beam under very high temperatures induces higher stresses in the column and has a significant effect on its buckling response, which in turn makes the column deflect more in the east-west travel direction.

The beam axial force response in the east-west travel direction shows a higher maximum beam compressive force for the 133 kPa blast compared to that of the north-south direction while the maximum beam compressive force for the 183 kPa blast is lower. Moreover, the maximum compressive force for the 183 kPa blast in the east-west travel direction is higher than that of the 133 kPa blast by about 2.7 % of the beam length. The axial force response also decreases as maximum temperatures increases. The deformation of the frame for the initial 133 kPa blast for the 3 temperatures studied is shown in Figure 5.19.

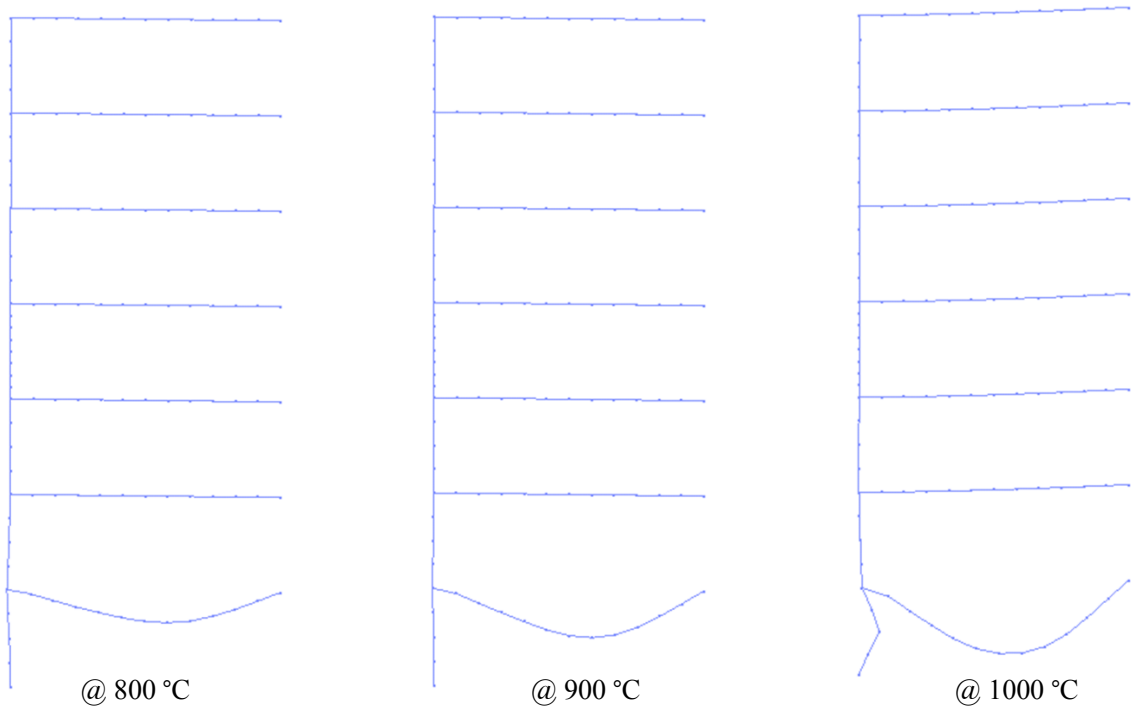

Figure 5.19. Deformation of the frame under the 133 kPa blast and travelling fire for different maximum temperatures (4x magnification of displacements).

5.6 Effects of fire size

The effect of fire size on steel frames under blast and travelling fires is also studied considering the 133 kPa and 183 kPa blast pressures applied at the ground floor of the numerical model followed by a horizontally travelling fire with a maximum compartment temperature of 800 °C. This study is conducted considering fire sizes of 10 %, 25 % and 50 % of the floor area.

5.6.1 North-south travel direction

The beam displacement response at mid-span, column lateral displacement response at mid-height and beam axial force response in the first storey for different fire sizes is shown in Figure 5.20. The beam displacement response shows that the time for maximum beam displacement to occur increases as the fire size increases. Smaller fire sizes will take longer to move across the floor if moving at a fixed rate resulting in a higher total fire duration when compared with larger fire sizes. As a result, the beam experiences maximum displacement quicker for smaller fire sizes. For the 133 kPa blast pressure, it is observed that the maximum beam displacement increases as the fire size increases, which is due to the beam being exposed to prolonged periods of heating for smaller fire sizes. Nevertheless, for the 183 kPa blast, the maximum displacement decreases as the fire size increases which shows the significance of high blast loads on the fire response. However, the difference is quite negligible in this travel direction as it is about 0.03 % of the beam length.

The maximum column lateral displacement is also observed to increase in the inward direction as the fire size increases for the 133 kPa blast, while the maximum displacement decreases generally for the 183 kPa blast. Comparing the lateral displacement response of both blast loads show that the effect of fire size is more evident for the 183 kPa blast as it is observed that there is a larger difference between the times of maximum column displacement compared to that of the 133 kPa blast. This is due to the high blast pressure which has a significant influence on the effect of fire spread rate on the column. Nevertheless, the maximum compressive axial force is about the same for the three fire sizes. However, the maximum tensile force is observed to decrease as the fire size increases. This is attributed to the longer total fire duration of the smaller fire sizes. Figure 5.20 shows that the time it takes the beam axial force to change from compression to tension increases as the fire size increases. This is as a result of the lower fire spread rate for smaller fire sizes so that cooling of the beam will occur relatively faster for a smaller fire size.

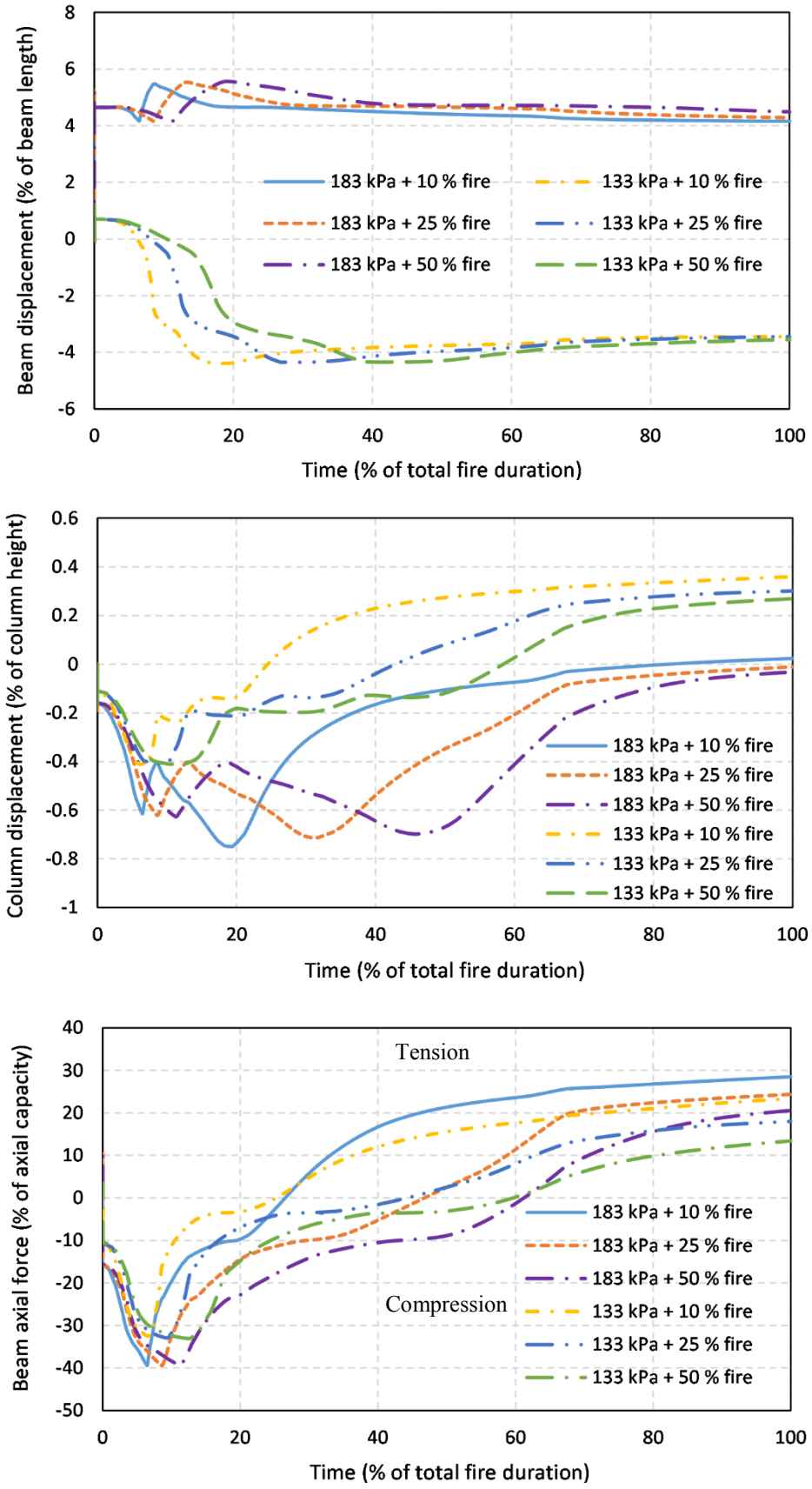

Figure 5.20. Structural response of the frame for fire travelling in the north-south direction showing the effect of increasing fire sizes.

5.6.2 East-west travel direction

The structural response for different fire sizes travelling in the east-west direction is shown in Figure 5.21. Comparing the beam displacement response in this travel direction with that of the north-south direction shows that in the east-west travel direction, the maximum beam displacement increases as the fire size increases for the 133 kPa blast while the maximum displacement of the beam decreases for the 183 kPa blast. However, the difference between the beam displacement values of the 25 % and 50 % fire sizes is smaller compared to the difference between the 10 % and 25 % fire sizes, especially for the 133 kPa blast. The 133 kPa blast is observed to produce a difference of 0.87 % of the beam length between the 10 % and 25 % fire sizes and a difference of 0.2 % of the beam length between the 25 % and 50 % fire sizes. This shows that for the fire travelling in the east-west direction with a longer total fire duration and an initial low blast pressure, there may be a lower displacement in the beam for smaller fire sizes. This lower beam displacement for smaller fire sizes is due to a smaller portion of the beam being subjected to burning in this travel direction.

The column lateral displacement response shows that the column displacement is higher in the east-west travel direction compared to the north-south travel direction for the 133 kPa blast, but it is lower for the 183 kPa blast. Also, the column displacement is observed to generally increase in the outward direction and decrease in the inward direction as the fire size increases especially for the 183 kPa blast. The increase in lateral displacement in the inward direction for increasing fire sizes is attributed to the duration of maximum compartment temperature, which is relatively higher for larger fire sizes. Moreover, the decrease in the lateral displacement during the cooling period is due to the reduction in the rate of cooling as the fire size increases.

The beam axial force response in Figure 5.21 shows that the maximum beam compressive force is lower in the east-west travel direction for the 183 kPa blast compared to the north-south direction. It is also observed that the maximum beam axial force decreases as fire size increases in the east-west travel direction for the 133 kPa blast. However, for the 183 kPa blast, the maximum compressive force increases while the maximum tensile force decreases. Also, in most cases, the time it takes the axial force to change from compression to tension is longer in this travel direction. This is due to the different temperature-time histories along the length of the beam which can have a significant influence on the thermal stresses induced in the beam at a particular time making it take longer for tensile forces to act on the beam.

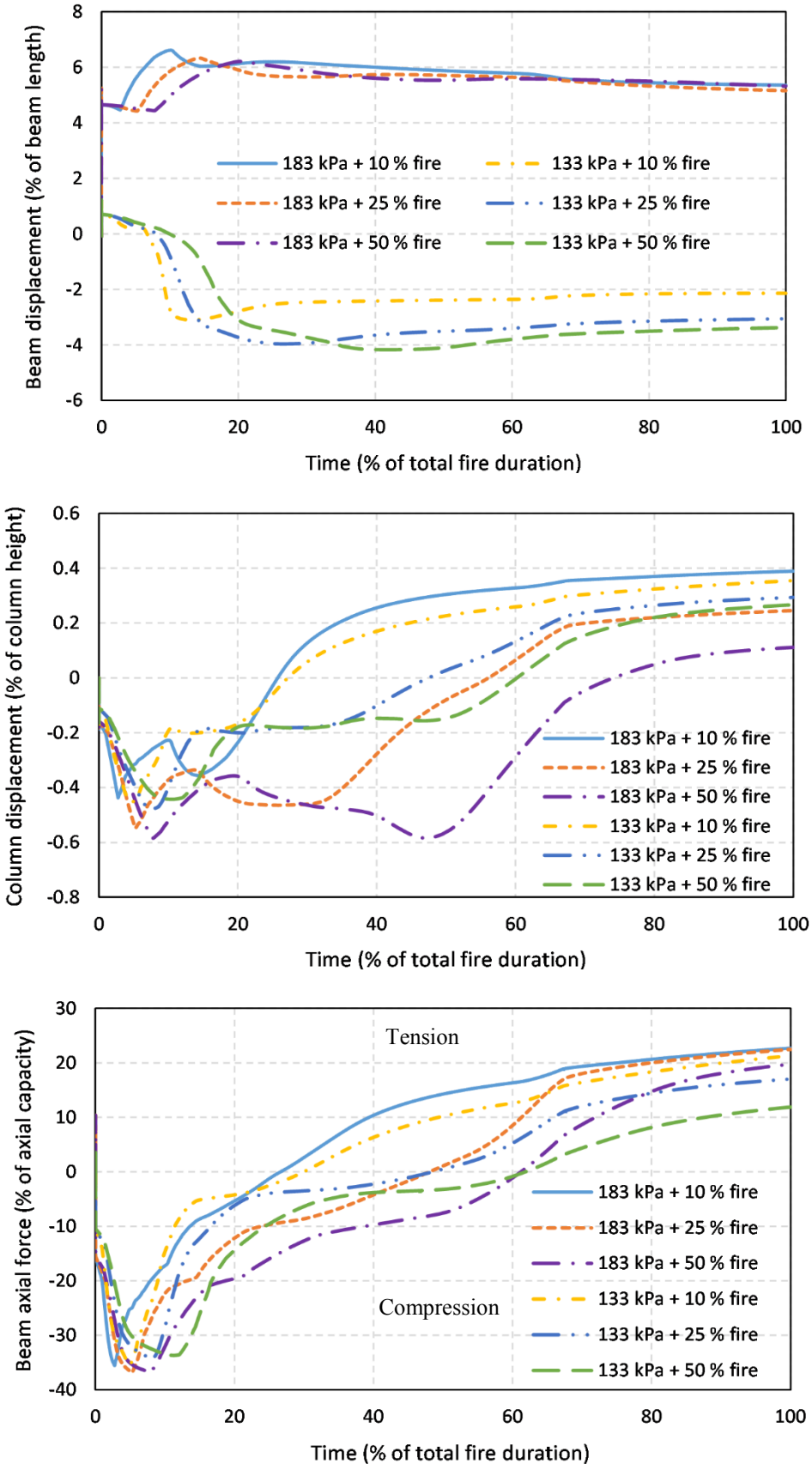

Figure 5.21. Structural response of the frame for fire travelling in the east-west direction showing the effect of increasing fire sizes.

5.7 Conclusions

The analyses carried out in this chapter demonstrate how blast pressures, fire parameters and direction of fire travel can affect the structural response of steel structures under blast and travelling fires. From the study, it can be concluded that under these actions:

1. The first storey or ground floor compartment is likely to be the most critical floor when the fire is a horizontally travelling fire burning simultaneously on multiple floors, a horizontally travelling fire on a single floor or a vertically travelling fire.
2. Upward or downward beam displacements can occur depending on the amount of initial blast pressure and travel direction of the fire.
3. High blast pressures will have a more significant effect on beam displacements compared to the subsequent travelling fire.
4. Increasing maximum compartment temperatures will result in an increase in beam displacements.
5. The effect of fire size is likely to be more significant in the east-west travel direction and in some cases, higher values of structural response can occur for smaller fire sizes.
6. The direction of travel and maximum compartment temperature can have a significant effect on the column lateral displacement, especially in the east-west travel direction where higher values of column displacement were observed particularly for higher compartment temperatures.
7. The axial force in the beam is easily affected by the direction of travel and fire size, and lower values of axial force can occur when the fire travels in the east-west direction.

The results of this study show the importance of considering all possible fire scenarios in design, especially travelling fires as lower fire sizes in some cases may have a larger impact on the frame when there is an initial blast pressure (Teslim-Balogun et al., 2019). Moreover, an understanding of the behaviour of structural members under these actions can assist structural engineers in improving the performance of structures to effectively resist multi-hazard scenarios involving blast and travelling fires.

Chapter 6
Performance-based Post-blast Travelling Fire Assessment of Steel Frames

6.1 Introduction

The importance of considering multi-hazard scenarios, in particular post-blast travelling fires and their effect on the performance of steel buildings has been discussed in the previous chapter. In this chapter, the PEER performance-based framework is used to assess the performance of steel buildings under the effect of post-blast travelling fires. Initially, a study is carried out to investigate the difference in structural behaviour of structural systems with different beam-to-column stiffness ratios under post-blast travelling fires. A performance-based assessment is then carried out for the different beam-to-column stiffness ratios. The assessment is expected to show the effects of both structural and loading parameters on the overall structural response when a probabilistic framework is used to assess steel structures subjected to post-blast travelling fires. The probability of exceeding the selected engineering demand parameters is determined and used to evaluate the probability of failure of the steel frame based on a given failure criterion.

6.2 Effects of steel beam-to-column stiffness ratio

Non-linear finite-element analyses are carried out in OpenSees on the numerical model presented previously in Chapter 3 (Figure 3.17) for different beam-to-column stiffness ratios. Scenarios with 133 kPa and 183 kPa blast pressures individually applied at the first storey are considered. These blasts are followed by a horizontally travelling fire with a fire size of 25 % of the floor area and a maximum compartment temperature of 800 °C. The fire is assumed to occur in the region near the blast and two directions of travel are considered. The study is carried out for four different values of beam-to-column stiffness ratios. The sections of the structural members in this study and their stiffness ratios are shown in Table 6.1. The steel beam-to-column stiffness ratio is calculated using Equation 6.1.

$$\alpha = \frac{EI_b/l_b}{EI_c/l_c} \tag{6.1}$$

where α is the beam-to-column stiffness ratio, E is the elastic modulus of the steel material, I_b is the second moment of area of the steel beam, l_b is the span of the steel beam, I_c is the second moment of area of the steel column and l_c is the height of the steel column. In this study, the structural systems are categorized in terms of the second moment of area (I). System A with lower α values is characterised by $I_b < I_c$ while System B with higher α values is represented by $I_b > I_c$. Comparing the second moment of area of the steel beam and column in both systems shows that the beams of System A are less rigid than the columns while the beams of System B are more rigid than the columns. Also, the beams of α = 0.31, 0.49 and 0.67 have a higher stiffness compared to that of α = 0.18 while the columns of System A are stiffer than those of System B.

Table 6.1. Element sizes for different steel beam-to-column stiffness ratios.

Beam	Column	Stiffness ratio (α)	Structural system
457x191x106 UB	356x406x340 UC	0.18	System A
533x210x138 UB	356x406x340 UC	0.31	System A
533x210x138 UB	305x305x283 UC	0.49	System B
533x210x138 UB	356x368x177 UC	0.67	System B

The effects of the steel beam-to-column stiffness ratio are examined in terms of the mid-span vertical displacement of the first floor beam, the mid-height lateral displacement of the first storey column and the axial force of the first floor beam. The displacements are normalized by the lengths of the structural members. Also, the axial force of the beam is normalized against its axial capacity while the time is normalized by the total fire duration. The structural response parameters are expressed in percentages as in Chapter 5. The response is strongly influenced by the shape of the temperature-time history which shows a rise to maximum compartment temperature, a constant fire duration stage and then a decline stage back to ambient temperature. It is important to note that the response during both actions (blast and travelling fire) has already been described in detail in Chapter 5. As a result, only major differences in the different structural systems are discussed in this section. Results are discussed for both blast pressures and different directions of travel of the fire. It should be noted that the light blue rectangles in Figures 6.1 to 6.4 show the periods of maximum compartment temperature during the fire.

6.2.1 North-south travel direction

133 kPa blast pressure

The beam displacement, column lateral displacement and beam axial force response of the steel frame (in Figure 3.17) under the 133 kPa blast pressure and fire travelling in the north-south direction are shown in Figure 6.1. The beam displacement response shows that for the 133 kPa blast, the 0.18 stiffness ratio results in an upward beam displacement during the fire while the other stiffness ratios result in downward displacements of the beam during the fire. The 0.18 stiffness ratio also produces a residual deflection of 5 % of the beam length during the blast compared to 1 % for the other stiffness ratios. This is due to the high impact of the blast load on the 0.18 stiffness ratio as a result of its low beam stiffness since the second moment of area of the steel beam for $\alpha = 0.18$ is the lowest of the steel beams studied. From Figure 6.1, it can be observed that increasing the stiffness ratio of System B from 0.49 to 0.67 results in a maximum beam displacement decrease of 1.6 % of the beam length even with the same beam section. This decrease is due to the blast effects and the redistribution of forces between the beam and column during the fire so that with a reduced column stiffness, the displacement of the beam is lower for the same beam section and second moment of area. Also, a decrease in displacement in the opposite direction is observed when the stiffness ratio of System A increases from 0.18 to 0.31. This decrease is expected since the beam of the 0.31 stiffness ratio has a higher stiffness and resistance to blast loads compared to the beam of the 0.18 stiffness ratio.

The column lateral displacement response shows that $\alpha = 0.67$ results in the highest column displacement of 1 % of the column length. The response also shows that the column displacement increases in the outward direction when the stiffness ratio increases from 0.49 to 0.67 for System B, but the displacement decreases in the inward direction towards the end of the analyses. This is expected since the second moment of area of the columns in System B is lower than that of System A which will then result in higher column displacements during the heating phase of the fire. Nevertheless, during the period of maximum temperature for System A, it can be observed that the column displacement for the 0.18 stiffness ratio is higher compared to the 0.31 stiffness ratio even though they have the same second moment of area. This is as a result of the reduced stiffness of the steel beam for the 0.18 stiffness ratio so that more forces are distributed to the column resulting in higher column displacements.

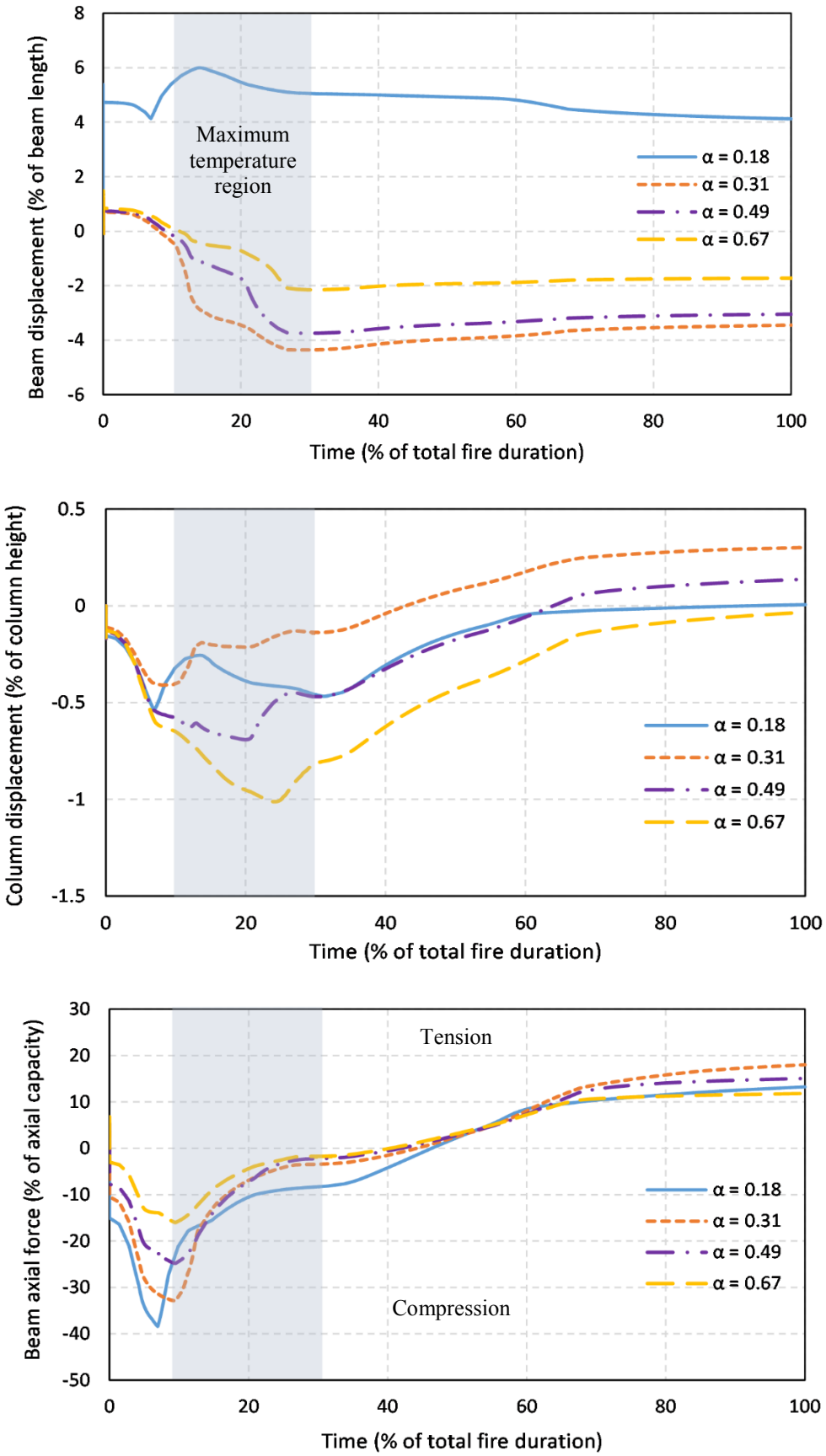

Figure 6.1. Structural response under the 133 kPa blast and fire travelling in the north-south direction for different beam-to-column stiffness ratios.

The beam axial force response in Figure 6.1 indicates that under the 133 kPa blast and travelling fire, the compressive force decreases as the stiffness ratio increases for both systems. The highest normalized compressive force recorded is 39 % of the beam axial capacity (for α = 0.18) while the lowest is 15 % (for α = 0.67). Although, the axial force in a member is a function of the area and compressive or yield strength, it is evident that under post-blast travelling fires, the interaction between the stiffness of the column and beam plays a role in determining the axial force. This is observed in Figure 6.1 which depicts that decreasing I_c can decrease the axial force acting on the beam. It is also observed that the tensile force in the beam increases as the stiffness ratio increases from 0.18 to 0.31 for System A while the tensile force decreases for System B. This is attributed to the rate of cooling of the fire temperatures and redistribution of thermal stresses between the beam and column in both structural systems.

183 kPa blast pressure

Figure 6.2 shows the structural response of the frame under an initial 183 kPa blast followed by a fire travelling in the north-south direction. For an initial blast pressure of 183 kPa, all stiffness ratios result in an upward displacement of the beam during the blast and then a decrease in beam displacement is observed for the higher α values during the travelling fire. The 0.18 stiffness ratio produces the highest beam displacement of 8.7 % of the beam length during the blast and 10.3 % during the fire. The beam displacement also decreases as the stiffness ratio increases from 0.18 to 0.31 which is expected since the second moment of area of the beam is higher for α = 0.31.

The beam displacement of System B is also observed to decrease as the stiffness ratio increases. This is observed up to about 27 % of the total fire duration for the 0.49 and 0.67 stiffness ratios. After this time, the displacement values are almost equal. This means that an increase in I_c in the systems with the higher α values does not produce significant reduction in the beam displacement in this particular scenario. This is attributed to the upward deflection from the blast which is observed to have a larger effect on the beam displacement response in comparison to the stiffness of the columns in System B. As a result, there is no significant effect on the beam displacement response even with a reduced second moment of area of the column especially during the cooling phase of the fire. The column displacement response for the 183 kPa blast also shows that the lateral displacement of the column increases as the stiffness ratio increases for both structural systems as expected. However, Figure 6.2 shows a difference of about 0.81 % between the column displacement of System A and B.

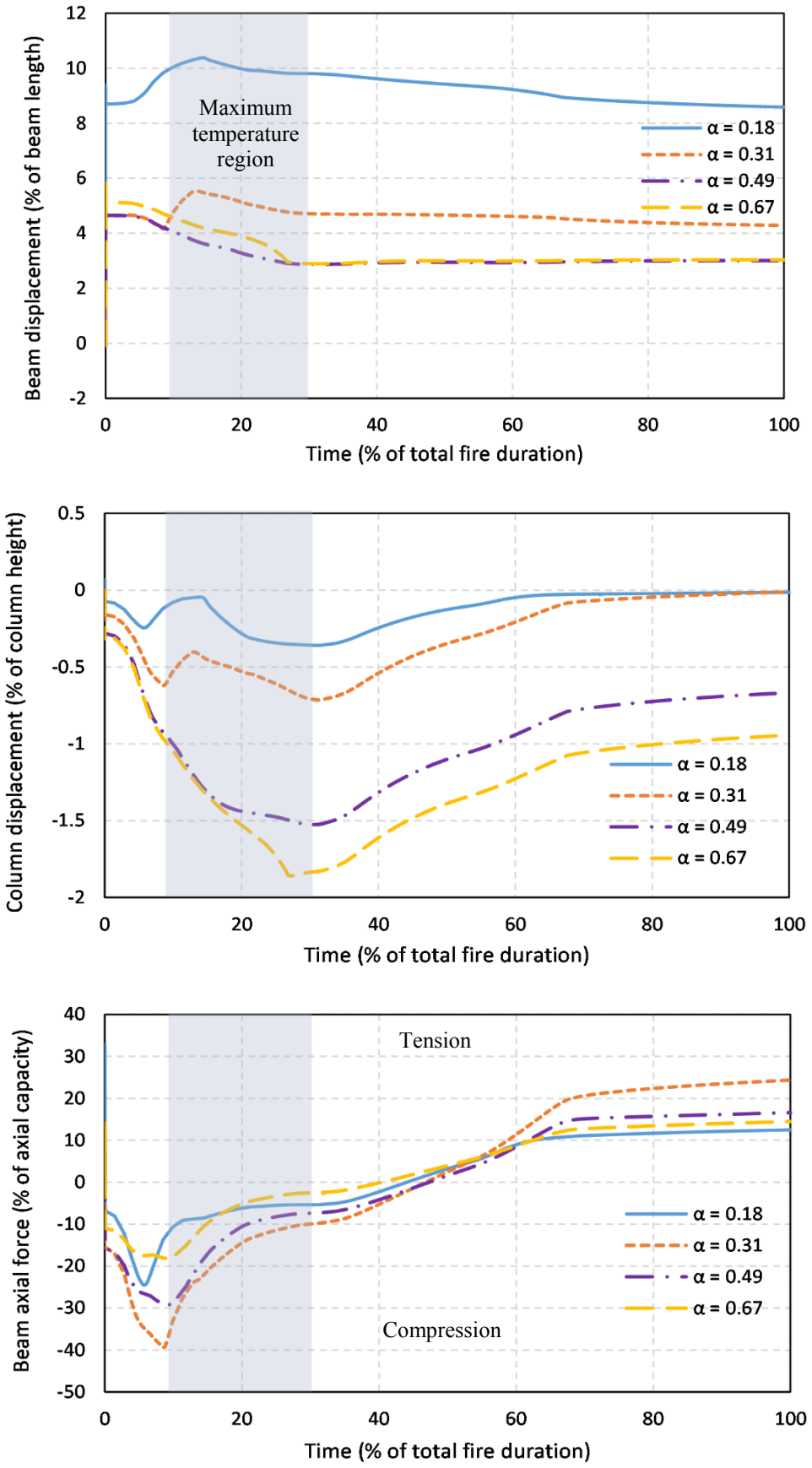

Figure 6.2. Structural response under the 183 kPa blast and fire travelling in the north-south direction showing the effect of different beam-to-column stiffness ratios.

This difference in the column displacement is as a result of the lower column stiffness in System B when compared with that of System A. The reduced stiffness decreases the resistance of the column under the blast and travelling fire thereby resulting in higher column displacements. The beam axial force response in Figure 6.2 shows that as the stiffness ratio increases, the compressive force decreases in System B while the compressive force increases in System A. This is due to the high tensile force during the blast which decreased the compressive stresses in the beam during the fire in System A, especially for $\alpha = 0.18$ which attains a normalized tensile force of 33 % of the beam axial capacity during the blast. This value is significantly higher in comparison with the normalized tensile force of the 0.18 stiffness ratio for the initial 133 kPa blast as depicted in Figure 6.2. Nevertheless, a maximum tensile force of 24 % of the beam axial capacity is observed for $\alpha = 0.31$ during the fire. This is higher than that of the 0.18 stiffness ratio by about 18 % of the beam axial capacity while the difference between the 0.49 and 0.67 stiffness ratios is significantly lower. This is due to the difference in the rate of cooling of the beam based on the different values of the maximum compressive stresses in the structural systems studied.

6.2.2 East-west travel direction

133 kPa blast pressure

Figure 6.3 shows the structural response of the frame under the 133 kPa blast pressure and the fire travelling in the east-west direction. Comparing the response in this travel direction to that of the north-south travel direction shows that the maximum beam displacement is higher for the 0.18 stiffness ratio and lower for the 0.31 stiffness ratio in this travel direction while the beam displacement response in both travel directions is similar for System B. This shows that the travel direction of the fire may have more impact on the beam displacement response for lower values of α. The high residual beam displacement during the blast of 5 % of the beam length, coupled with the thermal expansion from the repeated heating and cooling of the beam in this travel direction contributed to the increase in displacement of the 0.18 stiffness ratio structural system. The decrease in the 0.31 stiffness ratio may be due to the low residual displacement during the blast which caused a reduction in the effect of thermal stresses on the beam.

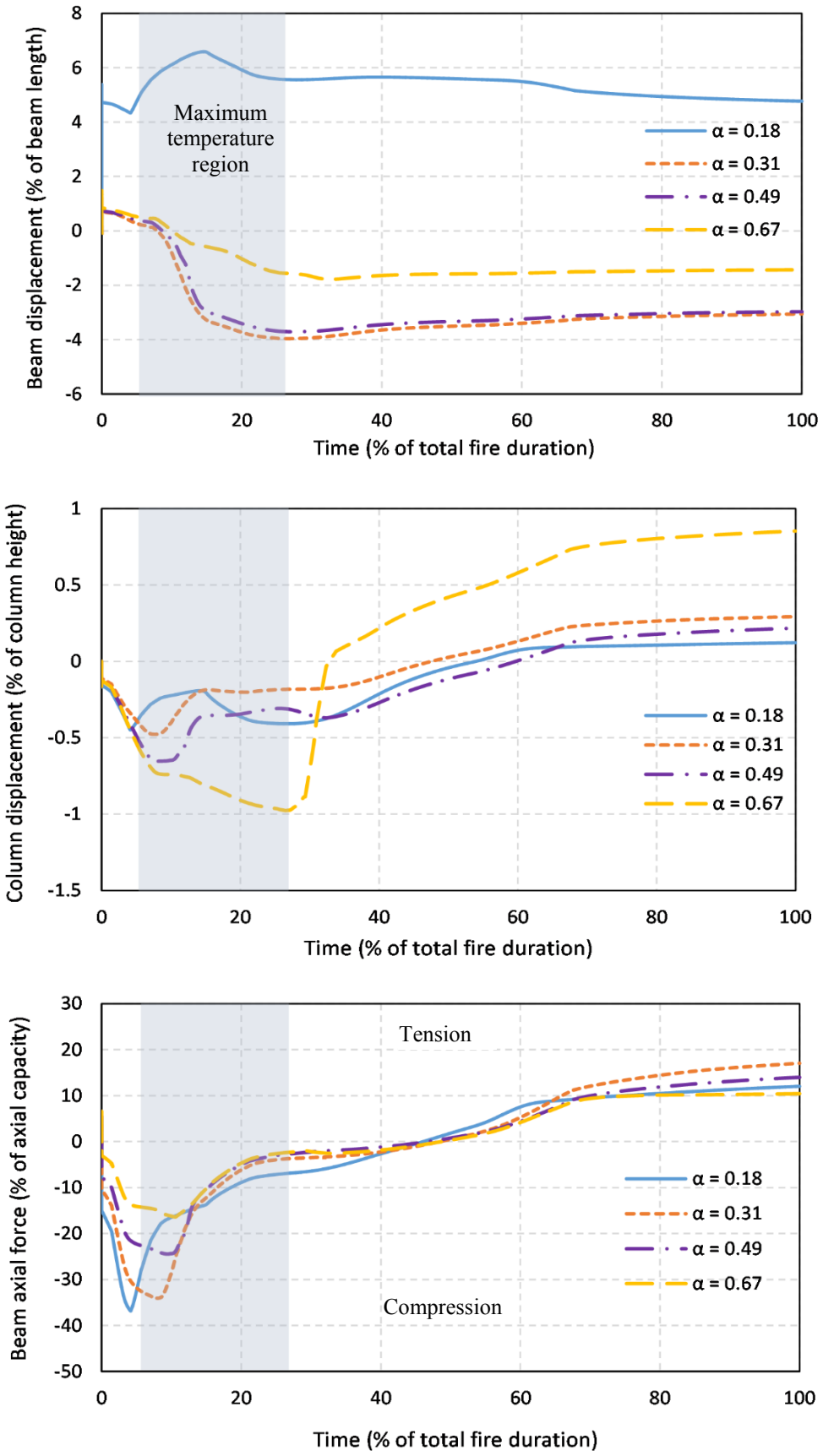

Figure 6.3. Structural response under the 133 kPa blast and fire travelling in the east-west direction showing the effect of different beam-to-column stiffness ratios.

The column displacement response for a fire travelling in the east-west direction is similar to that of the north-south direction except in the case of the 0.67 stiffness ratio. Figure 6.3 shows that when $\alpha = 0.67$, the column deflects inwards up to a time of about 33 % of the total fire duration and the deflection is about 0.8 % of the column length at the end of the analyses in comparison to that of the north-south direction. Also, the fire resistance of the column for $\alpha = 0.67$ is greatly reduced under the repeated heating and cooling of the beam so that it experienced higher displacements. As a result of this, the rate of cooling is significantly higher compared to other stiffness ratios once the compartment temperature begins to decrease resulting in a relatively higher inward displacement in comparison to other stiffness ratios.

The beam axial force response in this travel direction also shows that as the stiffness ratio increases, the maximum compressive force in the beam decreases while the maximum tensile force increases. The major difference between the axial force response during a fire travelling in the east-west direction and that of one travelling in the north-south direction is the time it takes for the beam to go from compression to tension. This occurred at a later time (of about 48 % of the total fire duration) when the fire travels in the east-west direction as opposed to the north-south direction (about 40 % of the total time) for most of the stiffness ratios studied. This is attributed to the differential heating of the beam in the east-west travel direction which induced compressive stresses in the beam for a longer period before decreasing temperatures caused the beam to go into tension.

183 kPa blast pressure

Figure 6.4 shows the structural response of the steel frame under a 183 kPa blast followed by a fire travelling in the east-west direction. The main difference when the beam displacement response in this travel direction (east-west) is compared with that of the north-south travel direction is the decrease in displacement when the stiffness ratio increases from 0.49 to 0.67 for System B. This difference is about 0.82 % of the beam length, however, in the north-south direction, an increase in beam displacement is observed just before the cooling of the beam and the beam displacement is equal for $\alpha = 0.49$ and 0.67. The decrease in beam displacement for both stiffness ratios in the east-west travel direction is due to the redistribution of forces between the beam and the column as a result of the reduced column stiffness for $\alpha = 0.67$. Therefore, reducing the stiffness of the column in a structural system with the same beam section produces a decrease in the beam displacement under this loading scenario.

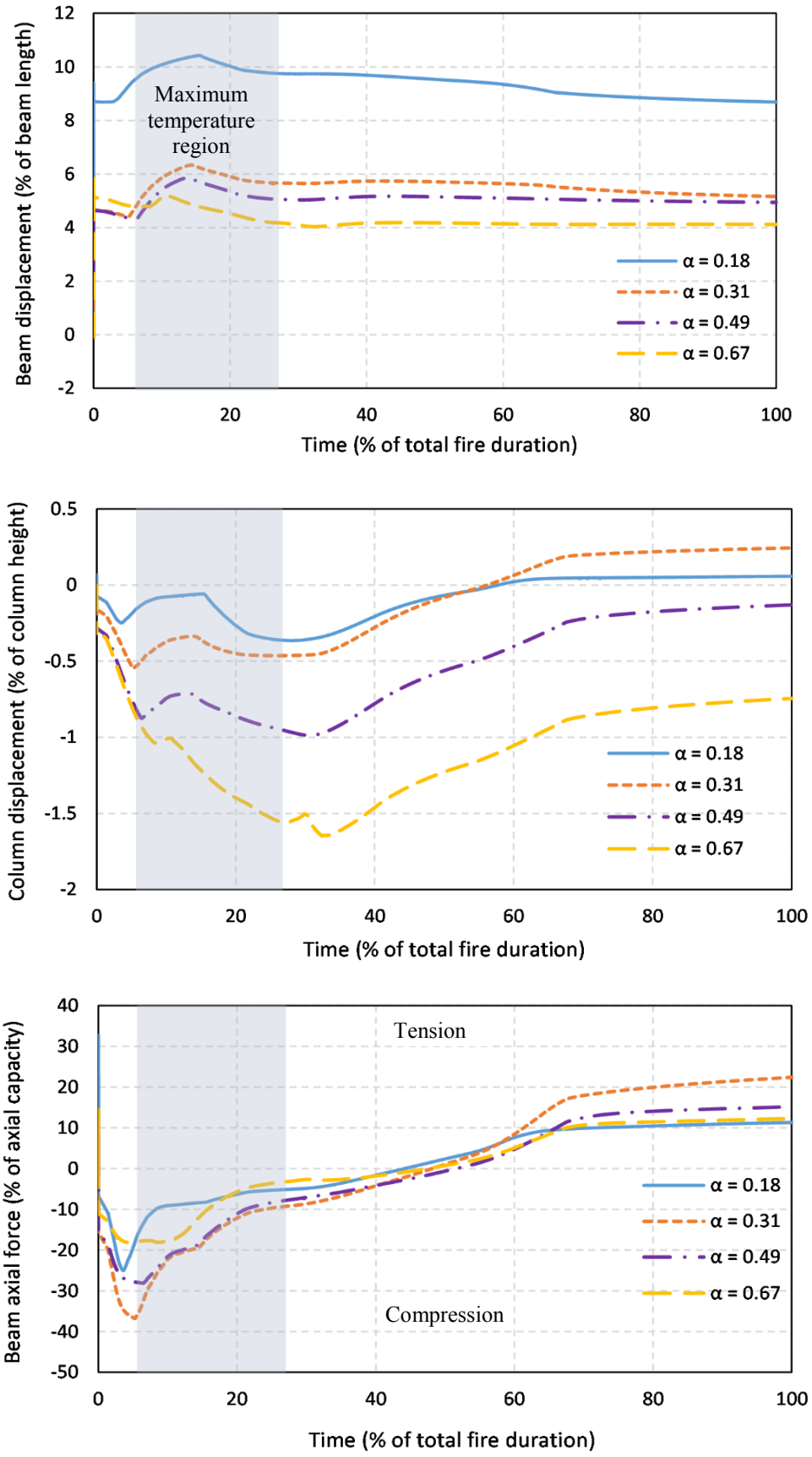

Figure 6.4. Structural response under the 183 kPa blast and fire travelling in the east-west direction showing the effect of different beam-to-column stiffness ratios.

The column lateral displacement response in the east-west travel direction shows that generally the column displacement increases as the stiffness ratio increases for both structural systems. In comparison with the north-south travel direction, it can be observed that the difference between the column displacements of both structural systems in the east-west travel direction is about 0.44 % of the column length which is about 50 % lower in comparison with that of the north-south direction. This means that the column displacement for System B is lower in the east-west travel direction. This is attributed to the lower thermal strains experienced in the column during the fire travelling in the east-west direction, in comparison with that of the north-south direction.

The beam axial force response in Figure 6.4 shows that during the fire, the maximum compressive force increases as the stiffness ratio increases for System A but the axial force decreases for System B. The opposite is the case for the maximum tensile force, as expected. The axial force response of the beam in this travel direction is quite similar to that of the north-south travel direction except that the maximum compressive and tensile forces are lower in this travel direction. It is possible that the effect of different thermal stresses on the beam in this travel direction is lower after the 183 kPa blast in comparison to the north-south travel direction because all parts of the beam are not subjected to heating and cooling at the same time.

6.2.3 Fire protection

Examining the results of the previous sections show that in some cases fire protection might be required to reduce the displacements arising from the effect of the travelling fire especially for very high maximum temperatures as demonstrated in Chapter 5. The numerical models in this thesis are not fire protected which assumes the worst case condition. This is because, after the blast, it is very likely that the fire protection may not have much effect on the fire resistance (especially for higher blast pressures) compared to when there is no initial blast event. However, it will be interesting to investigate how fire protection might affect the response of the structural systems previously discussed, on the assumption that the fire protection remains intact after the blast (especially for low blast pressures).

To this end, non-linear analyses are performed in OpenSees considering a 133 kPa blast occurring at the first storey and a subsequent fire travelling in the north-south direction. A fire size of 25 % and a maximum compartment temperature of 800 °C are assumed for the travelling fire. The fire protection adopted for this study is a sprayed mineral fibre protection (density,

ρ = 300 kg/m^3, thermal conductivity, k_i = 0.12 W/mK and specific heat, c_p = 1200 J/kgK). The thickness of the insulation is taken as 10 mm. The heat transfer analyses was carried out in SAFIR which produced the evolution of temperatures in the unprotected beams and also in the beams coated with a layer of insulation. The effect of fire protection is studied on the beam displacement of System A with beam to column stiffness ratios of 0.18 and 0.31. Figure 6.5 shows the temperature-time history in the beam flanges and slab for the protected and unprotected beams.

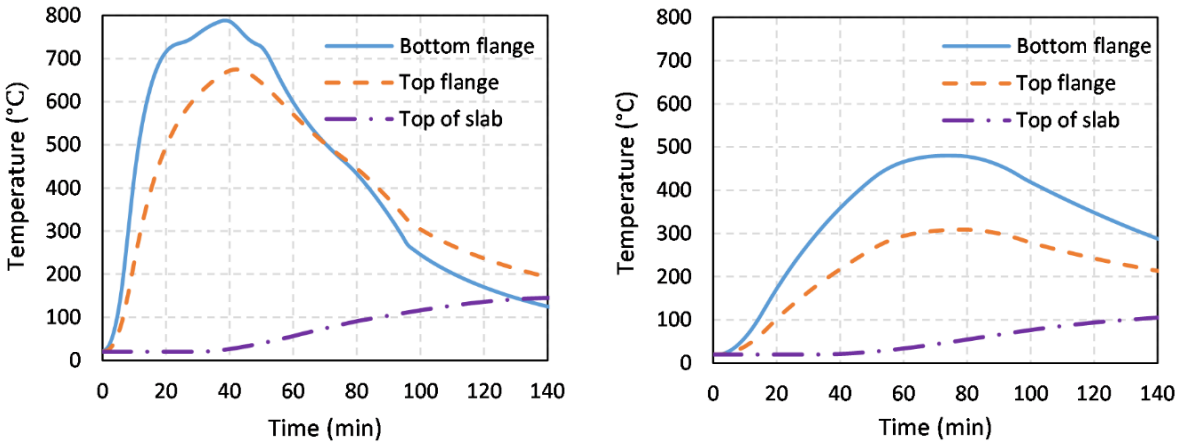

(a) Unprotected beam (b) Protected beam

Figure 6.5. Temperature-time history in the beam section for the protected and unprotected beams.

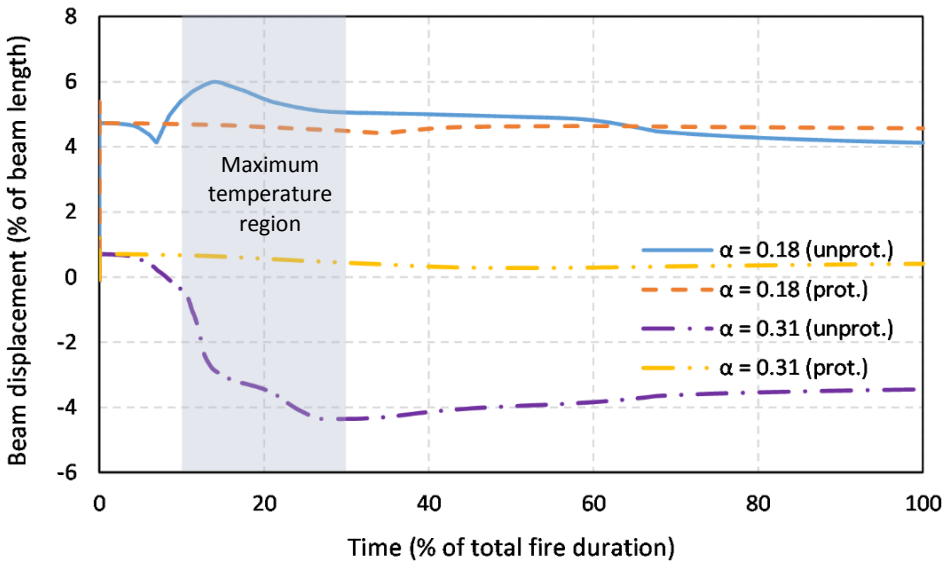

Figure 6.6. Beam displacement response for the protected and unprotected beams.

Only α = 0.18 and 0.31 are considered in this study because of the significant difference observed in the beam displacements between both stiffness ratios in the previous sections. The

vertical beam displacement response at mid-span for both structural systems for the protected and unprotected cases are presented in Figure 6.6. As discussed in the previous section, the unprotected beam with $\alpha = 0.18$ experiences a high upward displacement with a maximum displacement of 6 % of the beam length while a maximum downward displacement of about 4.2 % is observed for $\alpha = 0.31$. For the protected case, $\alpha = 0.18$ results in a maximum upward displacement of about 4.8 % of the beam length while a maximum upward displacement of 0.8 % is observed for $\alpha = 0.31$. The response shows that for $\alpha = 0.31$, the effect of fire protection is very significant as the protected beam does not deflect significantly during the fire in comparison to the unprotected beam. Moreover for $\alpha = 0.18$, the effect of fire protection is observed to be less significant as a result of the high residual displacement from the blast which reduces the effect of thermal strains on the beam.

6.2.4 Discussion

The effects of beam-to-column stiffness ratios on the structural response of the steel frame under consideration have been discussed. It was shown that under post-blast travelling fires; structural systems with lower α values may experience lower beam displacements, higher column lateral displacements and smaller beam axial forces while structural systems with higher α can experience higher beam displacements, lower column displacements and higher beam axial forces for low blast loads. In the event of a blast pressure in the region of the 183 kPa blast, high tensile forces may be experienced in the beam which can potentially decrease the beam axial force during the fire. Also, blast pressures and directions of travel of the fire can increase or decrease displacements and axial forces in the frame.

The study also revealed that when beam displacements need to be mitigated, a column section with a slightly smaller second moment of area (which does not undermine the integrity of the structure) can be used to accommodate this without changing the beam section. However, lower α systems will require a reasonable beam section or a degree of protection to avoid excessive beam displacements under very high blast loads and fire temperatures. The effect of fire protection is however observed to be insignificant for low blast loads that result in high upward beam displacements due to the stiffness of the beam. When downward beam displacements occur as a result of both actions, the effect of fire protection is more significant as it produces lower beam displacements. In this study, a stiffness ratio between 0.31 and 0.49 is found to be adequate enough to resist post-blast travelling fires.

6.3 Performance-based post-blast travelling fire assessment

The PEER performance-based travelling fire framework which was introduced in Chapter 2 and applied in Chapter 4 to travelling fire scenarios is extended in this section to include multi-hazard conditions involving post-blast travelling fires. This study is expected to assist structural engineers in the use of probabilistic approaches for designing and assessing steel buildings that may be susceptible to post-blast travelling fires during their design life. The first two parts of the framework – hazard and structural analyses are formulated first and probabilities of exceedance of the engineering demand parameters based on the combination of both actions are determined. The assessment is carried out for the different structural systems studied in the previous section.

6.3.1 Regression analyses

The numerical model presented in Figure 3.17 and the results of the analyses carried out in Chapter 5 are used in this section. The numerical model in Figure 3.17 has a steel beam-to-column stiffness ratio of 0.31. Numerical analyses are also carried out for the other beam-to-column stiffness ratios investigated in the previous section considering different blast and travelling fire scenarios. The following parts of this thesis consider an initial blast pressure applied at the first storey followed by a horizontally travelling fire at the ground floor compartment of that building. The structural response from the analyses were recorded and regression analyses are carried out to construct models that can be used to determine the relationship between key intensity measures (IM) and salient engineering demand parameters (EDP) for post-blast travelling fires. Three IMs and three EDPs are considered in this study. The IMs and EDPs employed are shown in Table 6.2.

The EDPs chosen are normalized against the member lengths and axial capacity, and they are expressed as percentages in Figure 6.7. The IMs are deemed to be able to effectively describe the severity of the blast and travelling fire based on the results described in Chapter 5. Also, the EDPs considered are known to adequately describe the structural response in these situations. The IMs and EDPs are assumed to follow a lognormal distribution based on initial assessment of the data by testing the fit of various distributions on the histogram of the data. A smaller sample data was used in this study compared to Chapter 4 as it is expected that the structural response under multi-hazard condition involving blast and fire will majorly be affected by the blast pressure, maximum compartment temperature and length of fire/fire size.

A scatter plot matrix of the parameters is presented in Figure 6.7 which shows univariate regression models for the natural log of the EDPs against the natural log of the IMs. The regression models are constructed using the equations in Chapter 4.

Table 6.2. Intensity measures and engineering demand parameters used in this study.

Intensity measure (IM)	**Description**	**Unit**
T_{max}	Maximum compartment temperature	°C
B_p	Blast overpressure	kPa
L_f	Length of fire	m
Engineering demand parameter (EDP)	**Description**	
MBD	Maximum beam displacement	% of beam length
MCD	Maximum column displacement	% of column height
MBC	Maximum beam compressive force	% of beam axial capacity

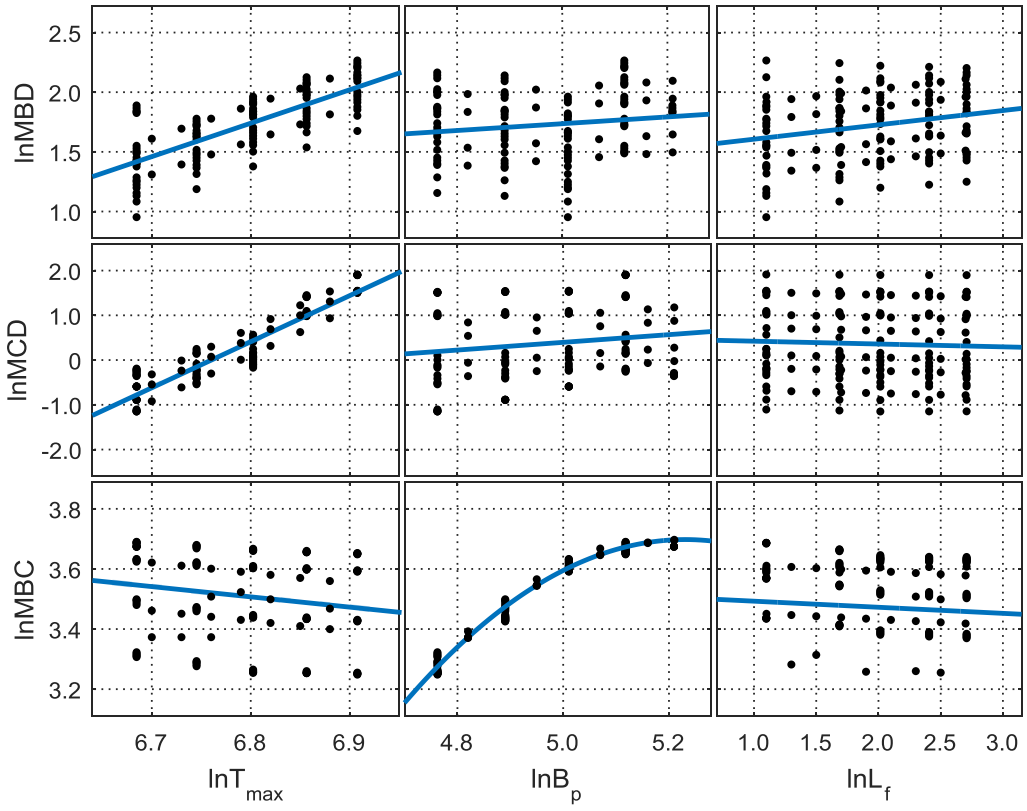

Figure 6.7. Scatter plot matrix of the natural logarithm of maximum beam displacement, maximum column displacement and maximum beam compressive force against the natural logarithm of the maximum compartment temperature, blast overpressure and length of fire.

The regression analyses are carried out to inform the application of the performance-based framework. From Figure 6.7, it can be observed that the IMs are well correlated with most of the EDPs considered. The scatter plot matrix shows that MBD and MCD increases as T_{max} increases which is expected. MBC is observed to decrease as T_{max} increases although the correlation between both parameters is low. The blast overpressure B_p is also observed to increase as MBD increases generally. Examining the scatter plot of lnMBD vs. lnB_p critically, it can be observed that sometimes increasing blast pressures might result in lower values of beam displacement for low blast loads. It should be noted that based on the results of Chapter 5, beam deflections may decrease during the fire in the downward direction due to high residual upward deflections from the blast. For higher blast pressures, upward beam deflections will occur in the frame which will increase as the blast pressure increases. MCD and MBC are also observed to increase as B_p increases due to increasing intensity of the blast with MBC showing strong correlations with B_p.

Figure 6.7 shows that increasing values of the length of fire L_f, which is directly related to the fire size results in an increase in MBD and a decrease in MBC. However, due to the effect of T_{max} and B_p, strong correlations are not observed for the plots of the EDPs against L_f. This is because high temperature values or blast overpressures can increase the EDP values even when the length of fire or fire size is low. The direction of travel of the fire can also affect the structural response. Nevertheless, it is important to note that the regression curves are only applicable to the range of IM values and the structural configuration considered.

The above explanation considers the influence of only one IM on the structural response (EDP) which is unrealistic in practical terms as the structure is subjected to two different types of loads which should be represented in the regression models. In this study, multivariate regression analyses are also carried out considering two intensity measures. As in Chapter 4, the IMs with the lowest value of standard deviation are considered to be the most efficient IMs for the performance-based post-blast travelling fire framework. The standard deviation values of the natural log of EDP|IM for both the univariate and multivariate regression analyses are presented in Table 6.3. From this table, it can be observed that the most efficient IM vector is the combination of T_{max} and B_p for each EDP considered since it has the lowest value of standard deviation. Based on the results of the regression analyses, a Vector IM consisting of T_{max} and B_p is used as the IM for the performance-based post-blast travelling fire framework in this study.

Table 6.3. Standard deviation values of EDP|IM.

EDP	Standard deviation $\sigma_{EDP\|IM}$			Standard deviation $\sigma_{EDP\|IM_1,IM_2}$		
	T_{max}	B_p	L_f	T_{max}, B_p	B_p, L_f	T_{max}, L_f
MBD	0.190	0.294	0.289	0.127	0.288	0.178
MCD	0.300	0.884	0.891	0.198	0.887	0.299
MBC	0.154	0.022	0.098	0.013	0.022	0.099

It is important to note that there is a possibility that the blast overpressure may have a correlation with the length of fire based on previous studies that proposed the relationship between the diameter of fire balls and the mass of explosives (Gayle and Bransford (1965), Stull (1977), Baker et al. (1983)). Also, based on the results presented in this thesis, it is possible that there may be some correlation between T_{max} and B_p. However, these were not considered in this thesis as it is assumed that the fire characteristics will be mainly influenced by the fuel loads in the compartment. It is understood that the combination of random values of IMs used in the regression analyses may not adequately capture the real correlation between the IMs. As a result, three values of correlation (ρ = 0, 0.8 and -0.8) as in Chapter 4 are adopted. This considers the case of zero correlation, high positive correlation and high negative correlation between T_{max} and B_p. It is assumed that the actual correlation value will fall within these boundaries.

6.3.2 Hazard analysis

The hazard analysis determines the annual rate of exceeding the IM and it is an input into the second part of the performance-based framework i.e. the structural analysis. As explained before in Chapter 4, the annual rate of exceeding the IM (λ_{IM}) is determined by multiplying the rate of occurrence of the action λ_E by the probability of exceeding the IM denoted by $P(IM)$. A value of 1.0 is assumed in this thesis to represent the annual rate of occurrence of the combined actions (λ_E). The annual rate of occurrence will usually be determined from a database of records of post-blast travelling fires, which is then used to predict the probability of blast and travelling fires that occur in a year. Since two IMs are used, the Joint PDF and Probability of exceedance (POE) curves are determined for the two IMs. Figure 6.8 shows the PDF and POE curves for the two IMs. Figure 6.9 presents the Joint POE curves for the 3 values of correlation considered while Figure 6.10 shows the Joint PDF curves.

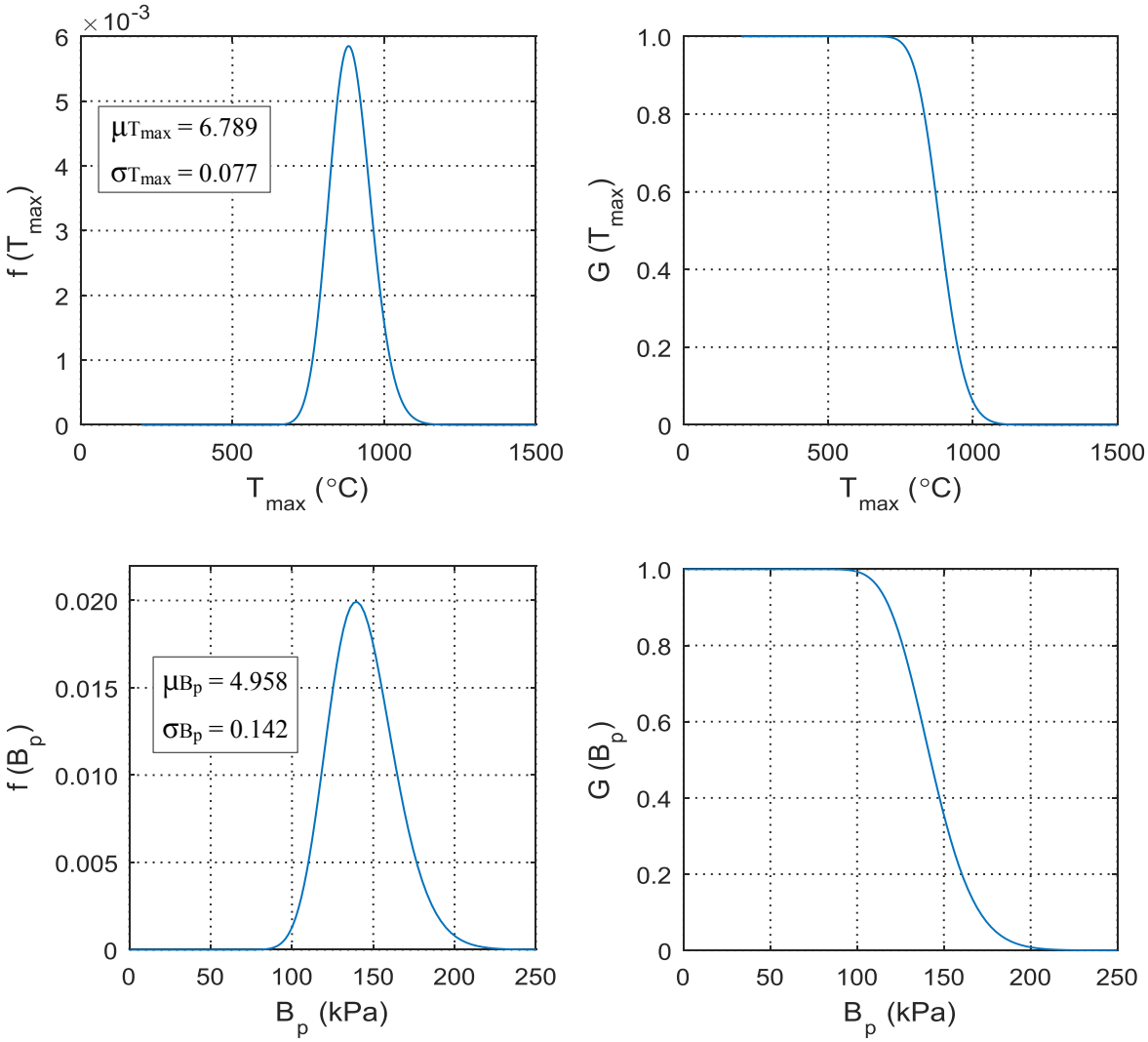

Figure 6.8. Probability distribution and Probability of exceedance curves for the maximum compartment temperature and blast overpressure.

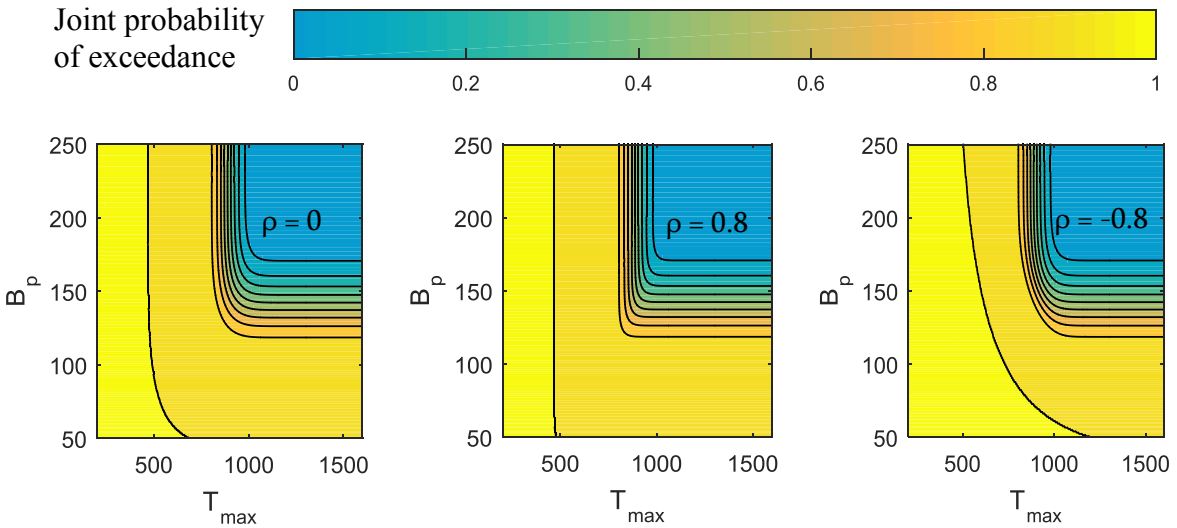

Figure 6.9. Joint probability of exceedance of maximum compartment temperature and blast overpressure.

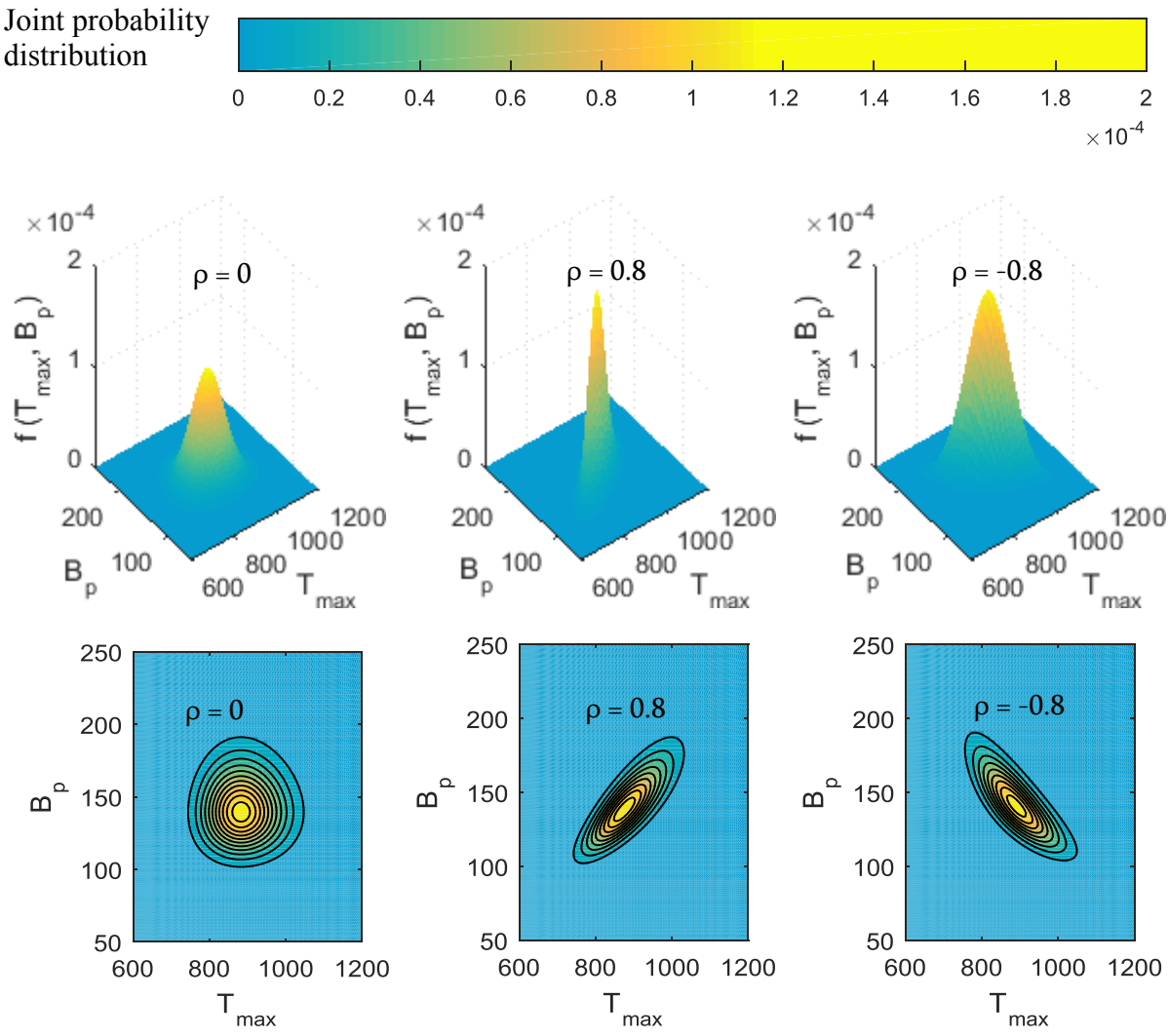

Figure 6.10. Joint probability distribution of maximum compartment temperature and blast overpressure (surface and contour plots).

6.3.3 Structural analysis

Three EDPs which are Maximum beam displacement (MBD), Maximum column displacement (MCD) and Maximum beam compressive force (MBC) are adopted for the structural analyses part of the performance-based assessment. As before, a lognormal distribution is assumed for the EDPs. The structural analysis part of the performance-based assessment yields the annual probability of exceeding the EDP which is evaluated numerically as the integral of the probability of exceeding the EDP given a value of IM i.e. $P(EDP|IM)$ with respect to the annual probability of exceeding the IM, i.e. λ_{IM}. The integration is carried out over the full hazard curve considering all possible combinations of both IMs. An adequate number of values for each IM is chosen to ensure that λ_{IM} adds up to 1. Figure 6.11 shows the probability distribution of the EDPs based on values of the Vector IM and it is observed to fit well with the

structural analyses data. The probability of exceedance of the EDPs are presented in Figure 6.12 to Figure 6.15 for the different beam to column stiffness ratios considering a Vector IM of T_{max} and B_p.

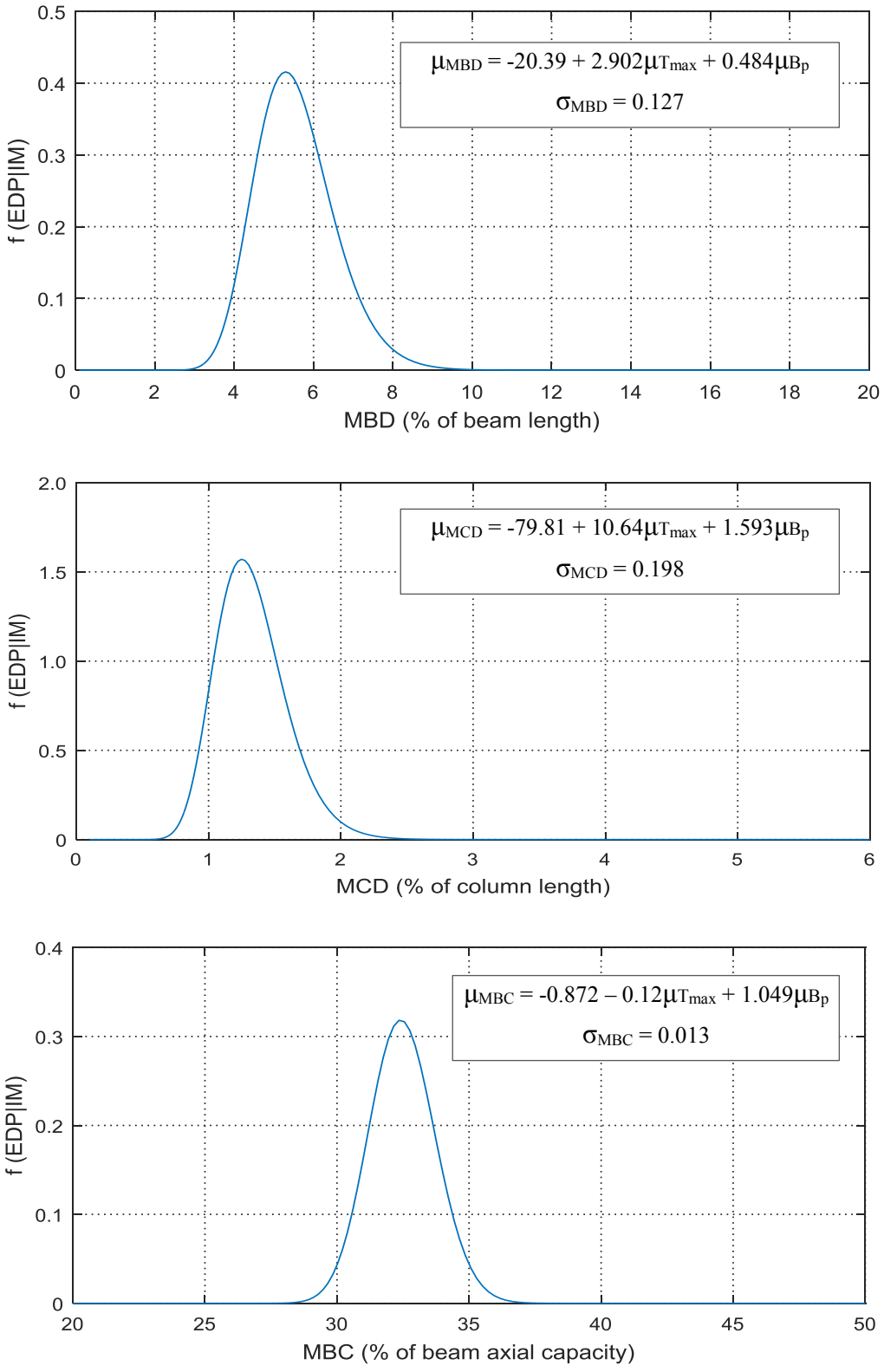

Figure 6.11. Probability distribution of the EDPs considering a Vector IM of T_{max} and B_p.

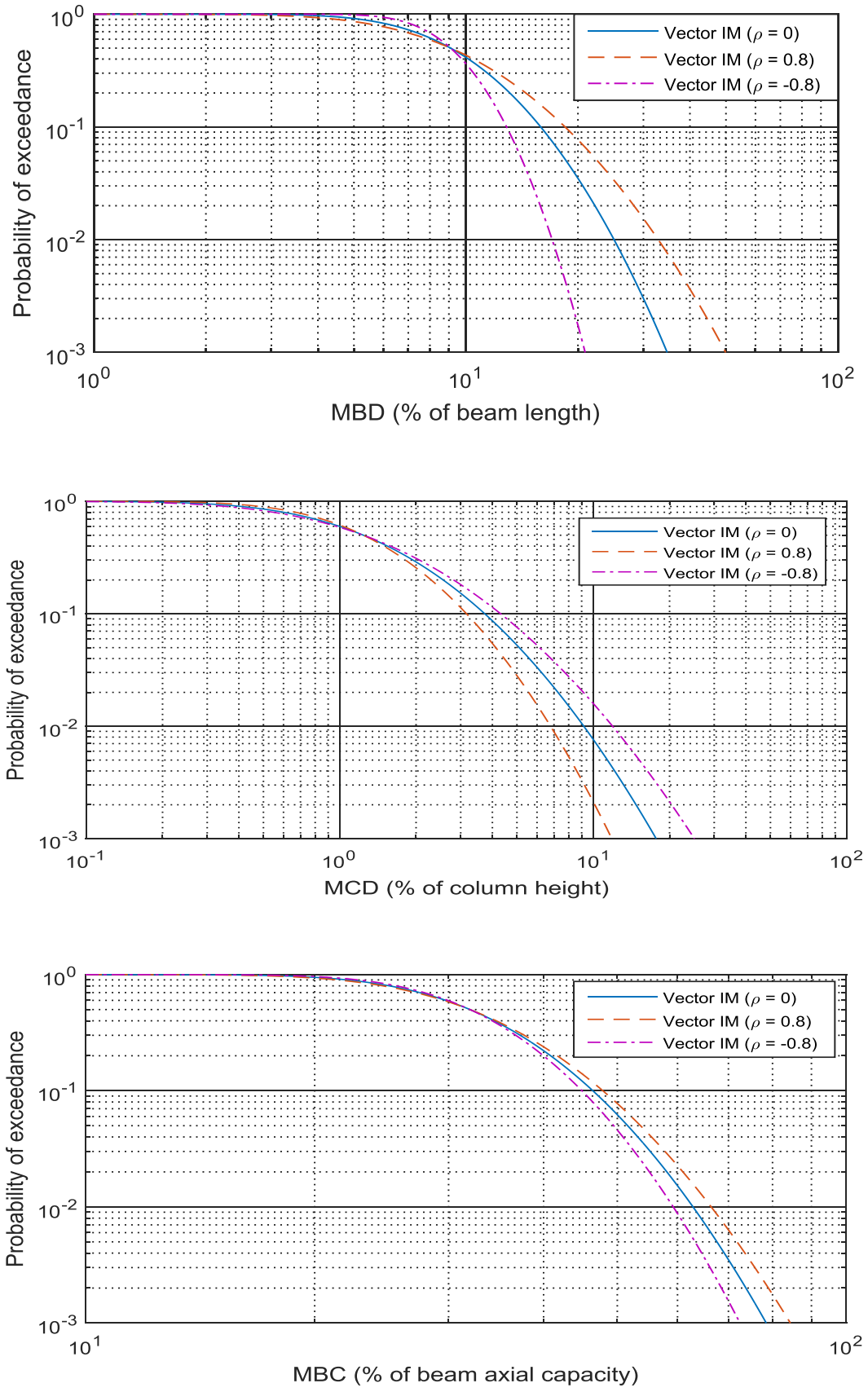

Figure 6.12. Probability of exceedance curves of the EDPs for the three values of correlation when $\alpha = 0.18$.

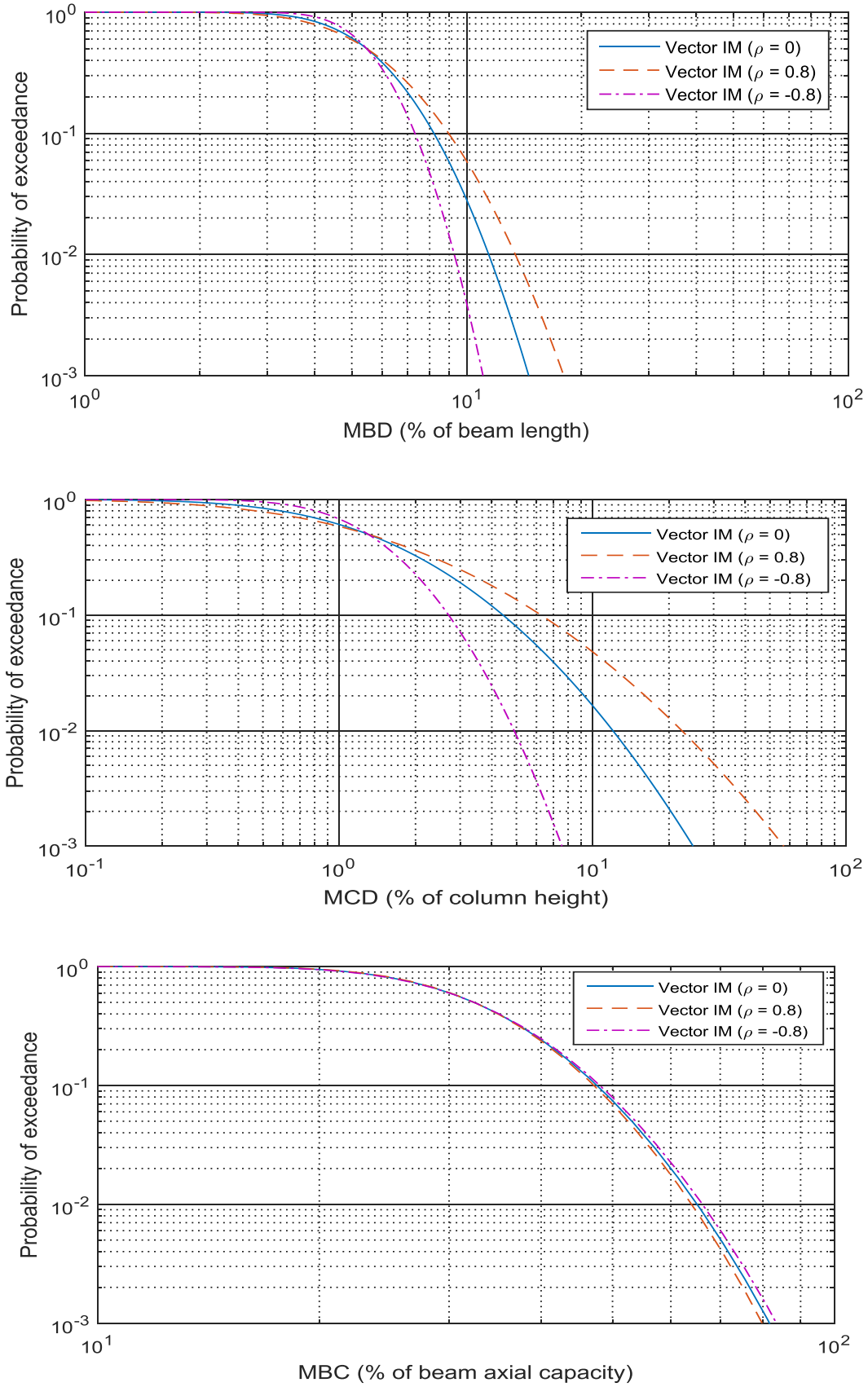

Figure 6.13. Probability of exceedance curves of the EDPs for the three values of correlation when $\alpha = 0.31$.

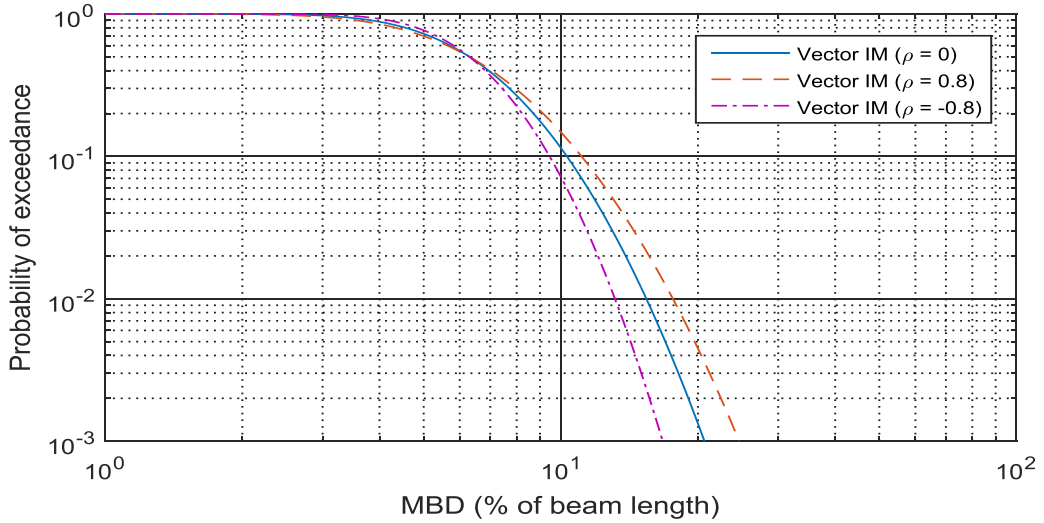

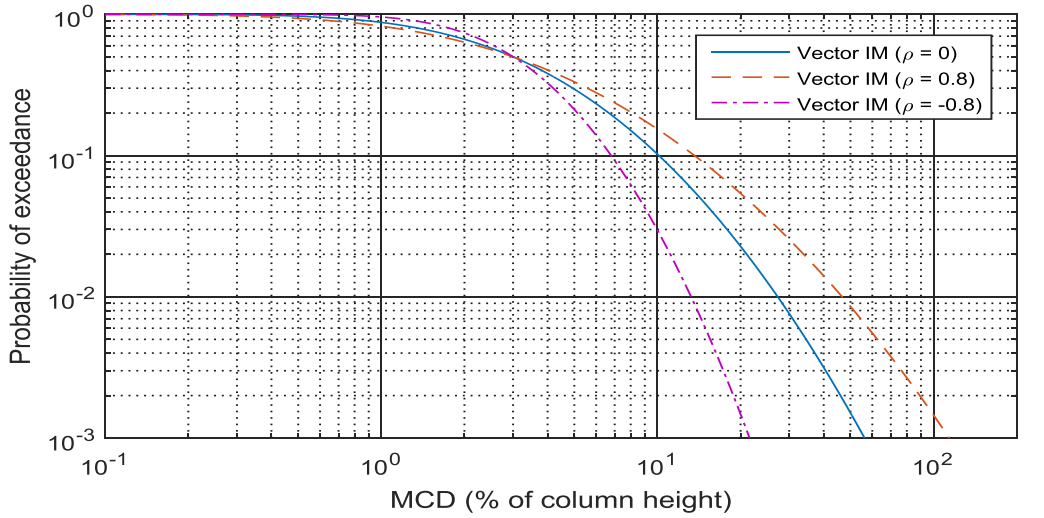

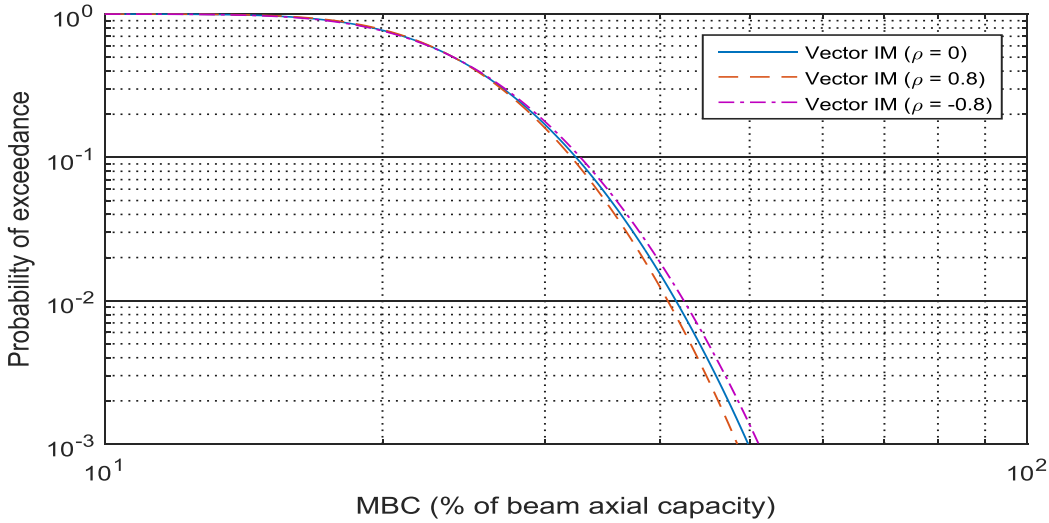

Figure 6.14. Probability of exceedance curves of the EDPs for the three values of correlation when $\alpha = 0.49$.

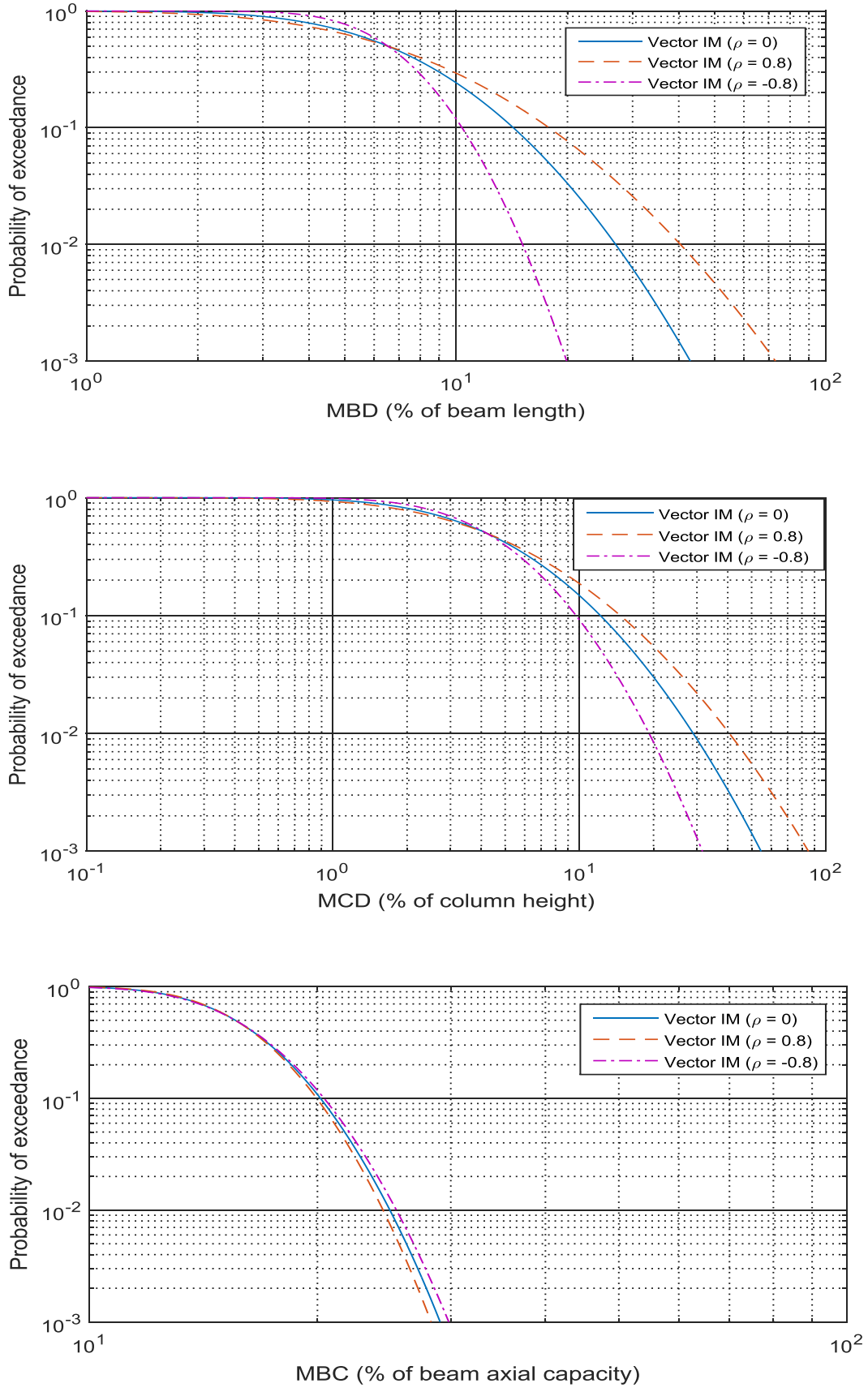

Figure 6.15. Probability of exceedance curves of the EDPs for the three values of correlation when $\alpha = 0.67$.

6.3.4 Discussion

Figure 6.7 demonstrates the effect of the selected IMs on the structural response of the frame under consideration. The maximum compartment temperature (T_{max}) and the blast overpressure (B_p) were found to be the most suitable IMs for the performance-based framework based on the results of the multivariate analyses. Also, the combination of both IMs results in a better prediction of the EDPs and reflects the contribution of both the blast and fire actions. The probability of exceedance curves of the EDPs in Figure 6.12 to Figure 6.15, which are presented in log scale, show the impact of high and zero correlation between T_{max} and B_p especially for low probabilities of exceedance. The plots also demonstrate the effect of the different structural systems on the performance of the structure.

From Figures 6.12 to 6.15, it is possible to deduce that the effects of high correlation between the IMs are more pronounced in the Maximum beam displacement (MBD) for $\alpha = 0.18$ and 0.67, and in the Maximum column displacement (MCD) for $\alpha = 0.31$ and 0.49 for low probabilities of exceedance. This is attributed to the high beam and column displacements associated with these stiffness ratios making the structural frame easily influenced by the significant correlation between the IMs. Also, high correlation is observed to have negligible effect on the Maximum beam compressive force (MBC) for all the stiffness ratios except for $\alpha = 0.18$ when low exceedance rates are considered. This is due to the high compressive forces in the frame especially for lower blast pressures. It is also observed that for $\alpha = 0.18$ at an exceedance rate of 0.001, a high positive correlation results in a percentage increase of 7.59 % from the zero correlation case while a negative correlation results in a percentage decrease of 8.86 %. The values of the EDPs for the high and zero correlation at an exceedance rate of 0.001 are presented in Table 6.4 for the different beam to column stiffness ratios. From this table, it can be observed that the highest value of MBD occurs when $\alpha = 0.67$ while the highest value of MCD and MBC occur when $\alpha = 0.49$ and 0.18 respectively and this can be used to assess performance levels.

Table 6.4. EDP values at a probability of exceedance of 0.001.

	MBD (%)			**MCD (%)**			**MBC (%)**		
α	**ρ = -0.8**	**ρ = 0**	**ρ = 0.8**	**ρ = -0.8**	**ρ = 0**	**ρ = 0.8**	**ρ = -0.8**	**ρ = 0**	**ρ = 0.8**
0.18	20	35	50	25	17	13	72	79	85
0.31	12	16	18	8	25	55	80	81	83
0.49	17	20	25	20	55	120	52	50	48
0.67	20	43	70	30	55	85	30	29	28

Probability of failure

The probability of failure of the steel frame can also be determined from the hazard curves, based on the probability of exceeding a value of EDP as a means of assessing the suitability of the structural system in resisting the blast and travelling fire actions. For instance, using a failure criterion of L/20 (5%) for the Maximum beam displacement (MBD) consistent with BSI (2009), the probability of failure of the building can be determined from the EDP exceedance curves for each beam to column stiffness ratio, which are presented in Table 6.5. These values can be multiplied by the annual rate of occurrence of the actions (to determine the annual rate of exceeding the MBD) and compared with a target probability of failure. Table 6.5 shows that the structural system with $\alpha = 0.31$ is the most efficient based on the failure criterion considered. Note that this ignores any uncertainty in the capacity at this failure limit.

Table 6.5. Probability of exceedance of MBD at a failure criterion of L/20 (for λ_E = 1.0).

Correlation (ρ)	**Beam to column stiffness ratio (α)**			
	α = 0.18	**α = 0.31**	**α = 0.49**	**0.67**
-0.8	0.986	0.653	0.767	0.770
0.0	0.915	0.611	0.726	0.669
0.8	0.860	0.592	0.699	0.633

6.4 Conclusions

This study demonstrates that under post-blast travelling fires, structural systems with stiffness ratios of 0.18 and 0.31 can experience higher beam displacements and axial forces while higher column lateral displacements can be expected in higher stiffness ratios. The regression analyses showed that a Vector IM of the maximum compartment temperature and blast overpressure is suitable for the PEER performance-based post-blast travelling fire framework. This study also proves that a performance-based assessment can be used over current design methods to determine the structural performance of buildings based on the EDP values at specified exceedance rates. It can also provide information on the need for blast and fire protection systems if the passive resistance of the structural members are insufficient to resist the overall effect of the actions. The framework formulated in this study is a fundamental step to understanding how the PEER performance-based framework can be adapted for post-blast travelling fire assessment. It is anticipated that further research will be carried out in this area.

Chapter 7
Conclusions and Future Work

This Chapter presents a summary of the findings of previous chapters of this thesis. Recommendations are also given with regards to assessment approaches that can be used by engineers and the limitations of the research are explained. Finally, several avenues of future research are outlined.

The main objective of this thesis was to study the performance of steel structures under travelling fires as well as post-blast travelling fires including the adoption of the PEER performance-based framework to assess the performance of structures under these actions. A detailed review which explored previous research in structural fire design, blast and performance-based design was performed. The review showed that current fire design methods are only applicable to smaller compartments and travelling fires will need to be considered. Also, travelling fires may be triggered by initial blast events and performance-based design is likely to be more suitable in assessing structures under these actions.

The finite element program, OpenSees was tested for its ability to analyse structures under blast and fire actions by comparing OpenSees results with those of previous experimental and numerical studies. The numerical models employed in this research were also discussed. To this end, a one-bay 7-storey slice of a typical steel-framed office building was selected. The sensitivity analyses carried out on the numerical model determined the adequate number of beam elements for the composite beams.

Furthermore, an assessment was carried out which determined the most efficient intensity measures for the PEER performance-based travelling fire framework. This was subsequently used in the performance-based framework to determine the probability of exceedance of the engineering demand parameters. Preliminary studies were undertaken to determine the most critical floor under different blast and travelling fire scenarios. Parametric analyses were then carried out to determine the effects of blast and travelling fire parameters on the performance of the steel frame under different post-blast travelling fire scenarios. Moreover, the effects of different beam to column stiffness ratios on the steel frame under post-blast travelling fires were also explored. Finally, a performance-based assessment was carried out to evaluate the probability of exceedance of selected EDPs for the steel frame, considering several post-blast

travelling fire scenarios and different structural systems. This was used to assess the performance of the building based on the probability of exceedance and probability of failure.

7.1 Conclusions and Recommendations

OpenSees for blast and fire actions

The capability of the OpenSees software was verified in Chapter 3 with regards to its ability to analyse blast and thermal actions. Previous numerical studies with regards to the structural fire response of steel beams, composite beams and steel frames were replicated in OpenSees and the results compared well with those of previous studies. Former studies on the blast response as well as blast and fire response of steel columns and frames also compared well with the results from OpenSees. Blast analyses have been carried out in OpenSees considering a recommended dynamic factor to accommodate strain rate effects (UFC, 2008). A representative analysis has also been used to combine the blast and fire analyses scripts in OpenSees. It was concluded that OpenSees is a suitable tool for analysing structures subjected to blast and fire actions in tandem. However, it is recommended that more sophisticated software with constitutive models that can handle both actions concurrently should be explored in future studies.

Performance-based assessment of steel structures under travelling fires

From the regression analyses carried out in Chapter 4, it has been concluded that the maximum compartment temperature and the length of fire or fire spread rate are adequate as Vector IMs for performance-based travelling fire assessment based on the EDPs and structural configurations considered. Also, EDP values might be overestimated or underestimated by up to 30 % if the correlation between the maximum compartment temperature and length of fire is ignored especially for very low probabilities of exceedance. This means that the length of fire which is directly proportional to the fire size is an important parameter in structural fire design, especially for buildings with large compartments. Therefore, it cannot be ignored as in current design methods which consider only the maximum compartment temperature, an approach that may lead to poor predictions of the structural response.

It is recommended that all possible fire scenarios including travelling fires be considered in structural fire design. Also, the PEER performance-based framework should be used to design or assess steel structures for fires in large compartments. This is because the performance of

the structure can be determined based on the value of exceedance rates of structural response parameters in comparison with a specified performance target. The outputs of the performance-based framework can also give significant and valuable information on the structural members requiring fire protection which can lead to great savings in the overall cost of building projects.

Effects of post-blast travelling fires on steel frames

Preliminary studies were carried out in Chapter 5 to determine the most vulnerable floor when the numerical model was analysed for different blast and travelling fire scenarios. These studies showed that for an initial blast pressure, the first floor beams might experience the largest displacements and axial forces under a single floor horizontally travelling fire, simultaneously burning multiple floor travelling fire as well as vertically travelling fire scenarios. Also, under these scenarios, the upper floor columns tend to have higher displacements when the blast pressure causes a displacement of less than 2 % of the column length. It was demonstrated that the first storey is most likely to be the most vulnerable floor in the building.

Parametric analyses were subsequently carried out to determine the effects of the blast pressure, fire size, direction of travel and maximum compartment temperature on the performance of the steel frame under different post-blast travelling fire scenarios. It was concluded that under post-blast travelling fires, blast pressures can cause an initial upward or downward residual deflection in the beam. Also, fires travelling in the east-west direction can cause lower axial forces and lower or higher beam displacements. Smaller fire sizes in some cases can produce higher displacements and axial forces. Maximum compartment temperature can also significantly increase beam and column displacements.

The study showed that the fire resistance is reduced when there is an initial blast event. Also, the fire size and direction of travel are important parameters that can affect the structural response other than the blast pressures and increasing temperatures. It is therefore recommended that structural engineers saddled with the responsibility of designing key facilities for blast and fire resistance ensure that first storey members are properly protected to avoid extensive damage or collapse under these actions. Moreover, adequate blast and fire protection should be provided to increase the resistance of the frame under these actions where necessary. Also, all possible directions of travel and realistic fire sizes need to be considered in design.

Performance-based post-blast travelling fire assessment

The performance of different structural systems under post-blast travelling fires was studied in Chapter 6. The structural behaviour of different beam-to-column stiffness ratios was first investigated. The study showed that increasing the beam-to-column stiffness ratio can result in a decrease in beam displacements and an increase in column displacement. Also, lower beam displacements, lower beam axial forces and higher column displacements can occur in structural systems with lower stiffness ratios such as 0.18 to 0.31 while higher beam displacements, higher beam axial forces and lower column displacements are expected in systems with higher stiffness ratios. The intensity of the initial blast load and the direction of travel of the fire can also have a significant influence on the structural response of both structural systems.

Subsequently, regression analyses were carried out considering Scalar and Vector IMs in order to determine the most efficient intensity measures (IM) under blast and travelling fires. A performance-based assessment was then performed to determine the performance of the steel frame for different structural systems. The study showed that the maximum compartment temperature and the blast overpressure can be used as a Vector IM for a performance-based post-blast travelling fire assessment. Also, the effect of high correlation between the maximum compartment temperature and the blast overpressure was found to be more significant for the Maximum beam displacement and Maximum column displacement for low probabilities of exceedance. A study on the probability of failure of the steel frame indicated that the structural system with a stiffness ratio of 0.31 was the most efficient system for the structure considering a failure criterion of L/20 of the Maximum beam displacement when a rate of occurrence of 1.0 was adopted.

It is recommended that engineers take advantage of the redistribution of forces between structural members in different structural systems when determining the appropriate sections for members designed to resist post-blast travelling fires. This can cause significant reduction in the amount of blast or fire protection required resulting in a more cost-effective and efficient solution. Also, a performance-based framework should be adopted when the efficiency or performance of steel structures under these actions are required so that important decisions can be made with regards to the acceptable risk level or performance target.

7.2 Limitations of research

This research was carried out considering a one-bay seven storey slice of a steel building supported by columns on the left and a reinforced concrete core on the right. Although the conclusions reached are expected to be generalizable, the results of this research are particularly relevant to this structural configuration. The sections of the composite beams and columns used in this thesis are also representative of particular practices and smaller section sizes with adequate fire protection might be used in some cases. Also, fully rigid connections at the beam - column joints were assumed in the thesis, while pin and semi-rigid connections may be more common in practice.

Only blast pressures from suitcase bombs are considered in this thesis. Moreover, only positive pressures were considered in this study for a simplified blast analyses, although based on the typical blast pressure-time history, negative blast pressures can be expected to be critical in some selected cases. It is also important to note that for internal explosions, repeated blast histories can occur with decreasing maximum blast pressures, but this was not considered in this thesis. Also, the coupling of blast and fire analyses in OpenSees as discussed in Section 3.3.2 represents a practical simplification for the purpose of the extensive analyses carried out in this thesis. The implication of shear failure occurring before flexural failure was not considered based on the fully rigid connections assumed for the beam-column joints.

Most of the fire analyses carried out in this research (especially post-blast travelling fires) considered a maximum compartment temperature of 800 °C. It is understood that higher temperatures can occur in building fires. However, 800 °C was used so that the numerical response under both blast and travelling fires can be achieved without convergence issues especially for higher blast pressures. This was observed for studies involving the 183 kPa blast and a travelling fire with a maximum compartment temperature of 1000 °C.

The combination of parameter values used for the regression analyses were randomly selected to represent bounding cases due to the lack of information on the actual correlation values and may not accurately represent the actual correlations between the intensity measures selected for the performance-based studies. Also, only two parts of the PEER performance-based framework (hazard and structural analysis) were adapted for travelling fires and post-blast travelling fires, and a value of 1.0 was assumed for the rate of occurrence of the actions which will have an impact on the values of the annual rate of exceeding the intensity measure. The

remaining parts of the framework i.e. damage and loss analyses were not considered in this study.

7.3 Future work

Based on the findings of the research and the limitations of the studies carried out, the following future work can be anticipated:

1. An investigation on the effects of different structural configurations and lateral support systems on the response of steel frames under blast and travelling fires.
2. Performance of typical steel composite buildings considering other beam sections for instance, beams with web openings under blast and travelling fires.
3. A study on the effects of different types of connections on the performance of steel frames under both actions.
4. Detailed investigation on the effects of fire protection on the structural performance of steel frames under post-blast travelling fires especially for high blast pressures.
5. An extension of the PEER performance-based framework formulated in this research to consider other parts of the framework for the actions studied. In particular, the damage and loss analyses part of the framework should also be formulated considering a proper hazard assessment with the actual value of the rate of occurrence in order to provide a more robust framework for assessing these actions.
6. Investigation of the response of steel frames under very high blast pressures and travelling fires. As the research mainly considered blast pressures between 117 kPa and 183 kPa, it will be interesting to see how explosives with higher pressures followed by travelling fires will affect the structural response of steel structures.
7. A more advanced method of coupling blast and fire analyses in OpenSees and its implications can be explored. Presently, there is no material model in OpenSees that can combine strain rate effects due to blast and mechanical degradation under elevated temperatures. It will be beneficial to implement new material models in OpenSees (being an open source program) that can predict the effect of both actions simultaneously.
8. Consideration of stochastic load models for blast and travelling fires as well as more physically motivated regression equations between the EDPs and IMs.

References

Alpert R. (1972) Calculation of response time of ceiling-mounted fire detectors. Fire Technology. 8, 181.

Asprone, D., Jalayer, F., Prota, A. & Manfredi, G. (2010) Proposal of a probabilistic model for multi-hazard risk assessment of structures in seismic zones subjected to blast for the limit state of collapse. *Structural Safety*. 32, 25-34.

Baker, W.E, Cox, P.A, Westine, P.S, Kulesz, J.J & Strehlow, R.A. (1983) *Explosions*. Hazards Evaluation. (Amsterdam: Elsevier).

Barbato, M., Petrini, F., Unnikrishnan, V. & Ciampoli, M. (2013) Performance-Based Hurricane Engineering (PBHE) framework. *Structural Safety*. 45, 24-35. Available from: doi:10.1016/j.strusafe.2013.07.002.

Bray J. D & Travasarou Th. (2003) Optimal ground motion intensity measures for assessment of seismic slope displacements. In: *2003 Pacific conference on earthquake engineering*, New Zealand, February 13-15.

British Standards Institution (2002) BS EN 1991-1-2:2002. *Eurocode 1: Actions on structures. Part 1-2: General actions - Actions on structures exposed to fire*. BSI.

British Standards Institution (2005) BS EN 1994-1-2:2005. *Eurocode 4: Design of composite steel and concrete structures. Part 1-2: General rules - Structural fire design*. BSI.

British Standards Institution (2009) BS 476-10:2009. *Fire tests on building materials and structures. Guide to the principles, selection, role and application of fire testing and their outputs*. BSI.

Buchanan, A.H (2002) *Structural Design for Fire Safety*. London, John Wiley & Sons.

Buratti, N. (2012) A comparison of the performances of various ground–motion intensity measures. *15th World Conference on Earthquake Engineering*. Lisbon, Portugal, September 24-28.

Burgess, I. & Alexandrou, M. (2014) Steel beams. In: Wald F., Burgess I., Kwasniewski L., Horová K., Caldová E. (eds.) *Benchmark studies. Verification of numerical models in fire engineering*. Czech Technical University, Prague, CTU Publishing House, 30-40.

Chen, H. & Liew, J. (2005) Explosion and fire analysis of steel frames using mixed element approach. *Journal of Engineering Mechanics*. 131(6), 606-616. Available from: doi:10.1061//asce/0733-9399/2005/131:6/606.

Clifton, G.C (1996) *Fire models for large firecells*. HERA Report R4-83. Heavy Engineering Research Association, Auckland, New Zealand.

Coile, R.V & Bisby, L. (2017) Initial probabilistic studies into a deflection-based design format for concrete floors exposed to fire. *Procedia Engineering*. 210, 488-495.

Cornell, A. & Krawinkler H. (2000) *Progress and challenges in seismic performance assessment*. PEER Center News, 3(2), 1-3.

Cornell, C.A., Jalayer, F., Hamburger, R.O. & Foutch, D.A. (2002). Probabilistic basis for 2000 SAC Federal Emergency Management Agency steel moment frame guidelines. *Journal of Structural Engineering*. 128(4), 526 - 533.

Dassault Systèmes (2008) Abaqus analysis user's manual.

Ding, Y., Wang, M., Li, Z.-X. & Hao, H. (2013) Damage evaluation of the steel tubular column subjected to explosion and post-explosion fire condition. *Engineering Structures*. 55, 44-55. Available from: doi:10.1016/j.engstruct.2012.01.013.

Drysdale, D. (2011) *An introduction to fire dynamics*. United Kingdom, John Wiley & Sons Ltd.

Elliot, C. (2009) Introduction. In: Cormie, D., Mays, G. & Smith, P. (eds.) *Blast effects on buildings*. United Kingdom, ICE Publishing.

Elsanadedy, H. M., Almusallam, T. H., Alharbi, Y. R., Al-Salloum, Y. A. & Abbas, H. (2014) Progressive collapse potential of a typical steel building due to blast attacks. *Journal of Constructional Steel Research*. 101, 143-157. Available from: doi:10.1016/j.jcsr.2014.05.005.

Fallah, A.S, Nwankwo, E. & Louca, L.A (2013). Pressure-Impulse Diagrams for blast loaded continuous beams based on dimensional analysis. *Journal of Applied Mechanics*. 80(5), 051011

Fang, C., Izzuddin, B. A., Elghazouli, A. Y. & Nethercot, D. A. (2011) Robustness of steel-composite building structures subject to localised fire. *Fire Safety Journal*. 46(6), 348-363. Available from: doi:10.1016/j.firesaf.2011.06.001.

Federal Emergency Management Agency (1997) *NEHRP Guidelines for the Seismic Rehabilitation of Buildings*. Report No. FEMA 273, Applied Technology Council for FEMA, Washington, D.C.

Fischer, E. C. & Varma, A. H. (2017) Fire resilience of composite beams with simple connections: Parametric studies and design. *Journal of Constructional Steel Research*. 128, 119-135. Available from: doi:10.1016/j.jcsr.2016.08.004.

Foster, S., Chladná, M., Hsieh, C., Burgess, I. & Plank, R. (2007) Thermal and structural behaviour of a full-scale composite building subject to a severe compartment fire. *Fire Safety Journal*. 42(3), 183-199. Available from: doi:10.1016/j.firesaf.2006.07.002.

Franssen J-M. (2005) SAFIR: A thermal/structural program for modelling structures under fire. *Engineering Journal-American Institute of Steel Construction Inc*. 42(3), 143-158.

Gayle, J.B & Bransford, J.W. (1965) *Size and Duration of Fireballs from Propellant Explosions*. Report Number NASA-TM-X-53314, George C. Marshall Space Flight Centre, Huntsville, Alabama.

Gernay, T. & Franssen, J. M. (2015) A performance indicator for structures under natural fire. *Engineering Structures*. 100, 94-103. Available from: doi:10.1016/j.engstruct.2015.06.005.

Hamilton, S. R. (2011) *Performance-Based Fire Engineering For Steel Framed Structures: A Probabilistic Methodology.* PhD Thesis. Stanford University. https://stacks.stanford.edu/file/druid:mh477sw7685/Dissertation%20Final%20Version-augmented.pdf.

Health and Safety Executive (2008) *Modelling of pool fires in offshore hazard assessments*. HSE information sheet. Offshore information sheet No.9/2008.

Hilber, H., Hughes, T. & Taylor, R. (1977) Improved numerical dissipation for time integration algorithms in structural dynamics. *Earthquake Engineering & Structural Dynamics*. 5(3), 283-292.

Huang, Z., Burgess, I.W. & Plank, R.J. (2003) Modelling membrane action of concrete slabs in composite buildings in fire. In: Theoretical development. *Journal of Structural Engineering*. 129(8), 1093-1102.

Izzuddin, B.A. (1991) *Nonlinear dynamic analysis of framed structures*. PhD Thesis. Imperial College, University of London.

Izzuddin, B. A., Song, L., Elnashai, A. S. & Dowling, P. J. (2000) An integrated adaptive environment for fire and explosion analysis of steel frames - Part II: verification and application. *Journal of Constructional Steel Research*. 53, 87-111.

Jiang, J., Li, G-Q. & Asif Usmani, A. (2015) Analysis of Composite Steel-concrete Beams Exposed to Fire using OpenSees. *Journal of Structural Fire Engineerin*g. 6(1), 1-20. Available from: https://doi.org/10.1260/2040-2317.6.1.1.

Jiang, Y., Kotsovinos, P., Usmani, A., Rein, G. & Stern-Gottfried, J. (2013) Numerical Investigation of Thermal Responses of a Composite Structure in Horizontally Travelling fires Using OpenSees. *Procedia Engineering*. 62, 736-744. Available from: doi:10.1016/j.proeng.2013.08.120.

Khan, S., Saha, S. K., Matsagar, V. A. & Hoffmeister, B. (2017) Fragility of Steel Frame Buildings under Blast Load. *Journal of Performance of Constructed Facilities*. 31(4), 04017019. Available from: doi:10.1061/(asce)cf.1943-5509.0001016.

Kirby, B. R., Wainman, D. E., Tomlinson, L. N., Kay, T. R. & Peacock, B. N. (1994) *Natural fires in large scale compartments*. [Online] British Steel. Available from: http://www.mace.manchester.ac.uk/project/research/structures/strucfire/DataBase/TestData/Cardington_NaturalFiresLargeScaleCompartments94.pdf.

Kotsovinos, P. (2013) *Analysis of the structural response of tall buildings under multifloor and travelling fires.* PhD thesis. The University of Edinburgh. https://www.era.lib.ed.ac.uk/handle/1842/8007.

Kotsovinos, P., Jiang, Y. & Usmani, A. (2013) Effect of vertically travelling fires on the collapse of tall buildings. *International Journal of High-Rise Buildings*. 2(1), 49-62.

Lange, D., Devaney, S. & Usmani, A. (2014) An application of the PEER performance based earthquake engineering framework to structures in fire. *Engineering Structures*. 66, 100-115. Available from: doi:10.1016/j.engstruct.2014.01.052.

Lange, D., Röben, C. & Usmani, A. (2012) Tall building collapse mechanisms initiated by fire: Mechanisms and design methodology. *Engineering Structures*. 36, 90-103. Available from: doi:10.1016/j.engstruct.2011.10.003.

Law, A., Stern-Gottfried, J., Gillie, M. & Rein, G. (2011) The influence of travelling fires on a concrete frame. *Engineering Structures*. 33(5), 1635-1642. Available from: doi:10.1016/j.engstruct.2011.01.034.

Lennon, T. & Moore, D. (2003) The natural fire safety concept—full-scale tests at Cardington. *Fire Safety Journal*, 38(7), 623-643. doi: 10.1016/s0379-7112(03)00028-6.

Lien, K. H., Chiou, Y. J., Wang, R. Z. & Hsiao, P. A. (2009) Nonlinear behavior of steel structures considering the cooling phase of a fire. *Journal of Constructional Steel Research*. 65(8-9), 1776-1786. Available from: doi:10.1016/j.jcsr.2009.03.015.

Liew, J. Y. R. (2008) Survivability of steel frame structures subject to blast and fire. *Journal of Constructional Steel Research*. 64(7-8), 854-866. Available from: doi:10.1016/j.jcsr.2007.12.013.

Liew, J. Y. R. & Ma, K. Y. (2004) Advanced analysis of 3D steel framework exposed to compartment fire. *Fire and Materials*. 28(24), 253-267. Available from: doi:10.1002/fam.850.

Louca, L.A & Boh, J.W. (2004) *Analysis and Design of Profiled Blast Walls*. Health and Sfety Executive, Research report 146.

Majdalani, A.H. & Torero, J.L (2011) *Compartment fire analysis for modern infrastructure*. 1^0 Congresso Ibero-Latino-Americano sobre Seguranca contra Incendio, Natal, Brazil.

Málaga-Chuquitaype, C., Elghazouli, A. Y. & Enache, R. (2014) Contribution of secondary frames to the mitigation of collapse in steel buildings subjected to extreme loads. *Structure and Infrastructure Engineering*. 1-16. Available from: doi:10.1080/15732479.2014.994534.

Martin, D., Kirby, B. & O'Connor, M. (1999) *The behaviour of multi-storey steel framed buildings in fire*. Moorgate, Rotterdam, UK, British Steel plc, Swinden Technology Centre.

McKenna, F. (1997) *Object Oriented Finite Element Programming: Frameworks for Analysis, Algorithms and Parallel Computing*. University of California, Berkeley, California, USA. http://opensees.berkeley.edu

Mesquita, L. M. R., Piloto, P. A. G., Vaz, M. A. P. & Vila Real, P. M. M. (2005) Experimental and numerical research on the critical temperature of laterally unrestrained steel I beams. *Journal of Constructional Steel Research*. 61(10), 1435-1446. Available from: doi:10.1016/j.jcsr.2005.04.003.

Milke, J., Kodur, V., Marrioon, C. (2002) *An Overview of Fire Protection in Buildings, FEMA 403 - World Trade Center Building Performance Stu*dy. Appendix A.

Modica A. & Stafford P.J. (2014) Vector fragility surfaces for reinforced concrete frames in Europe. *Bulletin of Earthquake Engineering*, 12, 1725-1753.

Nassr, A. A., Razaqpur, A. G., Tait, M. J., Manuel Campidelli, M. & Foo, S. (2012) Experimental performance of steel beams under blast loading. *Journal of Performance of Constructed Facilities*. 26(5), 600-619. Available from: doi:10.1061/(ASCE)CF.1943-5509.0000289.

Nigro E., Bilotta, A., Asprone, D., Jalayer, F., Prota, A. & Manfredi, G. (2014) Probabilistic approach for failure assessment of steel structures in fire by means of plastic limit analysis. *Fire Safety Journal*. 68, 16-29.

Ngo,T., Mendis, P., Gupta, A. & Ramsay, J. (2007) Blast loading and blast effects on structures – An Overview. *Electronic Journal of Structural Engineering Special Issue: Loading on Structures*. Available from: http://www.ejse.org/Archives/Fulltext/2007/Special/200707.pdf

Qin, C. & Mahmoud, H. (2019) Collapse performance of composite steel frames under fire. *Engineering Structures*. 183, 662-676. Available from: doi:10.1016/j.engstruct.2019.01.032.

Rackauskaite, E. & El-Rimawi, J. (2014) A Study on the Effect of Compartment Fires on the Behaviour of Multi-Storey Steel Framed Structures. *Fire Technology*. 51(4), 867-886. Available from: doi:10.1007/s10694-014-0419-0.

Rackauskaite, E., Hamel, C., Law, A. & Rein, G. (2015) Improved Formulation of Travelling Fires and Application to Concrete and Steel Structures. *Structures*. Available from: doi:10.1016/j.istruc.2015.06.001.

Rackauskaite, E., Kotsovinos, P. & Rein, G. (2017) Structural response of a steel-frame building to horizontal and vertical travelling fires in multiple floors. *Fire Safety Journal*. 91, 542-552. Available from: doi:10.1016/j.firesaf.2017.04.018.

Rein, G., Abecassis-Empis, G. & Carvel, R. (eds.) (2007) *The Dalmarnock fire tests: Experiments and modelling*. School of Engineering and Electronics, University of Edinburgh.

Rezvani, F. H. & Ronagh, H. R. (2015) Structural response of a MRF exposed to travelling fire. *Proceedings of the ICE - Structures and Buildings*. 168(9), 619-635. Available from: doi:10.1680/stbu.14.00046.

Rini, D. & Lamont, S. (2008) Performance Based Structural Fire Engineering for Modern Building Design. *Structures Congress 2008*, *24-26 April 2008*, *Vancouver, Canada*. American Society of Civil Engineers. pp. 1-12.

Röben, C., Gillie, M. & Torero, J. (2010) Structural behaviour during a vertically travelling fire. *Journal of Constructional Steel Research*. 66(2), 191-197. Available from: doi:10.1016/j.jcsr.2009.08.007.

Rubert, A., Schaumann, P. (1986) Structural steel and plane frame assemblies under fire action. *Fire Safety Journal*. 10, 173-184.

Rush, D., Bisby, L., Ioannou, I. & Rossetto, T. (2014) Towards fragility analysis for concrete buildings in fire: Residual capacity of concrete columns. *8th International Conference on Structures in Fire*. Shanghai, China, June 11-13.

Schleyer, G.K & Hsu, S.S (2000) A modelling scheme for predicting the response of elastic–plastic structures to pulse pressure loading. *International Joural of Impact Engineering*. 24(8), 759-777.

Sleich, J.B, Cajot, L.G, Pierre, M., Joyeux, D., Aurtenetxe, G., Unanua, J., Pustorino, S., Heise, F.J, Salomon, R., Twilt, L. & Van Oerle, J. (2002) *Valorisation project - Natural fire safety concept*. European commission technical steel research.

Smith, P. & Cormie, D. (2009) Blast loading. In: Cormie, D., Mays, G. & Smith, P. (eds.) *Blast effects on buildings*. United Kingdom, ICE Publishing.

Pitts, W.M, Butler, K.M & Junker, V. (2005) *Federal building and fire safety investigation of the World Trade Centre disaster: Visual evidence, damage estimates, and timeline analysis*. NIST NCSTAR 1-5A.

Spacone E., Filippou, F.C & Taucer, F.F (1996) Fibre beam–column model for non-linear analysis of r/c frames: Part I. Formulation. *Earthquake Engineering and Structural Dynamics*. 25, 711-725.

Stern-Gottfried, J. & Rein, G. (2012a) Travelling fires for structural design–Part I: Literature review. *Fire Safety Journal*. 54, 74-85. Available from: doi:10.1016/j.firesaf.2012.06.003.

Stern-Gottfried, J. & Rein, G. (2012b) Travelling fires for structural design-Part II: Design methodology. *Fire Safety Journal*. 54, 96-112. Available from: doi:10.1016/j.firesaf.2012.06.011.

Stull, D.R. (1977) *Fundamentals of Fire and Explosion*. AlChE Monograph Series Number 73, (New York: American Institute of Chemical Engineering).

Tan, Y., Xi, F., Li, S. & Zhou, Z. (2017) Pulse shape effects on the dynamic response of a steel beam under combined action of fire and explosion loads. *Journal of Constructional Steel Research*. 139, 484-492. Available from: doi:10.1016/j.jcsr.2017.10.001.

Teslim-Balogun, A., Malaga-Chuquitaype, C. & Stafford, P.J (2017) Assessment of efficiency of intensity measures for performance-based travelling fire design. In: *39th IABSE Symposium: Engineering the future*, Vancouver, Canada, September 21-23.

Teslim-Balogun, A., Malaga-Chuquitaype, C. & Stafford, P.J (2019) A Numerical Study on the Structural Response of Steel Structures under Post-Blast Travelling Fires. *Structures Congress 2019*, Orlando, Florida, April 24–27.

Thil, N., Mehreganian, N., Moatamedi, M., Louca, L.A & Fallah, A.S (2019) Dynamic plastic response of beams subjected to localised pulse loads. *International Journal of Protective Structures*. 10(2), 198-228.

Thyer, A.M., Kerr, D., Royle, M. & Willoughby, D. (2008). *The development of running pool fires on simulated offshore decking*, Report No. PS/08/08. The Health and Safety Laboratory, Buxton.

Torero, J.L (2011) Fire-induced structural failure: the World Trade Center, New York. *Forensic Engineering*. 164 (FE2), 69-77.

Torero, J.L., Law, A. & Maluk, C. (2017) Defining the thermal biundary condition for protective structures in fire. *Engineering Structures*. 149, 104-112.

Ufuah, E. (2012) The behaviour of stiffened steel plated decks subjected to unconfined pool fires. In: *Proceedings of the World Congress on Engineering and Computer Science*, San Francisco, USA, October 24-26.

United Facilities Criteria (2008) *Structures to resist the effects of accidental explosions*. US Army Corps of Engineers, Naval Facilities Engineering Command, Air Force Civil Engineer Support Agency, UFC 3-340-02, 5.

Usmani, A.S., Rotter, J.M., Lamont, S., Sanad, A.M., & Gillie M. (2001) Fundamental principles of structural behaviour under thermal effects. *Fire Safety Journal*, 36, 721-744.

Usmani, A., Zhang, J., Jiang, J., Jiang, Y. & May, I. (2012). Using OpenSees for structures in fire. *Journal of Structural Fire Engineering*. 3 (1), 57-70. Available from: https://doi.org/10.1260/2040-2317.3.1.57.

Wainman D.E. & Kirby B.R. (1988) *Compendium of UK standard fire test data - Unprotected structural steel-1*. British Steel Corporation, Ref. No. RS/RSC/S10328/1/98/B. Swinden Laboratories, Rotherdam.

Wang, Y. C. (2000) An analysis of the global structural behaviour of the Cardington steel-framed building during the two BRE fire tests. *Engineering Structures*. 22(5), 401-412.

Whittaker, A., Hamburger, R., Comartin, C., Mahoney, M., Bachman, R. & Rojahn, C. (2003) Performance based engineering of buildings and infrastructure for extreme loadings. In: *73rd Shock and Vibration Symposium, SAVIAC*. San Diego, CA.

Xu, L., Ma, T. & Zhuang, Y. (2018) Storey-based stability of unbraced structural steel frames subjected to variable fire loading. *Journal of Constructional Steel Research*. 147, 145-153. Available from: doi:10.1016/j.jcsr.2018.04.003.

Zhang, C., Li, G.-Q. & Usmani, A. (2013) Simulating the behavior of restrained steel beams to flame impingement from localized-fires. *Journal of Constructional Steel Research*. 83, 156-165. Available from: doi:10.1016/j.jcsr.2013.02.001.